

UNCLASSIFIED

~~CONFIDENTIAL~~



3 1176 00104 1319

**NASA TECHNICAL
MEMORANDUM**



NASA TM X-1101

C3

NASA TM X-1101

LIBRARY COPY

MAY 27 1965

LANGLEY RESEARCH CENTER
LIBRARY, NASA
LANGLEY STATION
HAMPTON, VIRGINIA

**INVESTIGATION OF ROUGHNESS-INDUCED
TURBULENT HEATING TO THE
HL-10 MANNED LIFTING ENTRY VEHICLE
AT A MACH NUMBER OF 8**

CLASSIFICATION CHANGED

by Philip E. Everhart and H. Harris Hamilton

UNCLASSIFIED

Langley Research Center

Langley Station, Hampton, Va.

To _____
By authority of *STAR* Date *12-31-70*
1.8 No. 24 *Rev*
3-16-71

NATIONAL AERONAUTICS AND SPACE ADMINISTRATION

WASHINGTON, D. C. • MAY 1965

UNCLASSIFIED
~~CONFIDENTIAL~~

UNCLASSIFIED
~~CONFIDENTIAL~~

NASA TM X-1101

CLASSIFICATION CHANGED

To UNCLASSIFIED

By authority of STAR Date 12-31-70
V. 8, No. 24 blm
3-16-71

INVESTIGATION OF ROUGHNESS-INDUCED TURBULENT HEATING

TO THE HL-10 MANNED LIFTING ENTRY VEHICLE

AT A MACH NUMBER OF 8

By Philip E. Everhart and H. Harris Hamilton

Langley Research Center
Langley Station, Hampton, Va.

GROUP 4
Downgraded at 3 year intervals;
declassified after 12 years

CLASSIFIED DOCUMENT-TITLE UNCLASSIFIED

This material contains information affecting the national defense of the United States within the meaning of the espionage laws, Title 18, U.S.C., Secs. 793 and 794, the transmission or revelation of which in any manner to an unauthorized person is prohibited by law.

NOTICE

This document should not be returned after it has satisfied your requirements. It may be disposed of in accordance with your local security regulations or the appropriate provisions of the Industrial Security Manual for Safe-Guarding Classified Information.

NATIONAL AERONAUTICS AND SPACE ADMINISTRATION

UNCLASSIFIED
~~CONFIDENTIAL~~

~~CONFIDENTIAL~~
UNCLASSIFIED

INVESTIGATION OF ROUGHNESS-INDUCED TURBULENT HEATING

TO THE HL-10 MANNED LIFTING ENTRY VEHICLE

AT A MACH NUMBER OF 8*

By Philip E. Everhart and H. Harris Hamilton
Langley Research Center

SUMMARY

An experimental investigation of a reentry configuration designated HL-10 having a hypersonic lift-drag ratio of about 1 has been conducted to determine the aerodynamic heating characteristics. The effects of roughness, angle of attack ($0 \leq \alpha \leq 60$), and Reynolds number (based on root chord) from 0.24×10^6 to 6.58×10^6 are assessed. The roughness caused boundary-layer transition near the roughness location from angles of attack of 20° to 40° at Reynolds numbers of 2.70×10^6 and 6.58×10^6 . The turbulent heating rates measured further rearward along the center line are in good agreement with a simple turbulent flat-plate theory in heating level, distribution, and variation with Reynolds number. The roughness had little effect on the heating over the elevons. Elevon deflections of 15° and 30° had little effect on the heat transfer to the rough model adjacent to the elevon location.

INTRODUCTION

Laminar heating characteristics for the HL-10 manned lifting entry vehicle at a Mach number of 8 are presented in reference 1 for Reynolds numbers (based on model root chord) from 0.24×10^6 to 2.70×10^6 . For actual flight conditions the boundary layer on portions of the configuration may be turbulent rather than laminar. Therefore, the present investigation using a roughness band near the nose of the HL-10 was undertaken to obtain the turbulent heating characteristics of the configuration and the results are presented herein. The investigation was made on an 8-inch calorimeter model in the Langley Mach 8 variable-density tunnel at Reynolds numbers (based on model root chord) from 0.24×10^6 to 6.58×10^6 . The model was tested at angles of attack from 0° to 60° and with elevon deflection angles of 0° , 15° , and 30° . The tests were made with and without roughness elements on the model nose. A comparison of the center-line data with turbulent strip theory is also presented.

*Title, Unclassified.

~~CONFIDENTIAL~~
UNCLASSIFIED

SYMBOLS

c	chord, 8 inches
c_w	specific heat of wall material
D_n	nose diameter, 0.75 inch
h	heat-transfer coefficient
h_o	calculated laminar stagnation-point heat-transfer coefficient on sphere having same radius as nose
k	thermal conductivity
m	weight of skin per unit heated surface area
M	Mach number
N_{Pr}	Prandtl number
N_{St}	Stanton number
p	pressure
r	radius of nose
R_c	free-stream Reynolds number based on root chord
R	Reynolds number
s	surface distance from plane of symmetry
t	time
T	absolute temperature
u	velocity
x,y,z	model coordinates (see fig. 1(a))
α	angle of attack (see fig. 1(a))
δ_e	elevon deflection angle in plane normal to hinge line, positive with trailing edge down
η_r	temperature recovery factor, $\frac{T_{aw} - T_l}{T_t - T_l}$
μ	dynamic viscosity

~~CONFIDENTIAL~~
UNCLASSIFIED

ρ density
 σ surface distance along model center line measured from midpoint of spherical nose

Subscripts:

2 free-stream conditions immediately behind normal shock
e elevon
l local conditions
L laminar
t total
T turbulent
w wall
aw adiabatic wall
 ∞ free-stream conditions

A primed symbol denotes values for reference temperature.

MODEL

The heat-transfer model tested was the 8-inch version of the HL-10 configuration used for the laminar tests reported in reference 1. Body ordinates for the HL-10 heat-transfer model tested are given in table 1 of reference 1. Model dimensions are given in figure 1(a) and the model instrumentation is presented in figure 1(b).

The thin-skinned, calorimeter, heat-transfer model was made of 0.031-inch-thick inconel sheet formed over a mandrel in two halves and then welded together. Details of the construction of the model and elevons may be found in reference 1. Photographs of the assembled model are shown in figure 2.

For the roughness tests, number 40 steel grit was spot-welded around the nose of the model in six rings forming a roughness band 0.25 inch wide. The average particle size (0.048 inch) is indicative of the roughness height. Closeup photographs of the roughness band are presented as figures 2(c) and 2(d). The roughness band had a mean diameter of 0.50 inch and was centered approximately around the expected stagnation point for an angle of attack of 30°. Iron-constantan thermocouples of number 30 wire (0.010-inch diameter) were spot-welded to the inner surface of the thin skin of the heat-transfer model at the locations shown in figure 1(b). Most of the instrumentation is located on the

~~CONFIDENTIAL~~

UNCLASSIFIED

center line of the model and along five spanwise stations at x/c equal to 0.125, 0.250, 0.500, 0.750, and 0.950.

TEST AND DATA REDUCTION

The model was tested in the Langley Mach 8 variable-density tunnel for which calibration data are given in reference 2. The tests were conducted in two phases. The model was initially tested with the tunnel operating at low pressure (80 to 1000 lb/sq in. abs) and discharging into a vacuum sphere. The second phase consisted of operating the tunnel at a higher pressure (2500 lb/sq in. abs) and discharging to the atmosphere.

Nominal tunnel conditions for the tests are given in the following table:

P_t , lb/sq in. abs	T_t , °F	M_∞	R_∞ per ft
80	750	7.59	0.35×10^6
275	850	7.85	1.16
1000	950	7.95	3.98
2500	1025	*8.00	9.87

*No calibration data are available for the tunnel operating at 2500 lb/sq in.; therefore, a tunnel design Mach number of 8 was used.

The model was tested with and without the roughness elements. All the tests which involved roughness were completed with the grit unaltered in order that the measured data would not vary as a result of the size and distribution of the roughness elements.

Heat-transfer data were obtained by means of a transient calorimetry technique. The tunnel was brought to the desired operating conditions, and then the sting-mounted model was rapidly injected into the airstream by a pneumatic piston from an enclosed recessed position directly under the test section. The time required for the model to pass through the tunnel-wall boundary layer and for steady flow to be established over the model was approximately 0.05 second. The model remained in the airstream for a period of 3 to 5 seconds. Between runs the model was cooled to room temperature by means of high-pressure air jets.

Thermocouple outputs were recorded on magnetic tape at a rate of 20 times per second by means of a high-speed analog to digital data recording system. Heat-transfer coefficients were calculated from the following equation:

$$h = \frac{mc_w}{T_{aw} - T_w} \frac{dT_w}{dt} \quad (1)$$

~~CONFIDENTIAL~~
UNCLASSIFIED

The weight of the material per unit surface area m was determined from the density, measured skin thickness, and an allowance for the surface curvature. The change in temperature with respect to time, required in equation (1), was obtained by first fitting a second-degree polynomial curve by the method of least squares to a group of 21 data points obtained over a period of 1 second. The equation fitted to this group of data points was then differentiated with respect to time and evaluated at the eleventh point on a card-programmed computer. The heat-transfer coefficients were computed at a time approximately 0.8 second after model injection.

The adiabatic-wall temperature required in equation (1) was calculated from $\frac{T_{aw}}{T_t} = \eta_r + \frac{T_l}{T_t}(1 - \eta_r)$ where $\eta_r = \sqrt{N_{Pr}}$ was used for the smooth model tests and $\eta_r = \sqrt[3]{N_{Pr}}$ was used for the tests with roughness. The Prandtl number was taken to be 0.7. The local temperature just outside the boundary layer was estimated by assuming that the flow expanded isentropically from the pressure behind a normal shock to the Newtonian pressure at the point in question. In the leeward region the pressure was assumed to be free-stream static pressure.

Estimates of the lateral conduction based on measured skin temperature distributions for the most severe conditions of the tests show that the measured heating may be low by as much as 12 percent at the stagnation point on the nose, 6 percent on the leading edge of the body, and 15 percent on the tip fin leading edge. The data are presented without correction since the calculated error was in general much smaller than that indicated previously.

The measured heat-transfer coefficients are presented as the ratio h/h_0 where h_0 is the reference laminar stagnation-point heat-transfer coefficient on a sphere having the same radius as the nose of the HL-10 model. The reference laminar heat-transfer coefficient h_0 was used in order to compare the present data with previous data (ref. 1) as well as to correlate the laminar data of the present investigation. Values of h_0 were calculated for the particular test conditions from the following equation, adapted from reference 3:

$$h_0 = 0.763 N_{Pr}^{0.4} k_2 \left(\frac{\rho_2}{\mu_2} \frac{du}{ds} \right)^{0.5} \quad (2)$$

The stagnation-point velocity gradient was obtained from modified Newtonian theory for the pressure distribution and is

$$\frac{du}{ds} = \frac{1}{r} \sqrt{\frac{2(p_{t,2} - p_\infty)}{\rho_{t,2}}}$$

Calculated values of h_0 for the nominal test conditions are shown in the following table:

~~CONFIDENTIAL~~
UNCLASSIFIED

p_t , lb/sq in. abs	Re	h_o , Btu/ft ² -sec-°F
80	0.24×10^6	0.0111
275	.77	.0206
1000	2.70	.0398
2500	6.58	.0617

These values of h_o are from 3 to $4\frac{1}{2}$ percent greater than those predicted by a modified form of the Fay and Riddell equation (ref. 4) for the heat transfer to the stagnation point of a blunt body in a perfect gas. It can be shown from theory that for any given point the laminar heat-transfer coefficient h_L and the laminar stagnation-point heat-transfer coefficient h_o are inversely proportional to the square root of the Reynolds number. Thus, for laminar flow, the heating ratio h_L/h_o is independent of Reynolds number. From turbulent theory the heat-transfer coefficient h_T is related to Reynolds number by $h_T \approx R^{-1/5}$. Therefore, the parameter h_T/h_o is dependent upon Reynolds number for turbulent flow and the dependence is expressed by $h_T/h_o \approx R^{0.3}$. This dependence of the heating ratio h_T/h_o on Reynolds number for turbulent flow must be accounted for in the application of the present turbulent data to conditions other than those tested.

THEORY

From reference 5 the turbulent heating on a flat plate, in terms of local reference-temperature conditions, is

$$\left[N'_{St}(R')^{1/5} \right]_l = \frac{0.0592}{2(N'_{Pr})^{2/3}} \quad (3)$$

The local turbulent Stanton number is, then

$$N_{St,l} = \frac{0.0296}{(N'_{Pr})^{2/3}(R_l)^{1/5}} \left(\frac{T_l}{T'} \right) \left(\frac{\mu'}{\mu_l} \frac{T'}{T_l} \right)^{1/5}$$

and hence, ideal air being assumed, the equation for the heat-transfer coefficient from turbulent strip theory is

$$h = 0.00829 \left(\frac{T_l}{T'} \right)^{0.8} \left(\frac{\mu'}{\mu_l} \right)^{0.2} \frac{p_l M_l}{(T_l)^{0.5} (R_l)} \left(\frac{1}{R_l} \right)^{0.2} \quad (4)$$

~~CONFIDENTIAL~~
UNCLASSIFIED

Modified Newtonian theory was used to obtain the local pressures since it was shown in reference 4 that Newtonian theory was in good agreement with the measured pressures on a blunt-nose delta wing for the angles of attack of primary interest. Local conditions of temperature and Mach number were based on stagnation conditions behind a normal shock wave. Reference temperatures were determined from local flow conditions by means of the following equation (ref. 6)

$$\frac{T'}{T_l} = 1 + 0.035M_l^2 + 0.45\left(\frac{T_w}{T_l} - 1\right) \quad (5)$$

Values of local Reynolds number were obtained by integrating the local unit Reynolds number over the surface distance along the model center line from the midpoint of the spherical nose using the following relation:

$$R_l = \int_0^\sigma 0.02856 \frac{p_l M_l}{\mu_l(T_l)^{0.5}} d\sigma \quad (6)$$

Heat-transfer coefficients were also calculated by using local Reynolds numbers obtained from local conditions at a point and the distance from the midpoint of the spherical nose to this point. However, the theoretical heat-transfer coefficients calculated by using the integrated local Reynolds numbers were in better agreement with the measured data and thus are used in this report.

RESULTS

Flow Pattern

Side-view schlieren photographs of the HL-10 model at various angles of attack are shown in figures 3 and 4. It can be observed in figure 3 that the shape and position of the bow shock, even in the vicinity of the trailing edge of the model, is unaffected by elevon deflection of 0°, 15°, and 30° at the two highest Reynolds numbers tested. However, deflecting the elevons did produce a shock just ahead of the elevons. The weak shocks in the regions just upstream of the elevons are evidently caused by some small surface imperfection since the screws holding the elevons to the model are located in this region. A comparison of the flow pattern for the configuration, with and without roughness, is shown in figure 4. No apparent effect of roughness on the shock shape and position is indicated, except possibly in the immediate vicinity of the roughness location.

Distribution of Heating Along Center Line

With roughness elements.- The ratio of the measured heat-transfer coefficient to the calculated stagnation-point heat-transfer coefficient h/h_0 along the center line of the HL-10 with roughness is presented in figure 5 for the angles of attack and Reynolds numbers tested. Elevon deflections of 0°, 15°,

~~CONFIDENTIAL~~
UNCLASSIFIED

UNCLASSIFIED

and 30° were tested; however, only the data for 0° elevon deflection are presented since they are representative of all the elevon deflections. Positive values of the parameter x/c indicate distance along the lower center line whereas distance along the upper center line is represented by negative values. The position of the roughness band is indicated on the figures by the vertical dotted areas. The roughness band caused considerable interference locally around the nose. Even at the thermocouple located in the center of the nose region ($x/c = 0$), unexpectedly high heating rates were measured. No significance can be attached to the measurements under and adjacent to the roughness and they will not be discussed further; however, the data are included for completeness.

The center-line distributions (fig. 5) of the heat-transfer ratio are similar at all the Reynolds numbers tested. The general trend of the heat-transfer ratio is to decrease with distance along the model center line. However, at the two highest Reynolds numbers (figs. 5(c) and 5(d)), inflections occur in the heat-transfer distribution for the high-angle-of-attack data.

Increasing the angle of attack, in general, increased the heat transfer to the lower surface and decreased that to the upper surface. Exceptions to this general trend occur at $R_c = 2.70 \times 10^6$ (fig. 5(c)) where the heat transfer to the forward portion of the model ($0.1 < x/c < 0.5$) was highest at $\alpha = 30^\circ$ and the highest heat transfer to the rearward portion of the model ($0.5 < x/c < 1.0$) occurred at $\alpha = 40^\circ$.

Increasing the Reynolds number by a factor of 10 (see figs. 5(a) and 5(c)) resulted in the heat-transfer ratio increasing by as much as 100 percent.

Without roughness elements.- The chordwise variation of the heat-transfer ratio on the HL-10 without roughness is presented in figure 6 for a Reynolds number of 6.58×10^6 , angles of attack from 0° to 40° , and elevon deflections of 0° , 15° , and 30° . In general, increasing the angle of attack decreased the heat transfer to the upper surface and increased that to the lower surface for the three elevon deflections tested. The heat-transfer ratio on the lower surface decreased with distance along the model center line except at an angle of attack of 40° where a substantial increase in the heating occurred over the rearward section of the model ($x/c > 0.5$).

Deflecting the elevons downward (figs. 6(b) and 6(c)) had little effect on the center-line heating except for 30° elevon deflection where at $\alpha = 40^\circ$ the heating on the rearward half of the model was lower than that for 0° and 15° deflections.

Spanwise Distribution of Heating

With roughness elements.- The spanwise distributions of the heat-transfer ratio at five chordwise stations on the HL-10 model with roughness are presented in figures 7 to 11. Parts (a), (b), (c), and (d) of each figure are for Reynolds numbers (based on root chord) of 0.24×10^6 , 0.77×10^6 , 2.70×10^6 , and 6.58×10^6 , respectively. Elevon deflections of 0° , 15° , and 30° were

UNCLASSIFIED

~~CONFIDENTIAL~~
UNCLASSIFIED

tested; however, only the data for $\delta_e = 0^\circ$ are presented since it was noted that the other deflection angles had little effect on the heating to the lower surface. The heating on the elevons is discussed in a later section. At $x/c = 0.125$, the distance parameter s/D_n begins at the lower center line and extends to the top center line; at other chordwise stations the data extends around the 90° of arc leading edge onto the relatively flat side of the vehicle. (See fig. 1(b).) The distribution of the heat-transfer ratio at $x/c \approx 0.950$ includes the thermocouples located on the lower elevon surface, also extends around the tip fin and includes a thermocouple on the leading edge of the tip fin and one on the inner surface of the tip fin. Cross sections and instrumentation details at each station are shown in figure 1(b).

The data from figures 7 to 10 show peak heating occurred on the leading edge of the model for most test conditions. However, at $x/c = 0.750$ (fig. 10) and angles of attack of 0° and 10° , the heating increased around the leading edge to a maximum value on the side of the model. In general, the peak heating increased with Reynolds number and decreased with distance from the nose (x/c). Similarly, the heating level on the entire lower surface increased as the Reynolds number increased and decreased toward the trailing edge. The lower surface heating was approximately constant in the spanwise direction at each chordwise station with an increase in the region of the cylindrical leading edge.

The effect of angle of attack on spanwise heat-transfer ratio is shown in parts (c) and (d) of figures 7 to 10. In general, the measured heating on the lower surface and the leading edge increased with increasing angle of attack. With increasing angle of attack, movement of the Newtonian stagnation line toward the lower surface results in a decrease in the heating to the side of the model.

The spanwise heat-transfer distribution at $x/c = 0.950$, which includes the heating to the elevon surface, is shown in figure 11 for the undeflected elevon. The level of heating to the elevon surface is nearly the same as on the lower surface center line. In general, the point of maximum heating occurred on the leading edge of the tip fin and decreased with increasing angle of attack. However, at the higher angles of attack the maximum heating occurred on the cylindrical leading edge of the lower surface.

Without roughness elements.— The measured spanwise distributions of heating at the five chordwise measuring stations are presented in figures 12 to 16 for the HL-10 model with zero roughness at a Reynolds number of 6.58×10^6 . Parts (a), (b), and (c) of each figure are for elevon deflections of 0° , 15° , and 30° . At most of the chordwise stations, the heat-transfer data increased toward the leading edge, the maximum heating occurring on the side of the model, and then decreased around the side of the model. However, at $x/c = 0.750$ (fig. 15) and low angles of attack ($\alpha \leq 20^\circ$), maximum heating occurred on the side of the model whereas at angles of attack of 30° and 40° , the maximum heating occurred on the leading edge.

~~CONFIDENTIAL~~

UNCLASSIFIED

~~UNCLASSIFIED~~

The spanwise heating on the lower surface and cylindrical leading edge increased with angle of attack, whereas the heating to the side of the model decreased with increasing angle of attack.

For the spanwise stations upstream of the elevon location, elevon deflection is seen to have little effect on the heating except at $x/c = 0.750$ (fig. 15) where for $\delta_e = 30^\circ$ and $\alpha = 40^\circ$, the spanwise heating on the lower surface is lower than that for the other elevon deflections.

Figure 16 presents the spanwise heat-transfer distribution at $x/c \approx 0.950$ for the elevon deflections tested. At this station the maximum heating occurred on the leading edge of the tip fin for angles of attack up to 20° and decreased with increasing angle of attack. At angles of attack of 30° and 40° , the maximum heating occurred on the cylindrical leading edge for the undeflected elevon whereas at elevon deflections of 15° and 30° , the maximum heating occurred on the elevons.

DISCUSSION

The object of this investigation was to obtain heating rates on the HL-10 for a turbulent boundary layer. The fact that turbulent flow was actually obtained over portions of the model will be shown from a comparison of the data for the model with and without roughness as well as from a comparison of the data with turbulent strip theory. A comparison of the measured heat-transfer ratios h/h_0 for the model, with and without roughness, is presented in figures 17 to 23 for the elevon deflections tested.

The heat-transfer data for the smooth model used in the comparison figures for angles of attack from 20° to 60° , elevon deflections of 0° and 30° , and for Reynolds numbers from 0.24×10^6 to 2.70×10^6 were obtained from reference 1 where it was shown that the heating was laminar. The remainder of the data for the smooth model was obtained from the present investigation. From the level and distribution of the data obtained in the present investigation on the smooth model (fig. 17), the heating also appears to be laminar except for the highest Reynolds number at angles of attack of 30° and 40° . For these two cases the heating increases downstream of the $x/c = 0.500$ station which suggests transition from laminar to turbulent flow. In the present analysis all heating rates for the model without roughness, except the two cases noted above, will be considered to be laminar.

It should be noted that for $\alpha = 0^\circ$ (fig. 17), the chordwise heating on both the rough and smooth models increases near the trailing edge. However, it is felt that this phenomenon is not the result of transition since the location of the increase in heating does not move forward with increasing Reynolds number and since similar effects are not observed at higher angles of attack as would be expected if this were transition.

Elevon deflection had little effect on the comparison of the data for the model with and without roughness; therefore the discussion of figures 17 to 22

* ~~CONFIDENTIAL~~

UNCLASSIFIED

~~CONFIDENTIAL~~
UNCLASSIFIED

at this point will be limited to the data for the 0° elevon deflection. The effect of elevon deflection on the heating to the smooth model was discussed in reference 1. This effect on the model with roughness will be discussed later.

Chordwise Heating

A comparison of the chordwise heat-transfer ratio for the model with and without roughness is presented in figure 17. The data show that the addition of roughness to the model had little effect on the measured heating for the two lowest Reynolds numbers tested ($R_c = 0.24 \times 10^6$ and 0.77×10^6). Previous work (ref. 1) has shown generally good agreement between the smooth model data and the heating rates calculated by laminar cross-flow theory; thus, agreement of the rough and smooth model results indicates that at these low Reynolds numbers the boundary layer on the rough model remained laminar.

For a Reynolds number of 2.70×10^6 , the addition of roughness to the model is seen to have little effect on heating at an angle of attack of 0° ; however, for higher angles of attack up to 40° , the addition of roughness was accompanied by a substantial increase in heating. This result suggests that transition occurred on the center line at $x/c \approx 0.250$ for $R_c = 2.70 \times 10^6$. For angles of attack of 50° (data not presented) and 60° , the data again show that the addition of roughness to the model had little or no effect on heating at $R_c = 2.70 \times 10^6$. For a Reynolds number of 6.58×10^6 , the addition of roughness to the model resulted in a large increase in heating for all angles of attack tested ($\alpha = 0^\circ$ to $\alpha = 40^\circ$).

Center-line heating rates calculated by turbulent strip theory for angles of attack of 40° or less are also shown in figure 17. At the lower angles of attack ($\alpha \leq 10^\circ$), the theory considerably overpredicted the level of the heating on the rough model for the two highest Reynolds numbers. The fact that the data are greater than the laminar values and less than those predicted by turbulent strip theory indicates that the data may be transitional. At angles of attack from 20° to 40° , however, the higher Reynolds number data are in excellent agreement with the turbulent theory, whereas the $R_c = 2.70 \times 10^6$ data are generally closer to the turbulent theory than to the smooth model results. Further examination of the data in figure 17 shows that for angles of attack from 0° to 40° , the difference between the heating on the rough and smooth models increases with increasing Reynolds number. As was discussed earlier, the parameter h/h_o is dependent upon Reynolds number for turbulent flow; thus, this increase in the heat-transfer parameter with Reynolds number is further evidence of turbulence within the boundary layer.

Based on these data it is concluded that boundary-layer transition occurred along the center line of the lower surface of the rough model just downstream of the roughness elements for Reynolds numbers of 2.70×10^6 and 6.58×10^6 throughout the angle-of-attack range of primary interest for this vehicle ($20^\circ \leq \alpha \leq 40^\circ$).

~~CONFIDENTIAL~~
UNCLASSIFIED

Spanwise Heating

The effect of roughness on the spanwise heat-transfer ratio at each of the chordwise stations is shown in figures 18 to 22 for the Reynolds numbers tested. At Reynolds numbers of 0.24×10^6 and 0.77×10^6 , little effect of roughness on the heating, particularly at the more rearward stations ($x/c \geq 0.500$), is indicated in these figures. It has been shown previously that the heating on the smooth model was laminar; therefore, at these low Reynolds numbers the heating on the rough model is also laminar. It is interesting to note that the addition of roughness had little effect on the heating rates provided the boundary layer remains laminar. This result is in agreement with the chordwise data of figure 17 which showed that turbulent flow did not exist on the model at these low Reynolds numbers.

Similarly, at $R_c = 2.70 \times 10^6$ (figs. 18 to 22), the spanwise data on the rough model are in agreement with that on the smooth model at angles of attack of 0° and 10° except for small regions ($x/c \leq 0.250$) where localized disturbances associated with the roughness elements result in higher heating rates. However, at $R_c = 6.58 \times 10^6$, higher heating was encountered on the rough model over the entire lower surface with the exception of a region near the trailing edge.

At angles of attack of 20° and 30° , the large difference in the heating on the rough and smooth models indicates that turbulent flow existed on the entire lower surface for $R_c = 2.70 \times 10^6$. At these angles of attack, turbulent flow also existed on portions of the cylindrical leading edge for the foremost stations ($0.125 \leq x/c \leq 0.500$). However, at $x/c = 0.750$ and 0.950 (figs. 21 and 22), the heating on the cylindrical leading edge appears to be laminar since the data for the rough and smooth models are in agreement. The data at an angle of attack of 40° show that the heating was laminar over the entire span at the most forward station. At $x/c = 0.250$, transition becomes evident on the center line, whereas at the more rearward stations, a region of turbulent flow spreads outward from the center line until at $x/c \approx 0.950$ the flow is turbulent over the entire span of the lower surface and part of the cylindrical leading edge. At angles of attack of 50° (data not shown) and 60° , no effect of roughness on the heat transfer for the model is shown. This result is thought to be caused by strong crossflow components which probably exist in the nose region of the model at these high angles of attack and cause the disturbed boundary layer to flow in a spanwise rather than a chordwise direction. Thus, the portion of the boundary layer which has passed over the roughness elements is probably removed from the lower surface before it can influence the downstream heating.

At $R_c = 6.58 \times 10^6$ and angles of attack of 20° and 30° , the data show a large increase in heating on the model with roughness, which indicates that the boundary layer was turbulent. A close examination of figures 18 to 22 shows that at the most forward stations ($x/c \leq 0.250$), the region of turbulent flow extends outward from the center line covering the entire lower surface and part of the cylindrical leading edge. For the more rearward stations ($x/c > 0.250$),

UNCLASSIFIED

the region of turbulent flow extends around the leading edge and well onto the side of the model. The data show that at an angle of attack of 40° the heating is turbulent over the entire lower surface and most of the cylindrical leading edge for chordwise stations upstream of $x/c = 0.750$. However, on the center line at $x/c = 0.750$ and on the entire lower surface and part of the cylindrical leading edge at $x/c \approx 0.950$, the heating on the rough and smooth models is approximately the same. This phenomenon is probably the result of a region of turbulent flow on the smooth model indicated previously; this region starts at the center line at $x/c \approx 0.750$ and spreads outward from the center line at the more rearward stations.

Elevon Heating

A comparison of the data on the model with roughness in parts (a), (b), and (c) of figures 17 to 22 shows that elevon deflections of 15° and 30° had little effect on the heat transfer to the adjacent surface of the model. The chordwise distributions of heat-transfer ratio on the elevons are presented in figure 23 for the deflection angles tested where only the data for Reynolds numbers of 2.70×10^6 and 6.58×10^6 are presented. At the two lowest Reynolds numbers the heating on the rough model was approximately the same as that on the smooth model as reported in reference 1. The level of heating on the elevons increased with angle of attack and with elevon deflection.

At $R_c = 2.70 \times 10^6$ (fig. 23(a)) little effect of roughness is shown at angles of attack of 0° and 20° for the elevon deflection angles tested. At an angle of attack of 40° , the elevon heating on the rough model was approximately twice that on the smooth model for elevon deflections of 0° and 15° ; however, for an elevon deflection of 30° the heating was considerably higher on the smooth model.

In reference 1 it was shown that the laminar boundary layer on the smooth model probably separated from the model surface upstream of the deflected elevon. However, the boundary layer on the model with roughness was turbulent and probably did not separate from the model surface. If the separated boundary layer on the smooth model becomes turbulent before reattachment, the heat transfer in the region of reattachment could be higher than the heat transfer for attached turbulent flow and would explain the difference between the heating on the smooth and rough models. At $R_c = 6.58 \times 10^6$ roughness had little effect on the heating over the elevon.

Heat Transfer to Tip Fin

The heat transfer to the leading edge of the tip fin presents a considerably greater problem for a turbulent boundary layer than for a laminar one. The highest heat transfer measured on the leading edge of the tip fin occurred at an angle of attack of 0° for the highest Reynolds number tested (see fig. 22) and was approximately 10 percent higher than the calculated laminar stagnation-point heating rate. This value represents approximately a 70-percent increase in heating over that for the smooth model.

UNCLASSIFIED

~~UNCLASSIFIED~~

CONCLUSIONS

A model of a manned lifting entry vehicle designated the HL-10 has been tested with and without roughness elements at a Mach number of 8, four Reynolds numbers from 0.24×10^6 to 6.58×10^6 , elevon deflections of 0° , 15° , and 30° , and angles of attack from 0° to 60° . From a comparison of the heating rates on the model with roughness with those on the smooth model as well as a comparison with turbulent strip theory, the following conclusions were obtained:

1. The roughness around the nose of the model caused boundary-layer transition near the roughness location at angles of attack from 20° to 40° at free-stream Reynolds numbers (based on root chord) of 2.70×10^6 and 6.58×10^6 . The turbulent heating rates measured further rearward along the center line are in good agreement with a simple turbulent flat-plate theory in heating level, distribution, and variation with Reynolds number.
2. Elevon deflections of 15° and 30° had little effect on the heat transfer to the rough model adjacent to the elevon location.
3. In general, the roughness had little effect on the heating over the elevons. However, at an angle of attack of 40° and a free-stream Reynolds number (based on root chord) of 2.70×10^6 , the elevon heating on the rough model was approximately twice that on the smooth model for elevon deflections of 0° and 15° .
4. The highest heat transfer on the leading edge of the tip fin of the rough model occurred at an angle of attack of 0° for a Reynolds number of 6.58×10^6 and was approximately 10 percent higher than the calculated laminar stagnation-point value.

Langley Research Center,
National Aeronautics and Space Administration,
Langley Station, Hampton, Va., March 5, 1965.

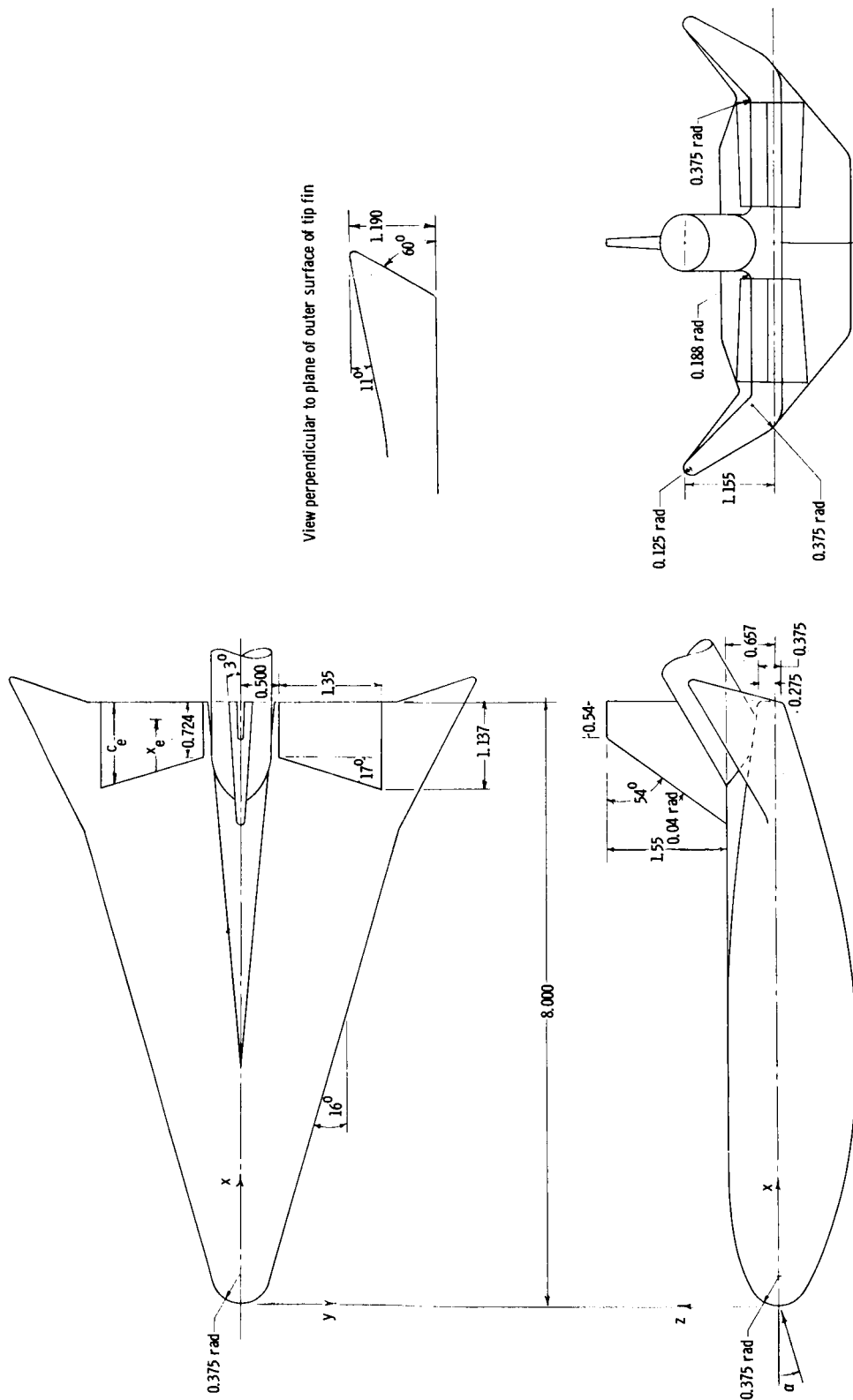
~~CONFIDENTIAL~~
UNCLASSIFIED

~~CONFIDENTIAL~~
UNCLASSIFIED

REFERENCES

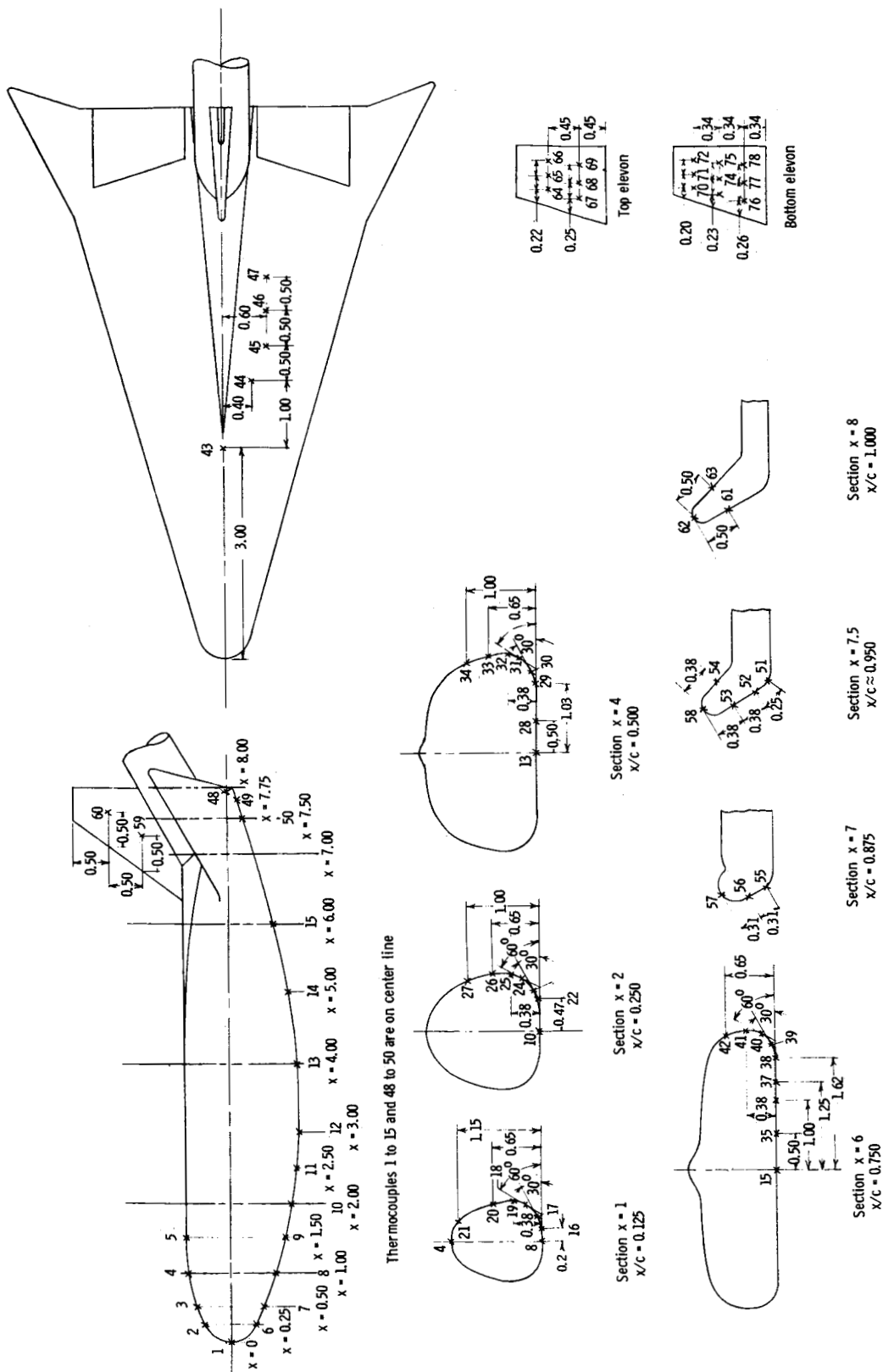
1. Dunavant, James C.; and Everhart, Philip E.: Investigation of the Heat Transfer to the HL-10 Manned Lifting Entry Vehicle at a Mach Number of 8. NASA TM X-998, 1964.
2. Stainback, P. Calvin: Heat-Transfer Measurements at a Mach Number of 8 in the Vicinity of a 90° Interior Corner Aligned With the Free-Stream Velocity. NASA TN D-2417, 1964.
3. Crawford, Davis H.; and McCauley, William D.: Investigation of the Laminar Aerodynamic Heat-Transfer Characteristics of a Hemisphere-Cylinder in the Langley 11-Inch Hypersonic Tunnel at a Mach Number of 6.8. NACA Rep. 1323, 1957. (Supersedes NACA TN 3706.)
4. Bertram, Mitchel H.; and Everhart, Philip E.: An Experimental Study of the Pressure and Heat-Transfer Distribution on a 70° Sweep Slab Delta Wing in Hypersonic Flow. NASA TR R-153, 1963.
5. Schlichting, Hermann (J. Kestin, trans.): Boundary Layer Theory. McGraw-Hill Book Co., Inc., 1955.
6. Sommer, Simon C.; and Short, Barbara J.: Free-Flight Measurements of Turbulent-Boundary-Layer Skin Friction in the Presence of Severe Aerodynamic Heating at Mach Numbers From 2.8 to 7.0. NACA TN 3391, 1955.

~~CONFIDENTIAL~~
UNCLASSIFIED



(a) Model geometry.

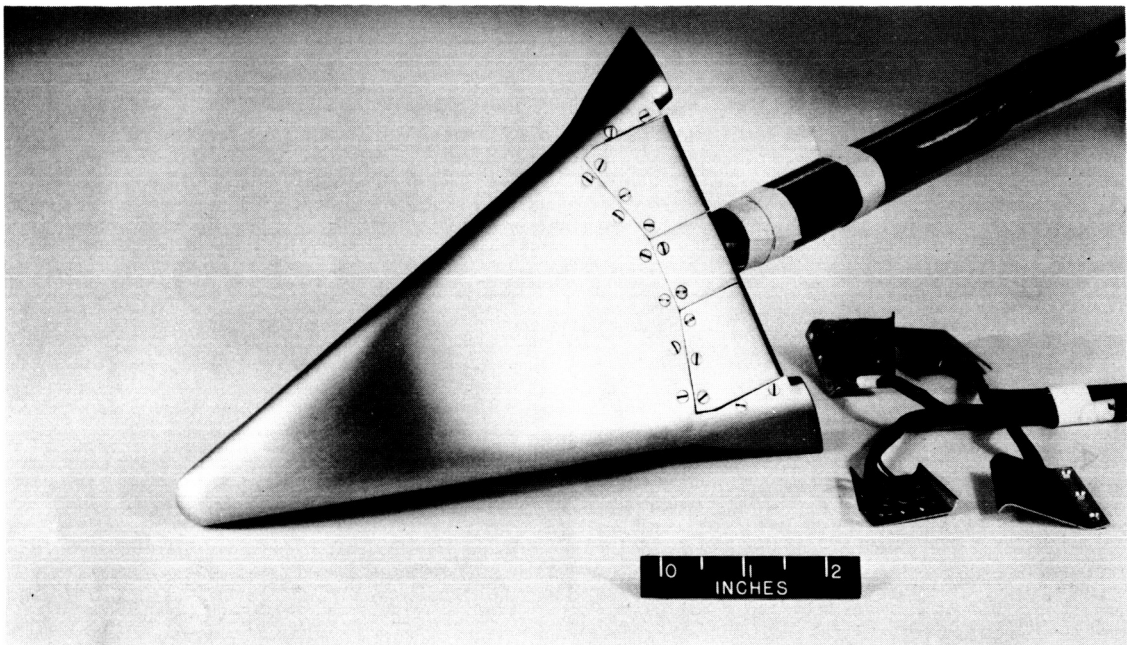
Figure 1.- Geometry and instrumentation of HL-10 configuration with fins D and E. All dimensions are in inches.



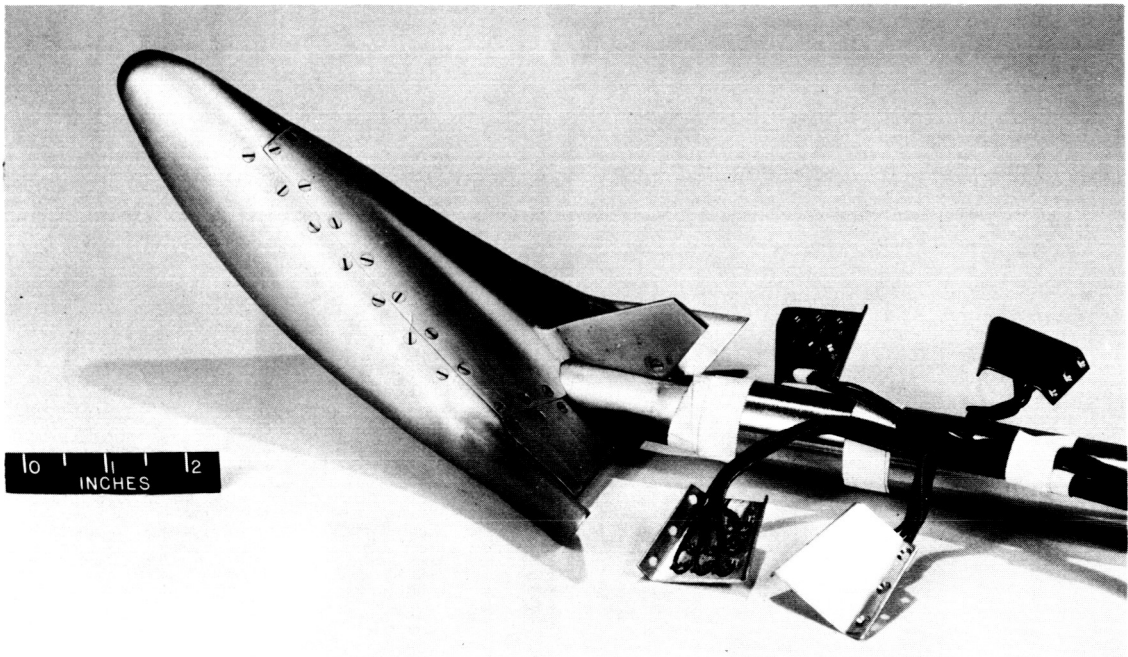
(b) Thermocouple locations.

Figure 1.- Concluded.

~~CONFIDENTIAL~~
UNCLASSIFIED



(a) Bottom view.

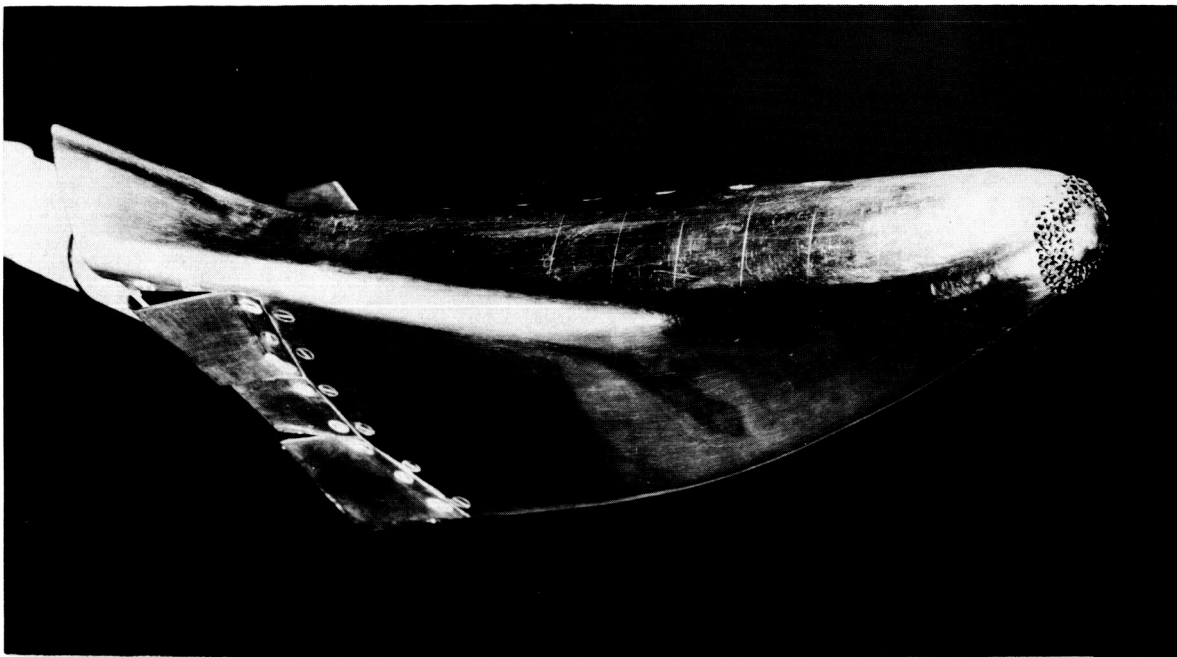


(b) Top view.

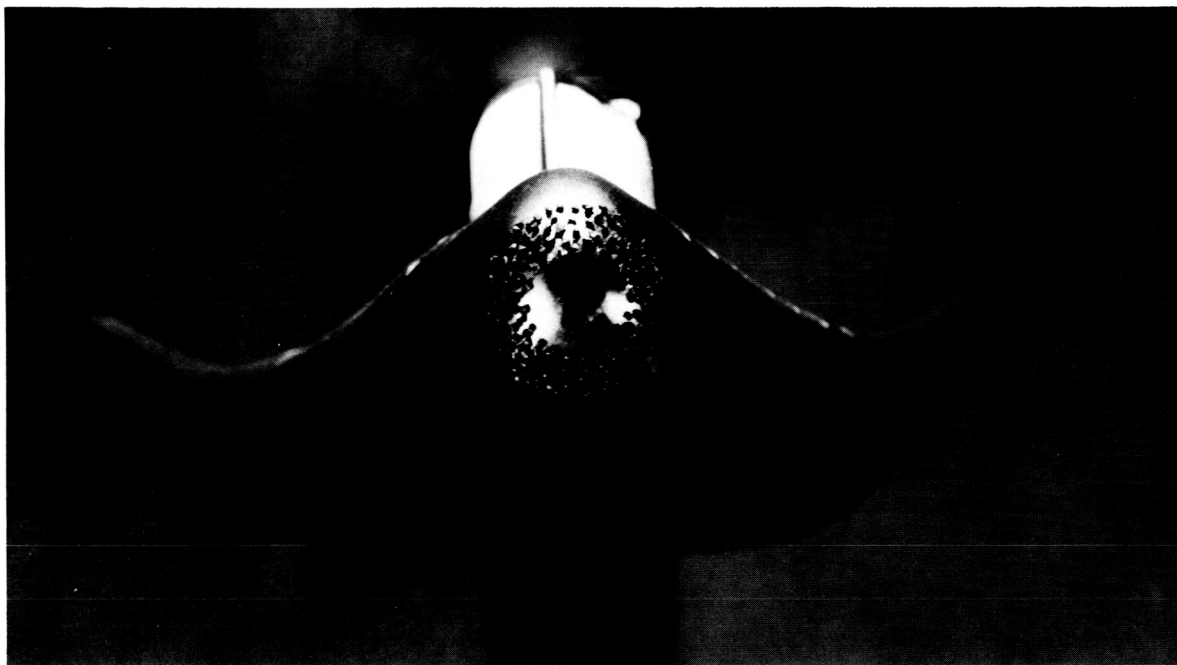
L-64-3055

Figure 2.- Photographs of HL-10 heat-transfer model.

~~CONFIDENTIAL~~
UNCLASSIFIED



(c) Side view of HL-10 with number 40 steel grit roughness.



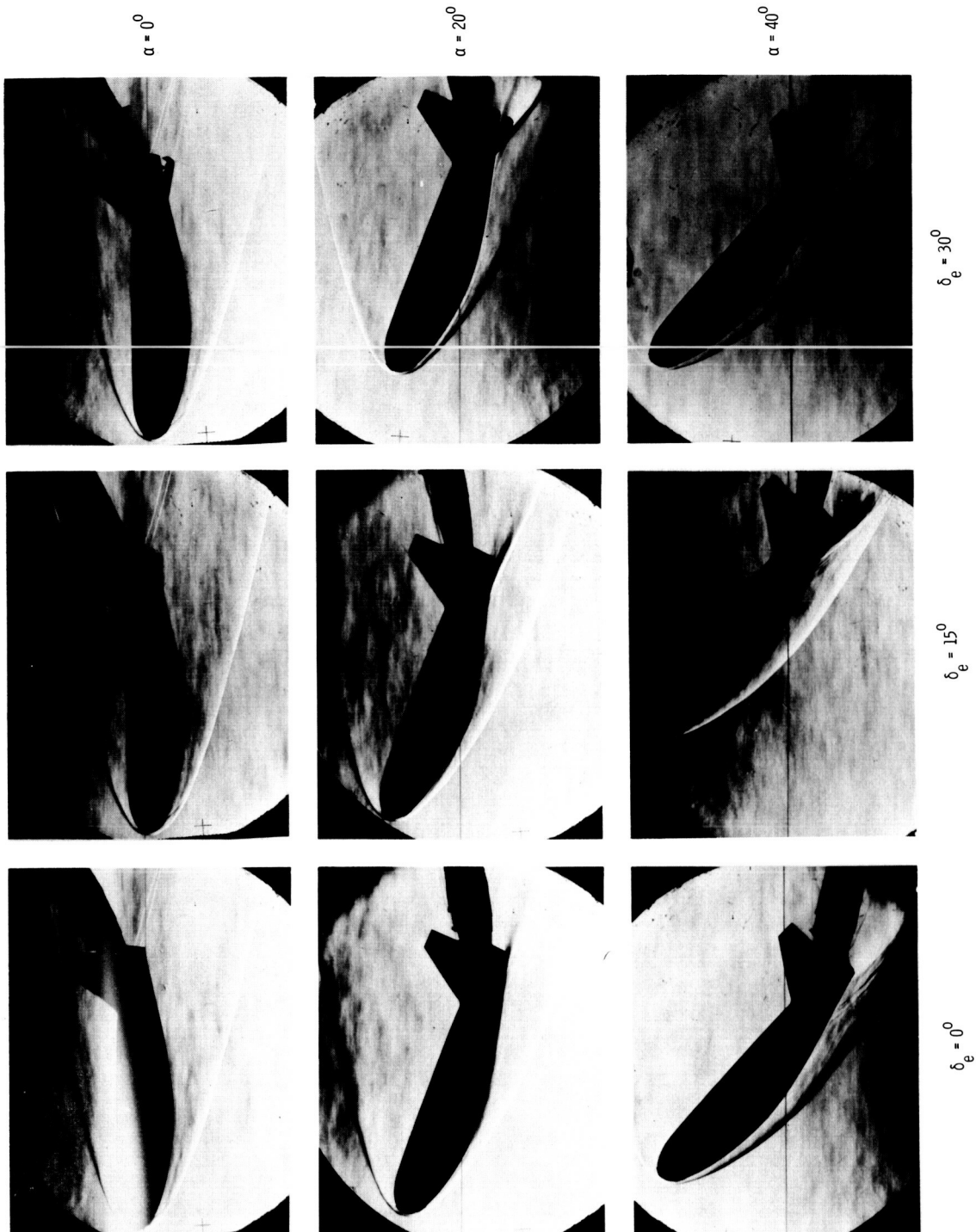
(d) Front view of HL-10 with number 40 steel grit roughness.

L-65-56

Figure 2.- Concluded.

UNCLASSIFIED

~~CONFIDENTIAL~~



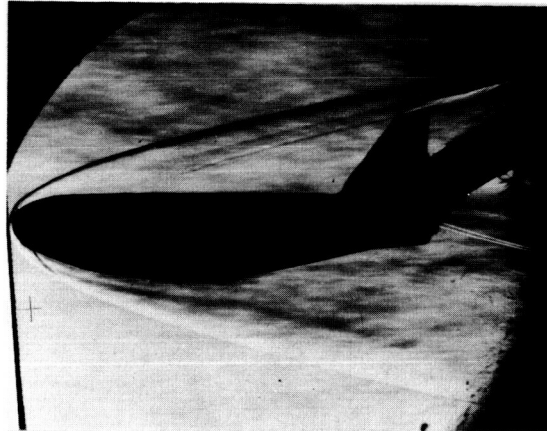
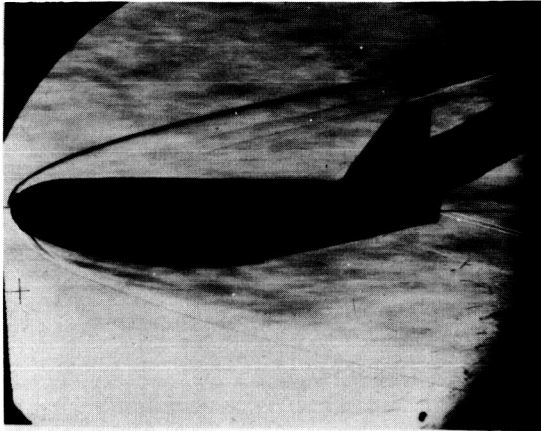
L-65-57

(a) $R_e = 2.70 \times 10^6$.

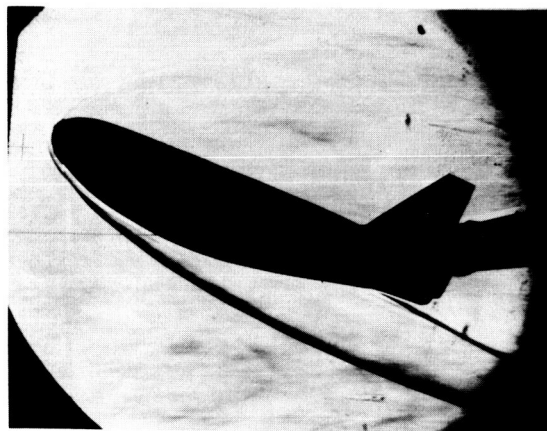
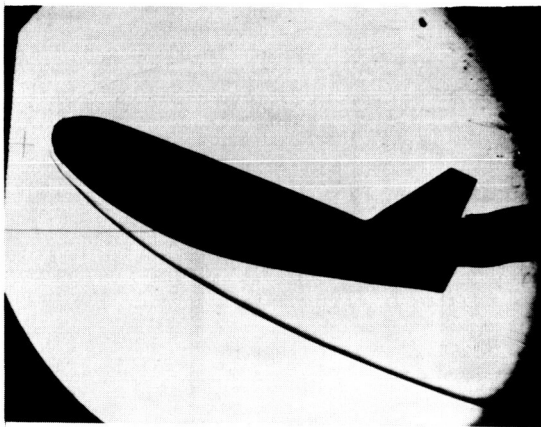
Figure 3.- Schlieren photographs of HL-10 with elevons deflected.

~~CONFIDENTIAL~~

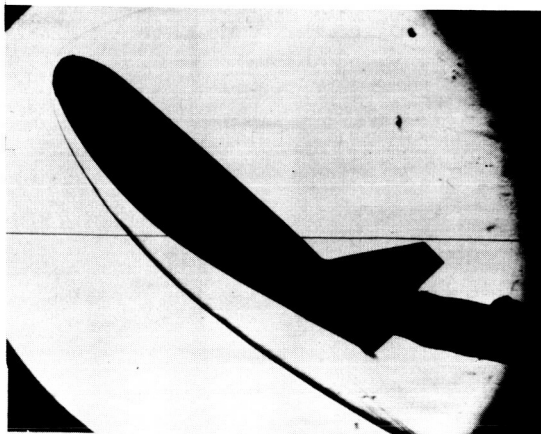
UNCLASSIFIED



$\alpha = 0^0$



$\alpha = 20^0$



No schlieren available.

$\alpha = 40^0$

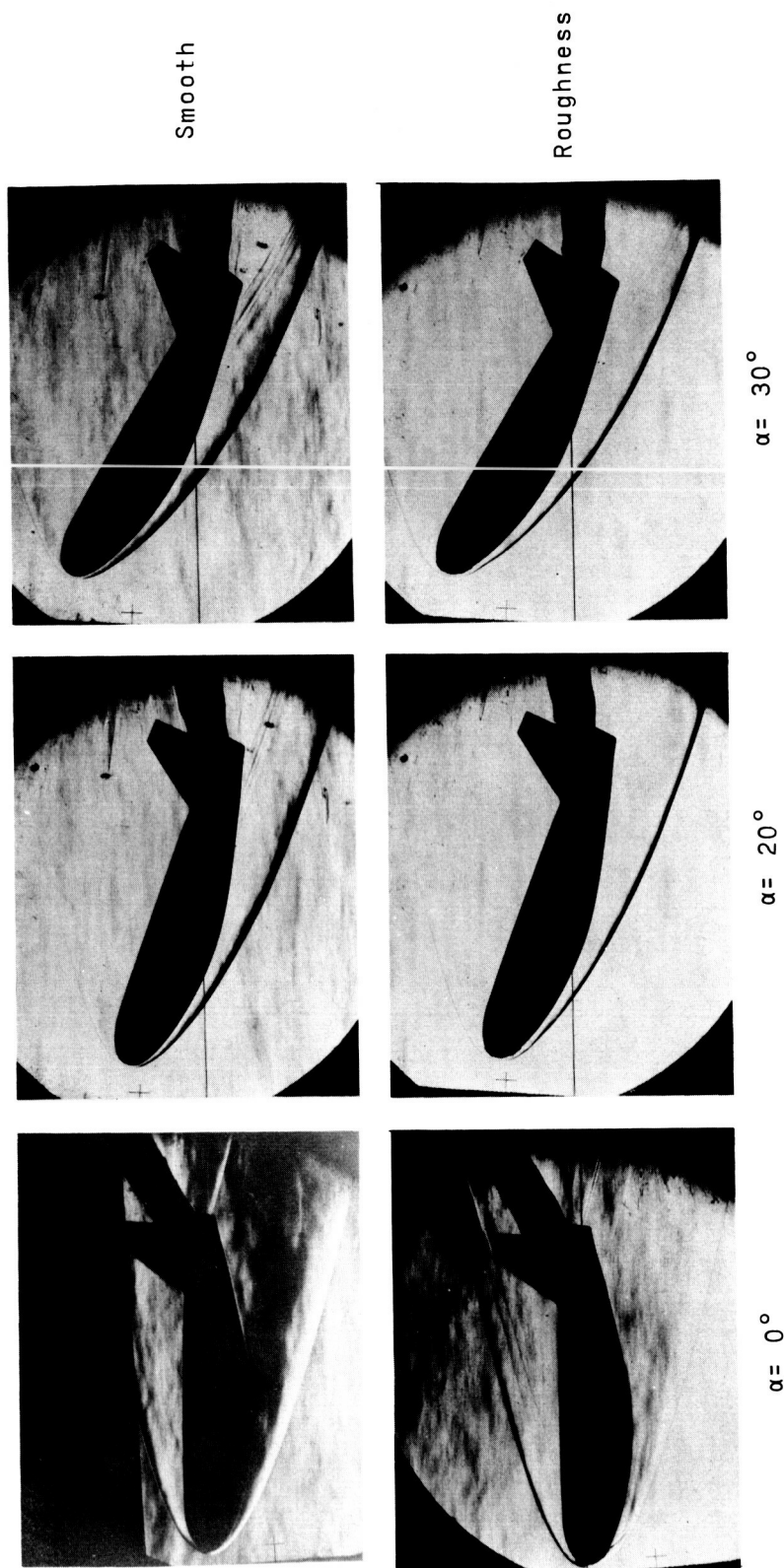
$\delta_e = 0^0$

$\delta_e = 15^0$

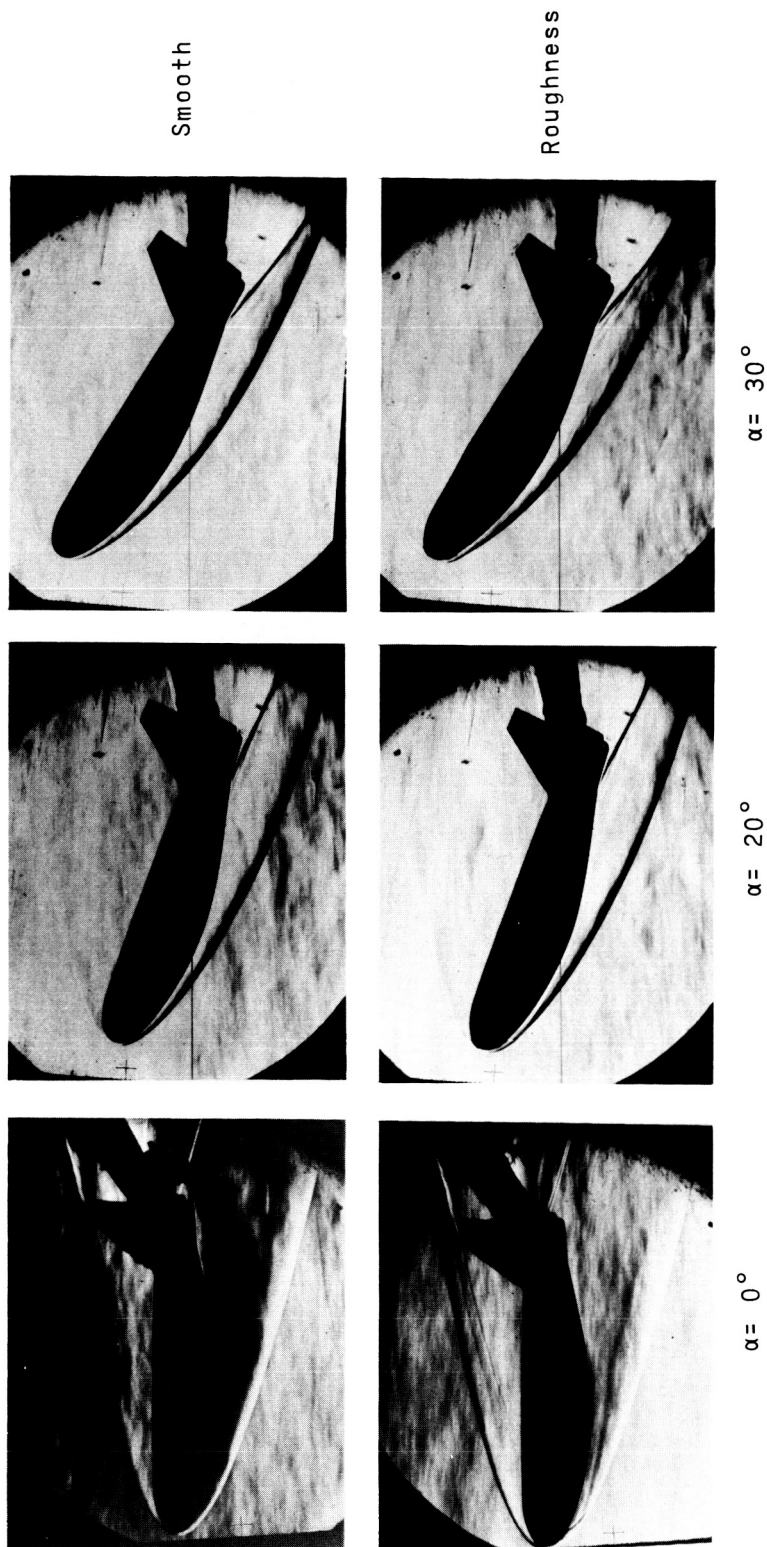
(b) $R_c = 6.58 \times 10^6$.

L-65-58

Figure 3.- Concluded.



(a) $\delta_e = 0^\circ$.
 L-65-59
 $R_e = 6.58 \times 10^6$.
 Figure 4.- Schlieren photographs of the HL-10 at angles of attack with and without roughness. $R_e = 6.58 \times 10^6$.



L-65-60

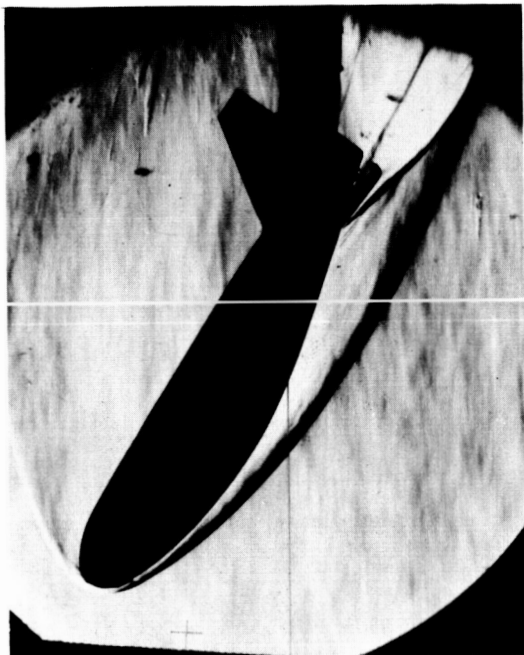
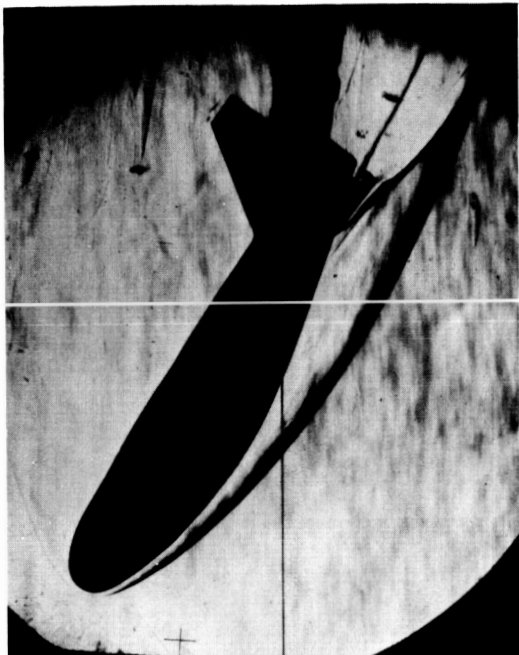
(b) $\delta_e = 15^\circ$.

Figure 4.- Continued.

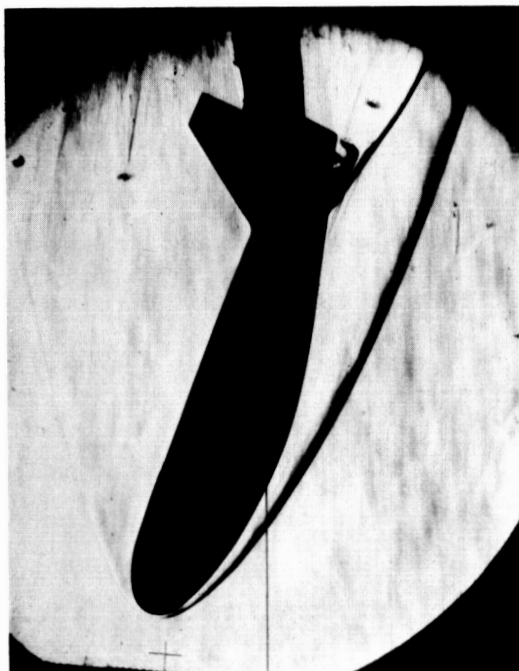
UNCLASSIFIED

Smooth

Roughness



$\alpha = 30^\circ$



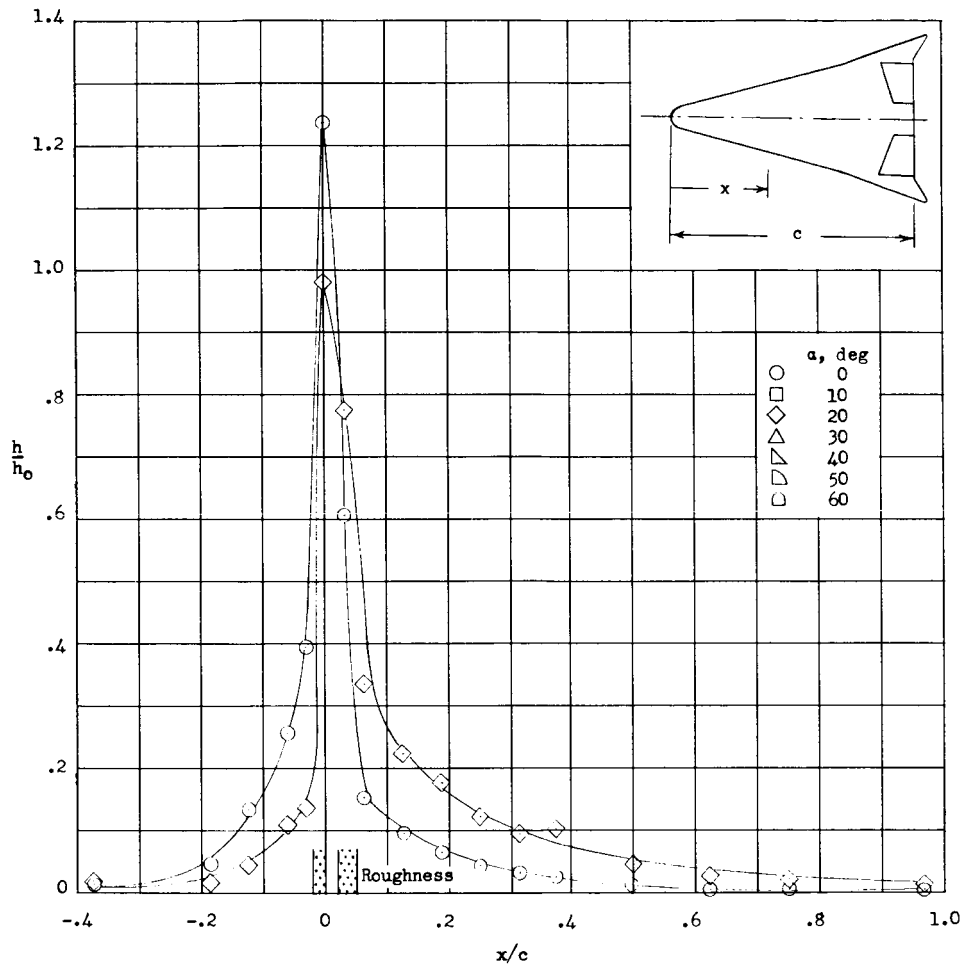
$\alpha = 20^\circ$

(c) $\delta_e = 30^\circ$.

Figure 4.- Concluded.

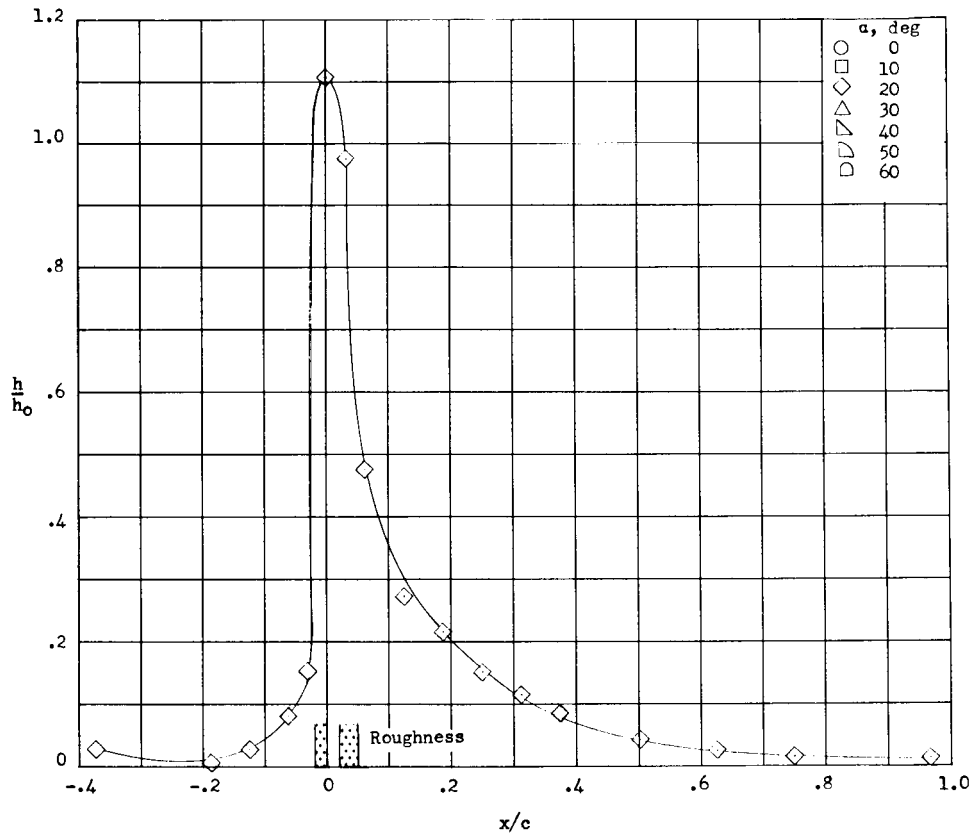
L-65-61

UNCLASSIFIED



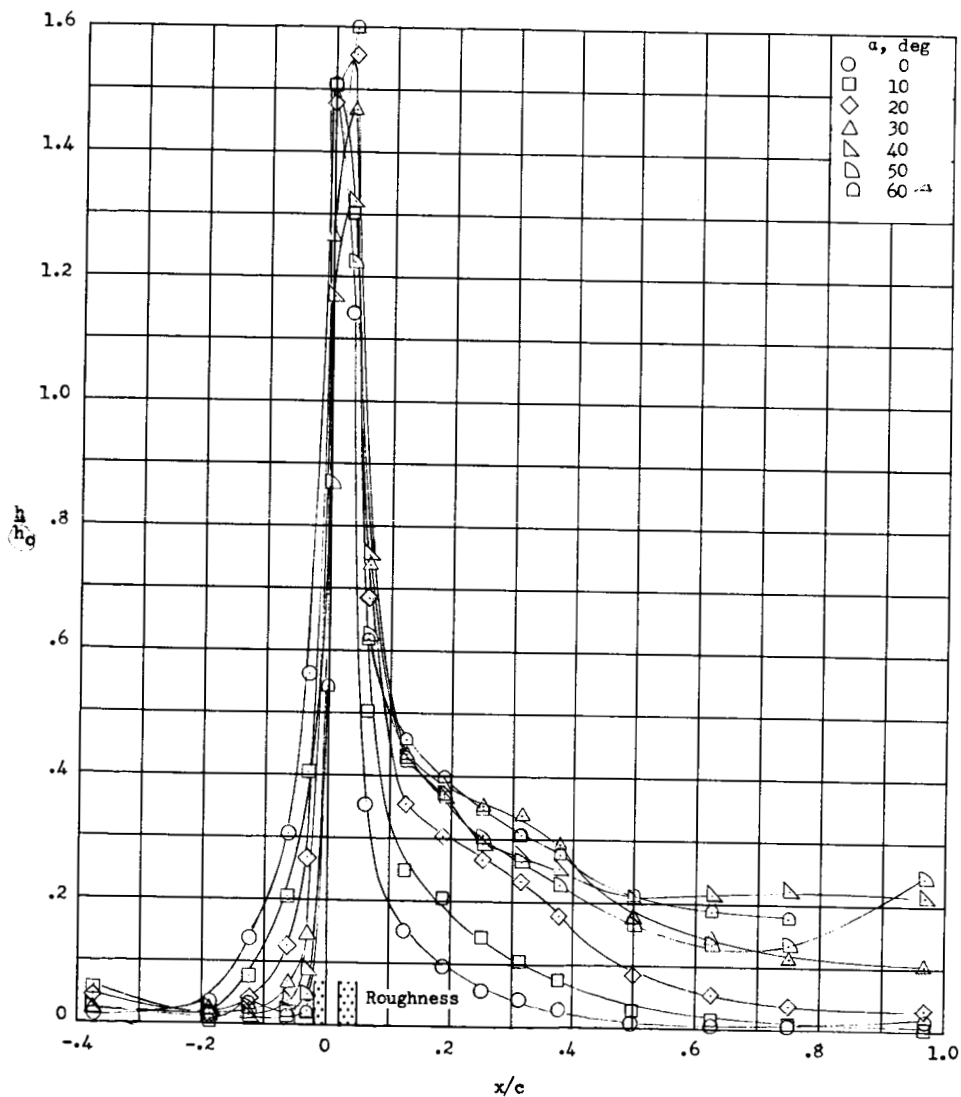
(a) $R_c = 0.24 \times 10^6$.

Figure 5.- Center line distributions of heat-transfer ratio on HL-10 with roughness at angle of attack. $\delta_e = 0^\circ$.



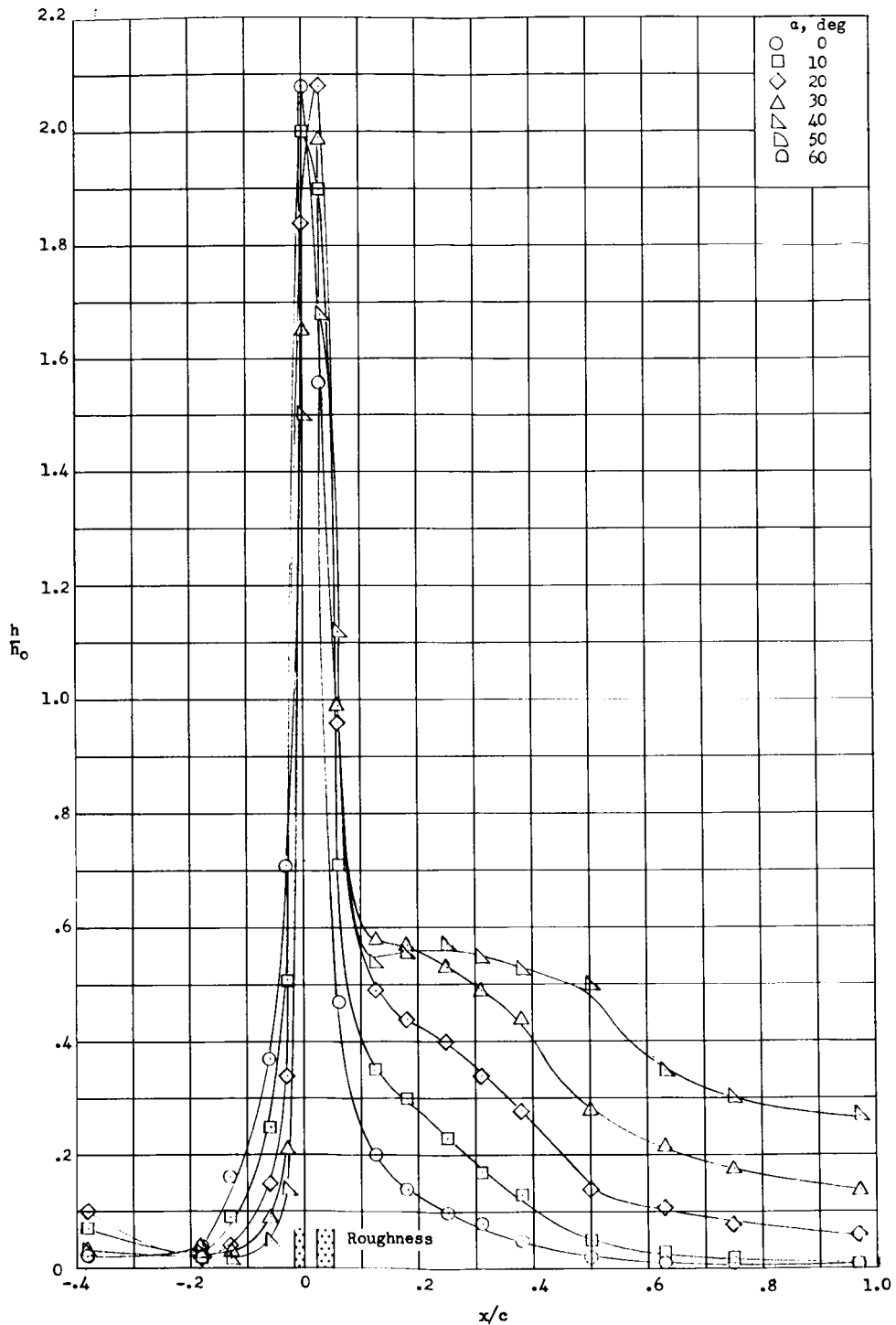
(b) $R_c = 0.77 \times 10^6$.

Figure 5.- Continued.



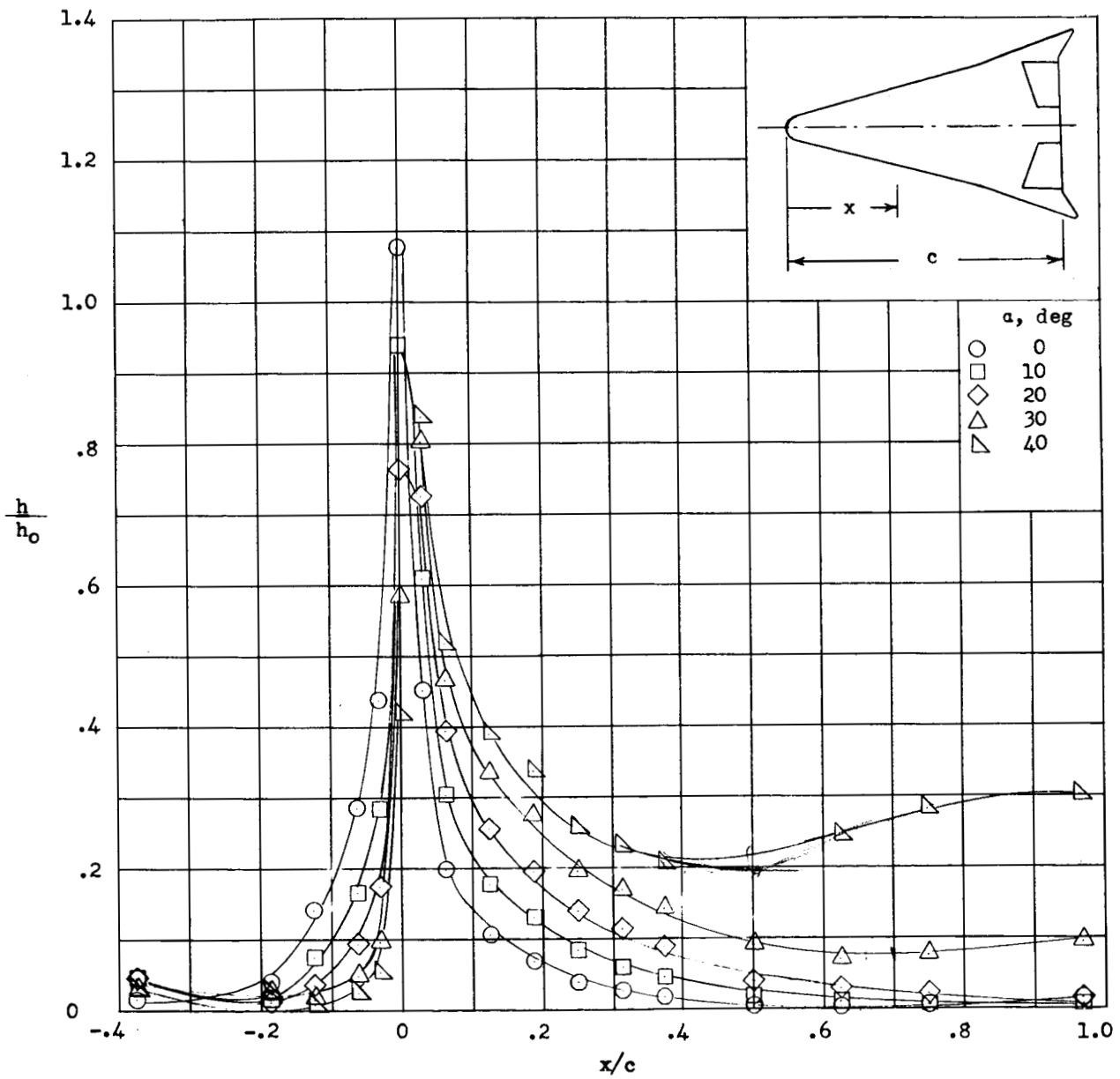
(c) $R_c = 2.70 \times 10^6$.

Figure 5.- Continued.



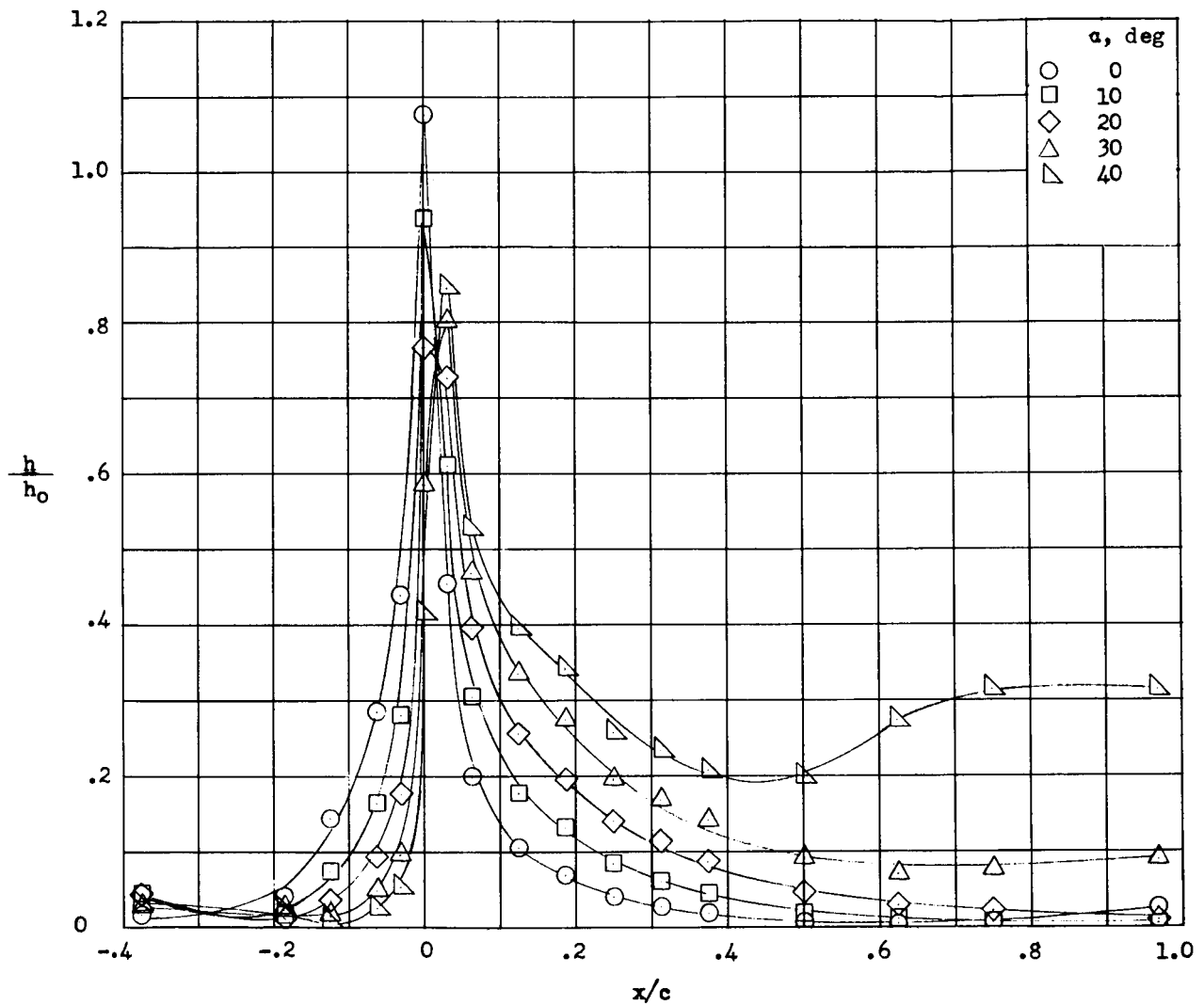
(d) $R_c = 6.58 \times 10^6$.

Figure 5.- Concluded.



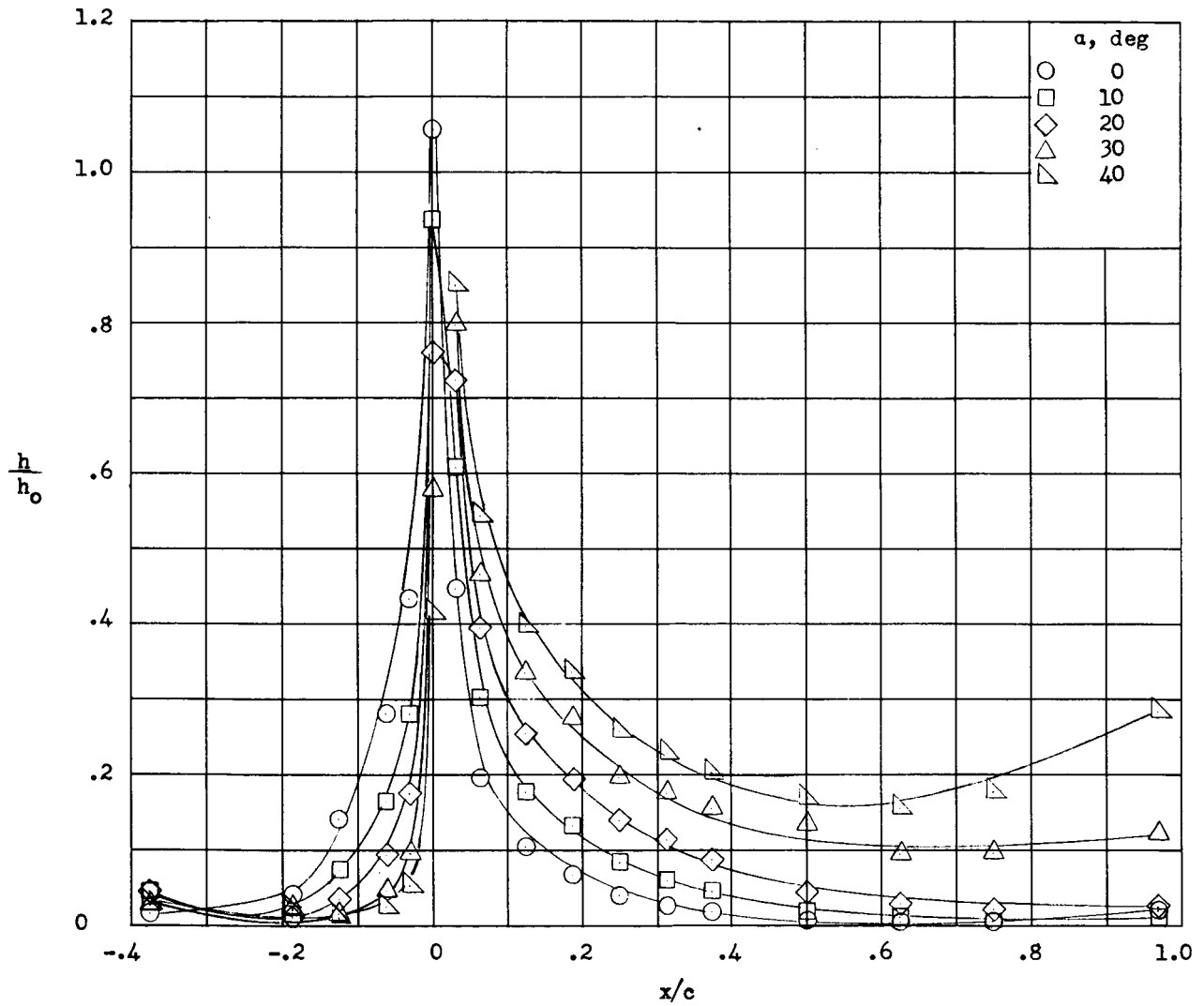
(a) $\delta_e = 0^\circ$.

Figure 6.- Variation of heat-transfer ratio on HL-10 without roughness at angle of attack.
 $R_c = 6.58 \times 10^6$.



(b) $\delta_e = 15^\circ$.

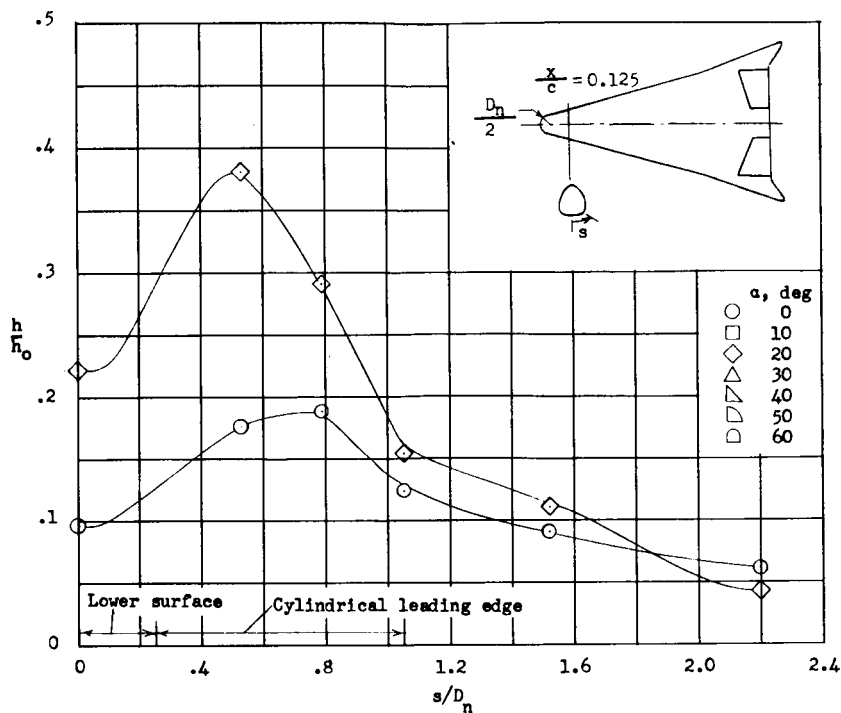
Figure 6.- Continued.



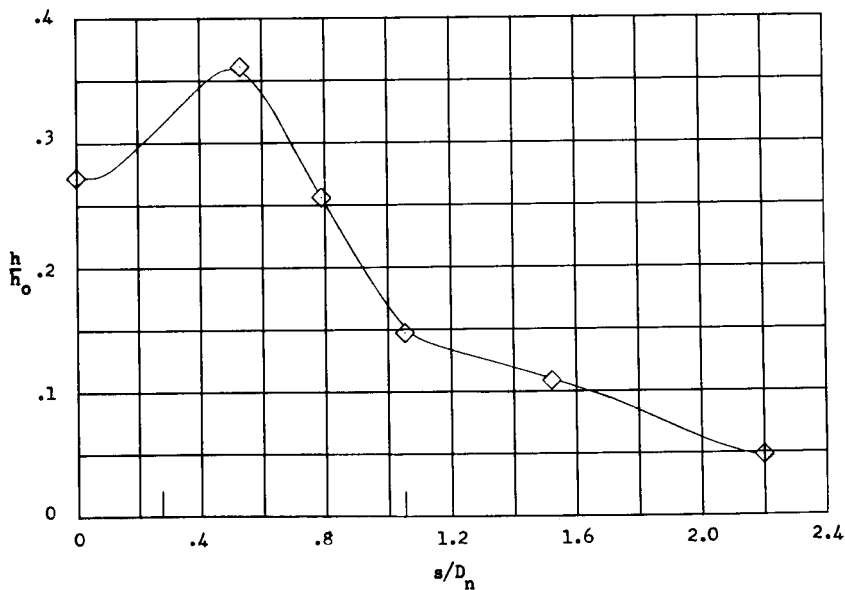
(c) $\delta_e = 30^\circ$.

Figure 6.- Concluded.

UNCLASSIFIED



(a) $R_c = 0.24 \times 10^6$.

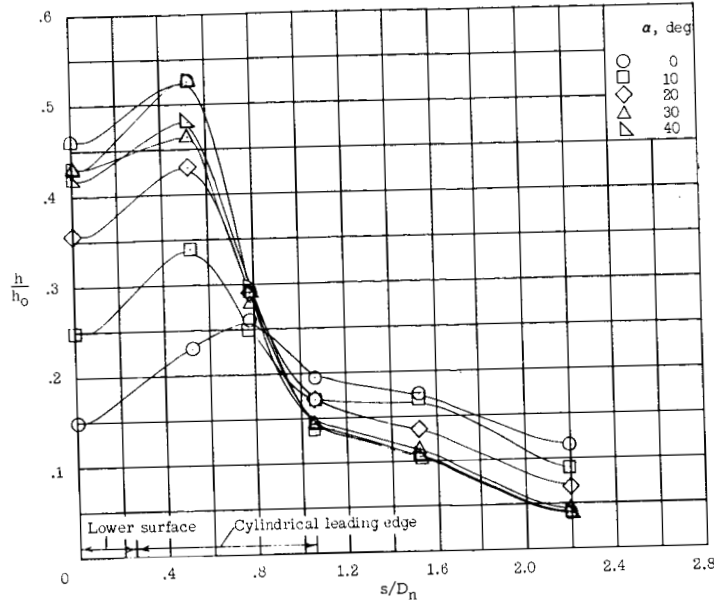


(b) $R_c = 0.77 \times 10^6$.

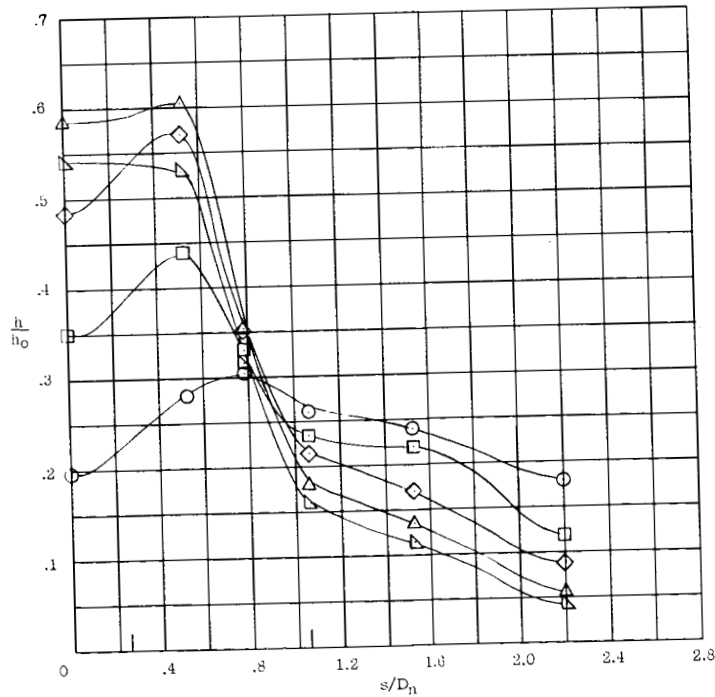
Figure 7.- Spanwise distributions of heat-transfer ratio on HL-10 with roughness at angle of attack at station $x/c = 0.125$. $\delta_e = 0^\circ$.

UNCLASSIFIED

UNCLASSIFIED



(c) $Re = 2.70 \times 10^6$.

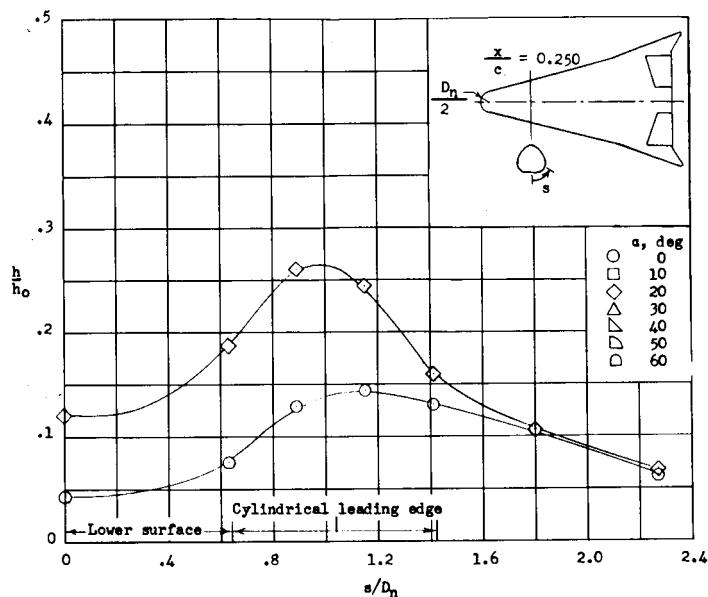


(d) $Re = 6.58 \times 10^6$.

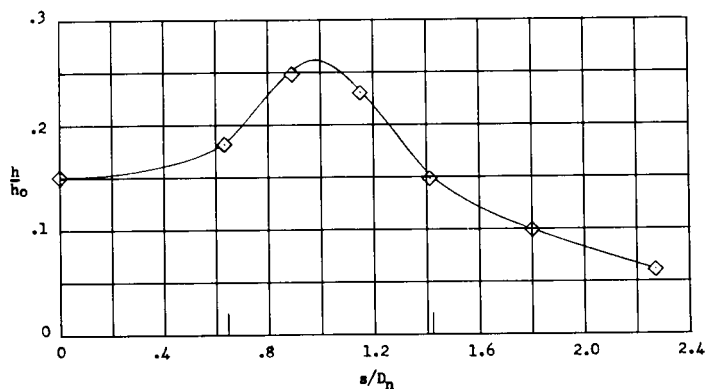
Figure 7.- Concluded.

UNCLASSIFIED

UNCLASSIFIED



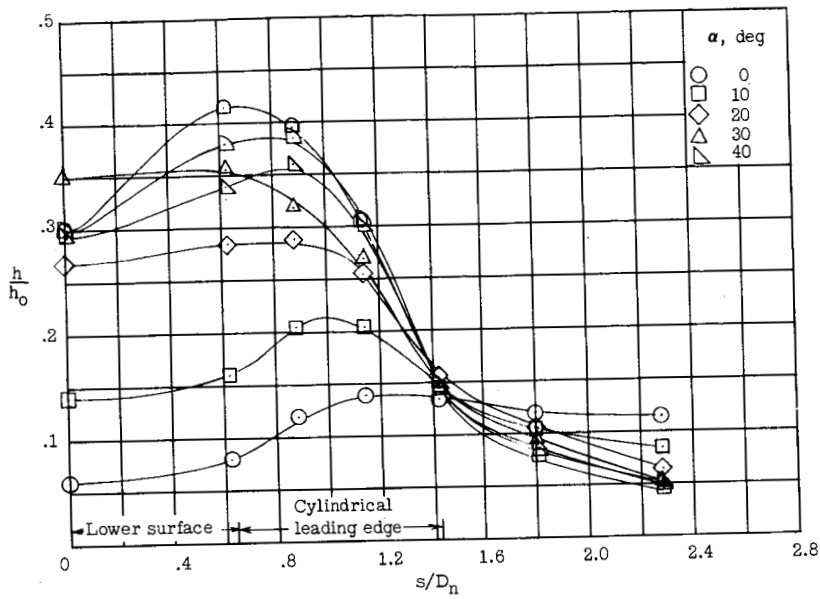
(a) $R_c = 0.24 \times 10^6$.



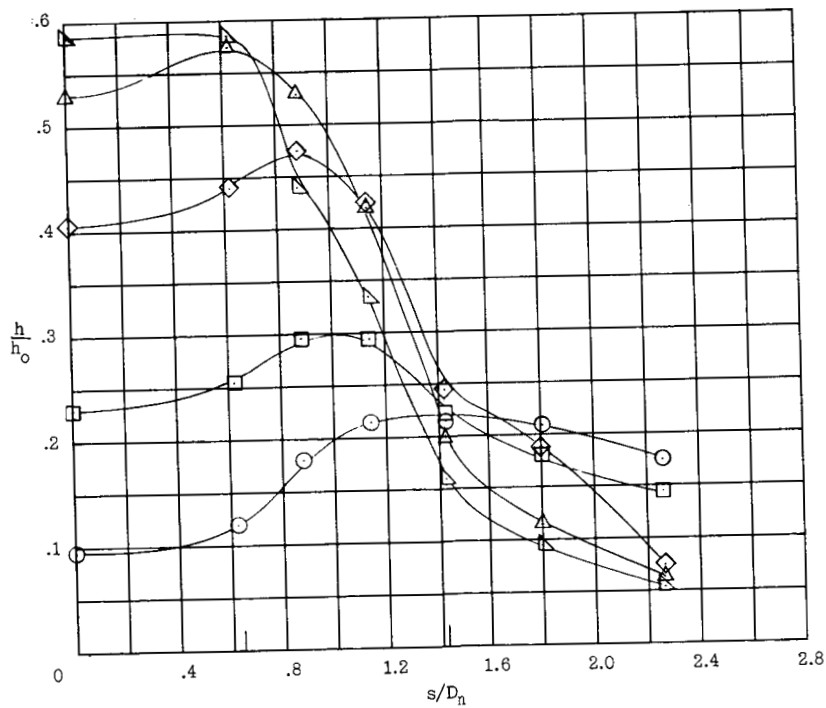
(b) $R_c = 0.77 \times 10^6$.

Figure 8.- Spanwise distribution of heat-transfer ratio on HL-10 with roughness at angle of attack at station $x/c = 0.250$. $\delta_e = 0^\circ$.

UNCLASSIFIED



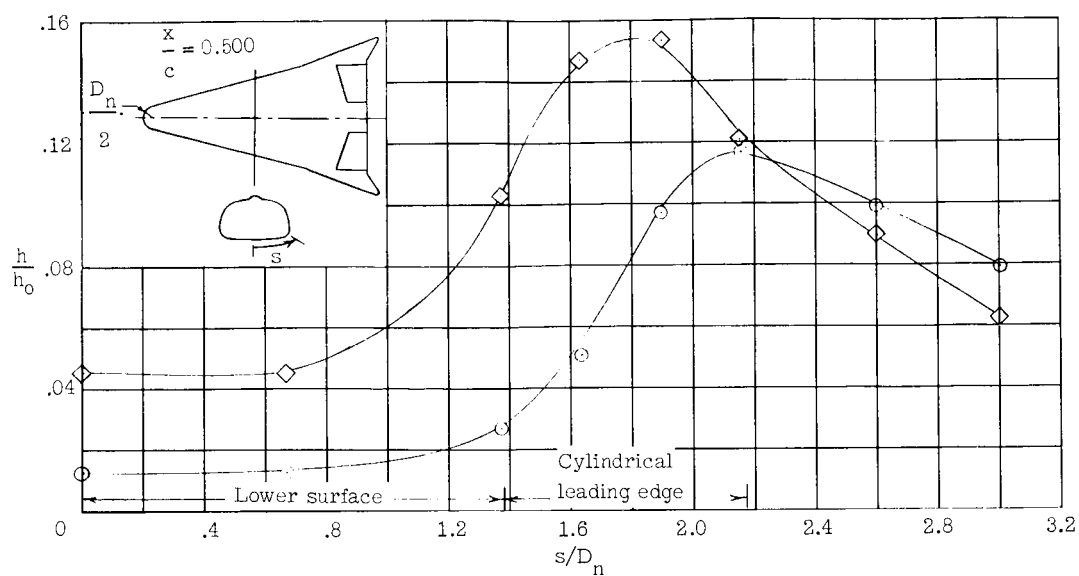
(c) $Re = 2.70 \times 10^6$.



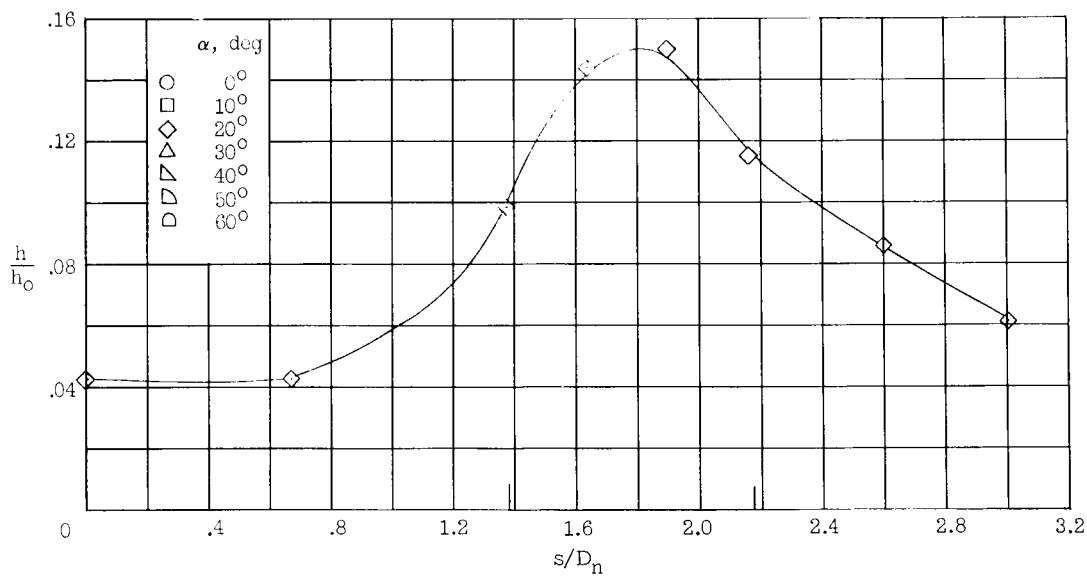
(d) $Re = 6.58 \times 10^6$.

Figure 8.- Concluded.

UNCLASSIFIED



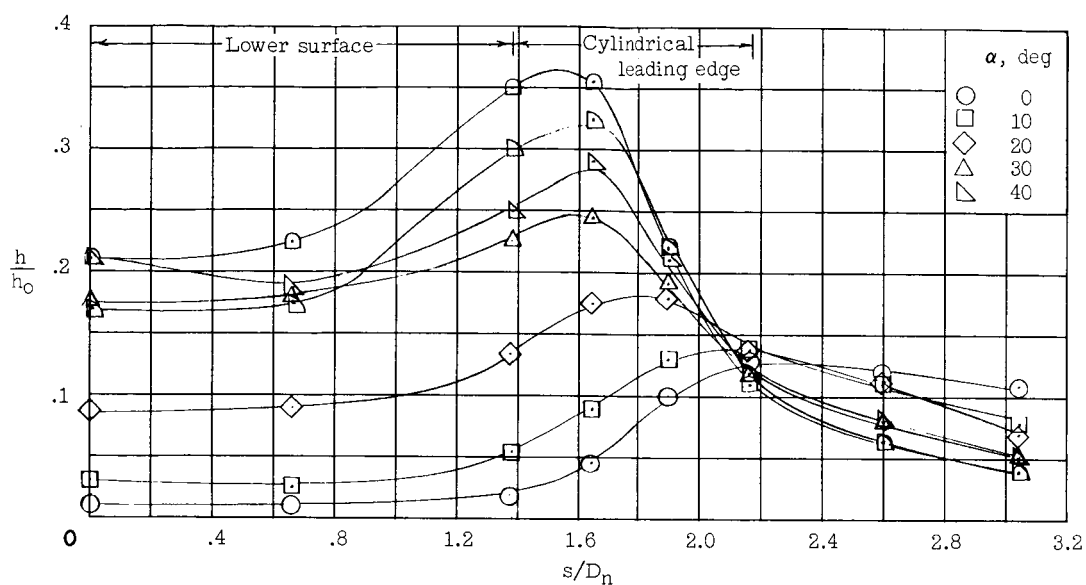
(a) $R_c = 0.24 \times 10^6$.



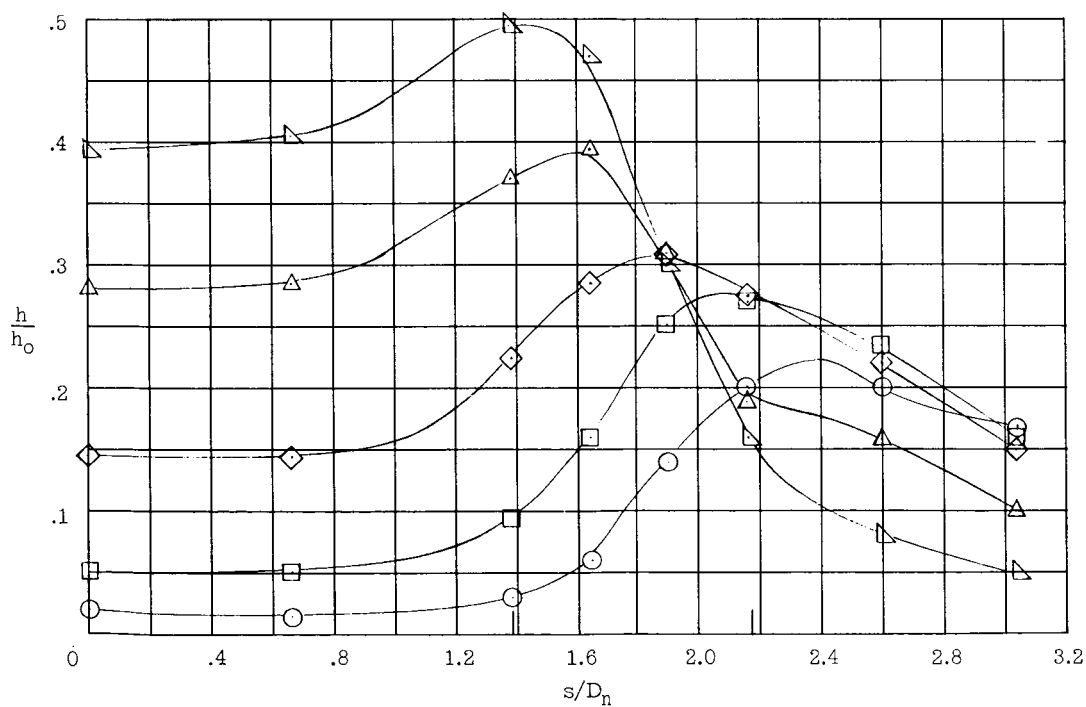
(b) $R_c = 0.77 \times 10^6$.

Figure 9.- Spanwise distributions of heat-transfer ratio on HL-10 with roughness at angle of attack at station $x/c = 0.500$. $\delta_e = 0^\circ$.

UNCLASSIFIED



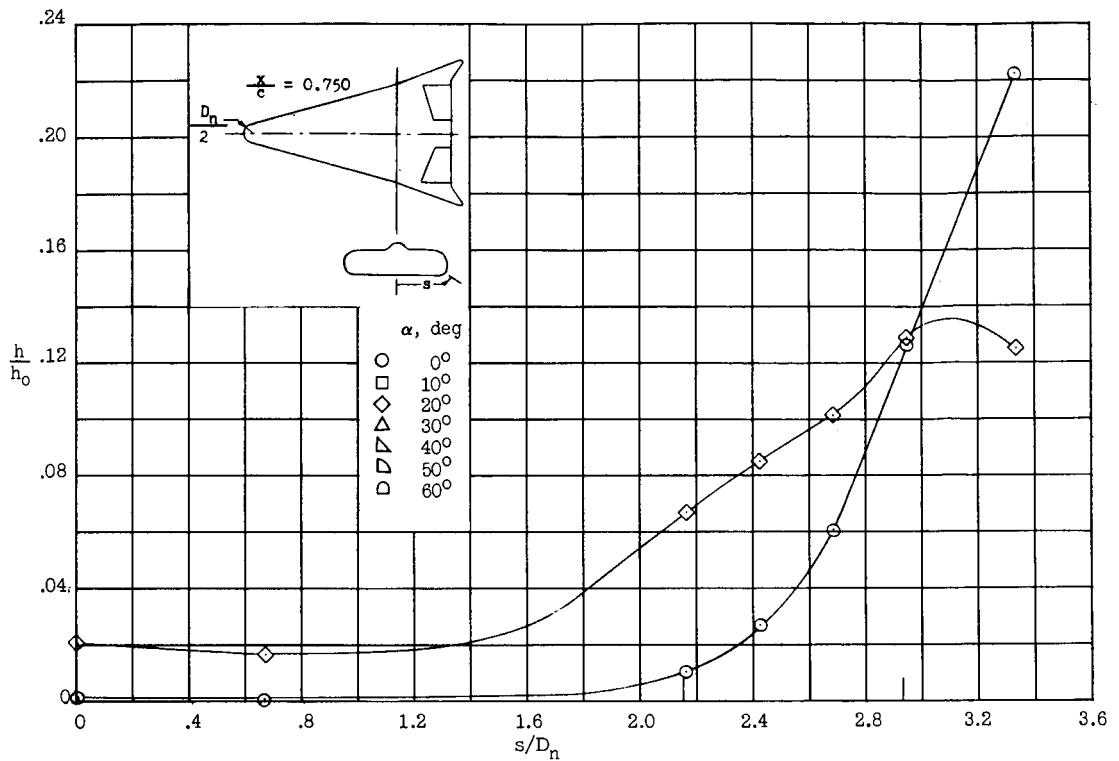
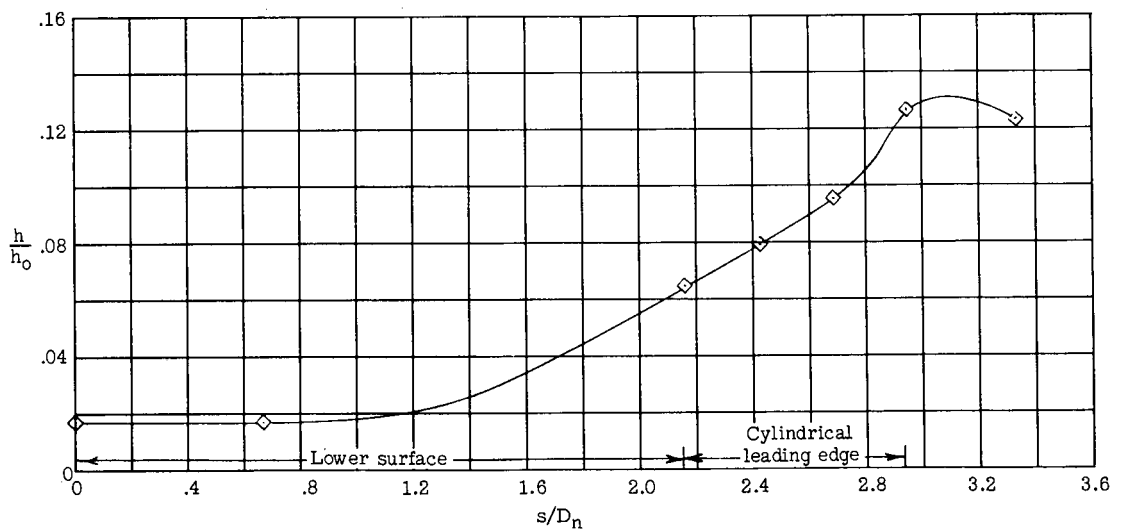
(c) $R_c = 2.70 \times 10^6$.

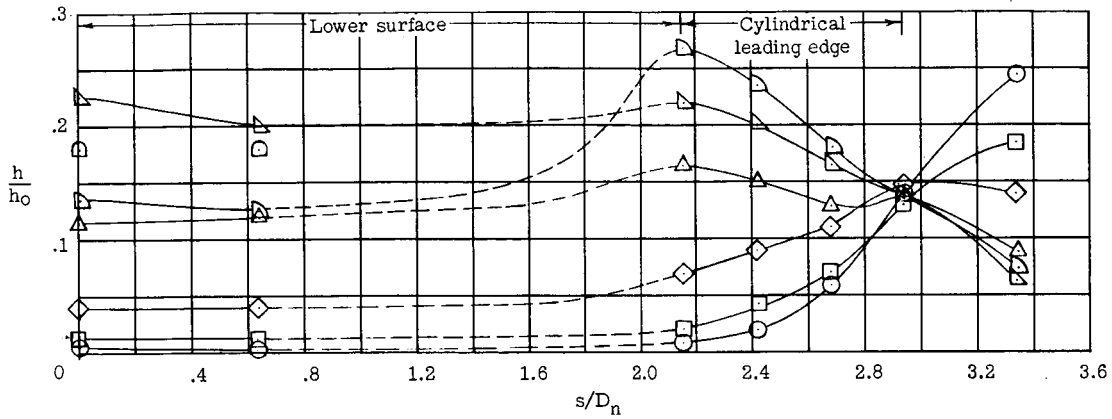


(d) $R_c = 6.58 \times 10^6$.

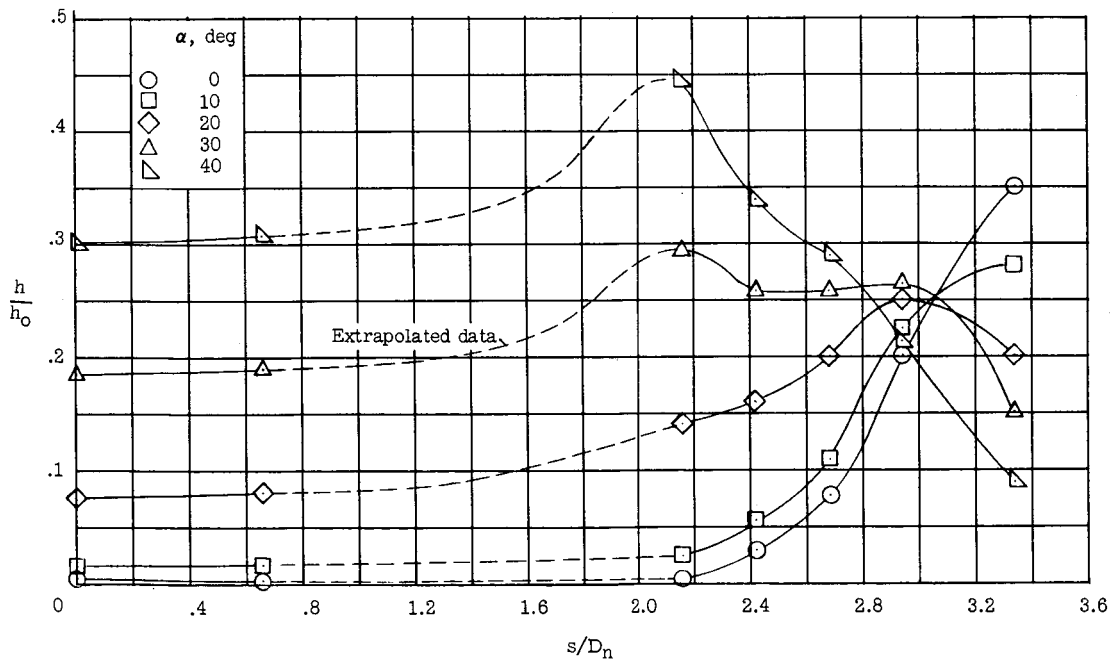
Figure 9.- Concluded.

UNCLASSIFIED

(a) $R_c = 0.24 \times 10^6$.(b) $R_c = 0.77 \times 10^6$.Figure 10.- Spanwise distributions of heat-transfer ratio on HL-10 with roughness at angle of attack at station $x/c = 0.750$. $\delta_e = 0^\circ$.

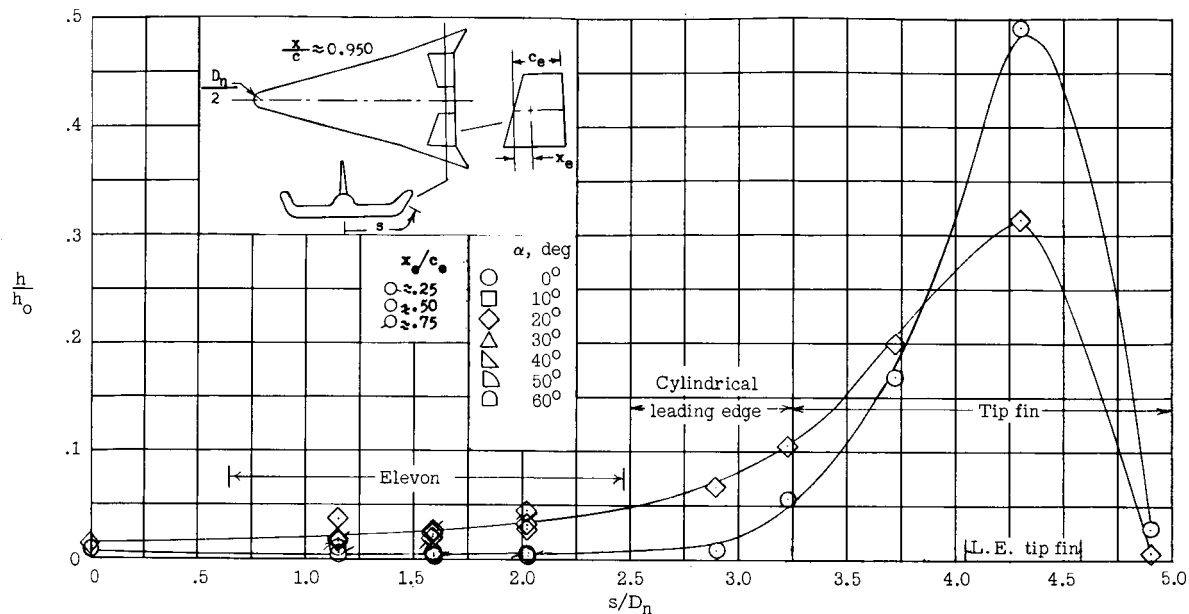


(c) $R_c = 2.70 \times 10^6$.

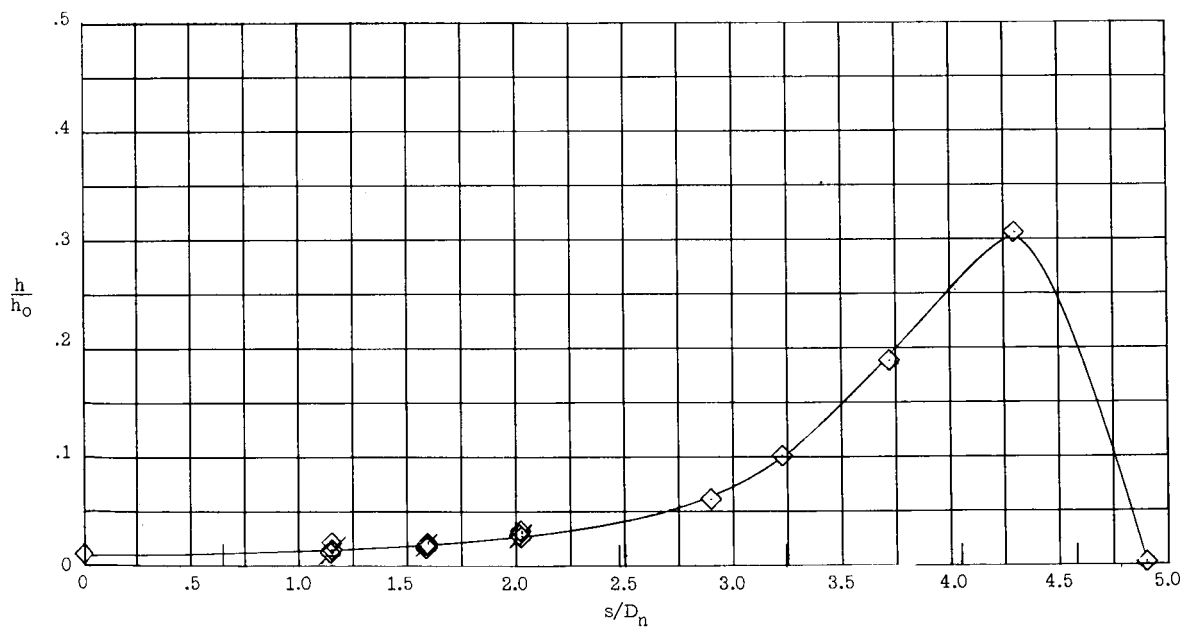


(d) $R_c = 6.58 \times 10^6$.

Figure 10.- Concluded.

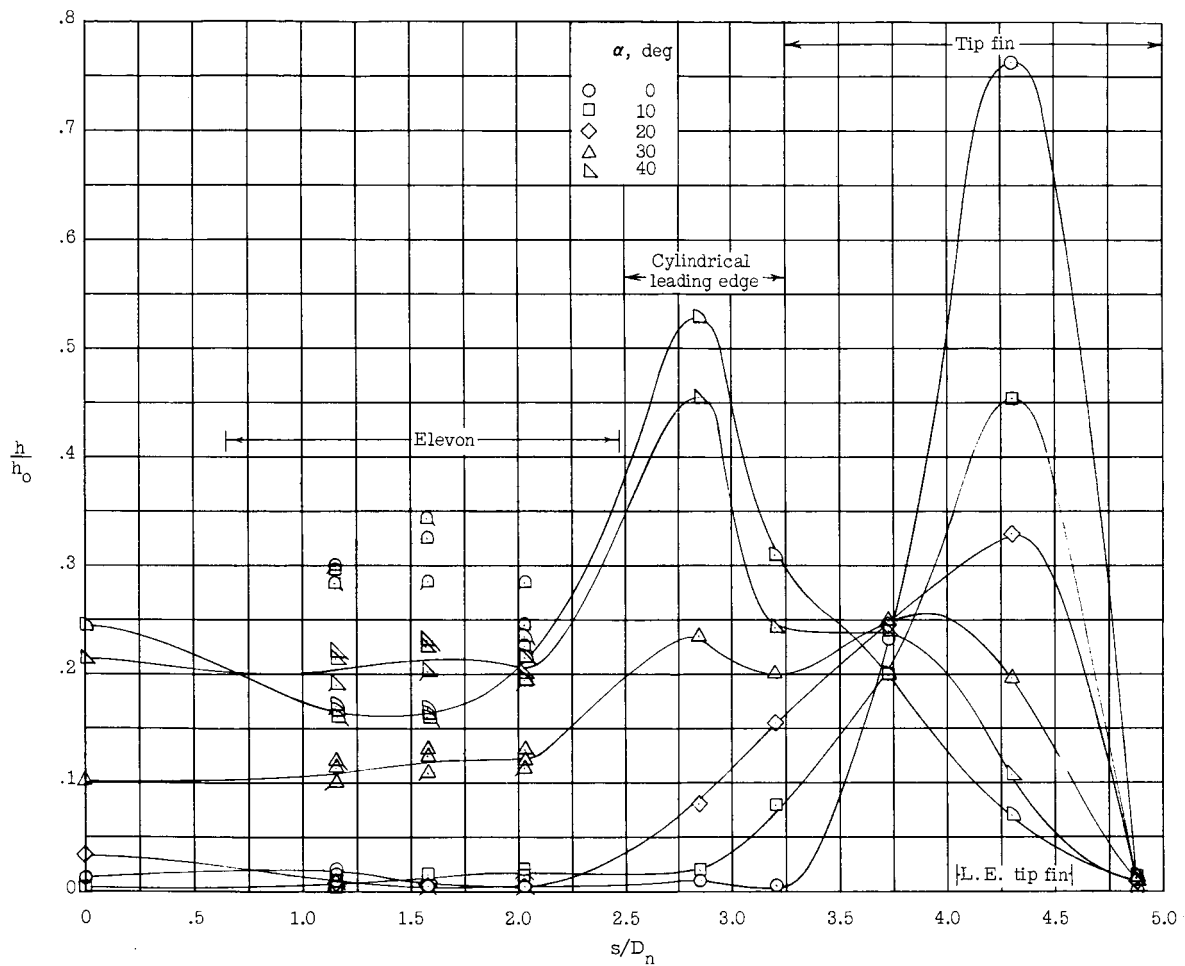


(a) $R_c = 0.24 \times 10^6$.



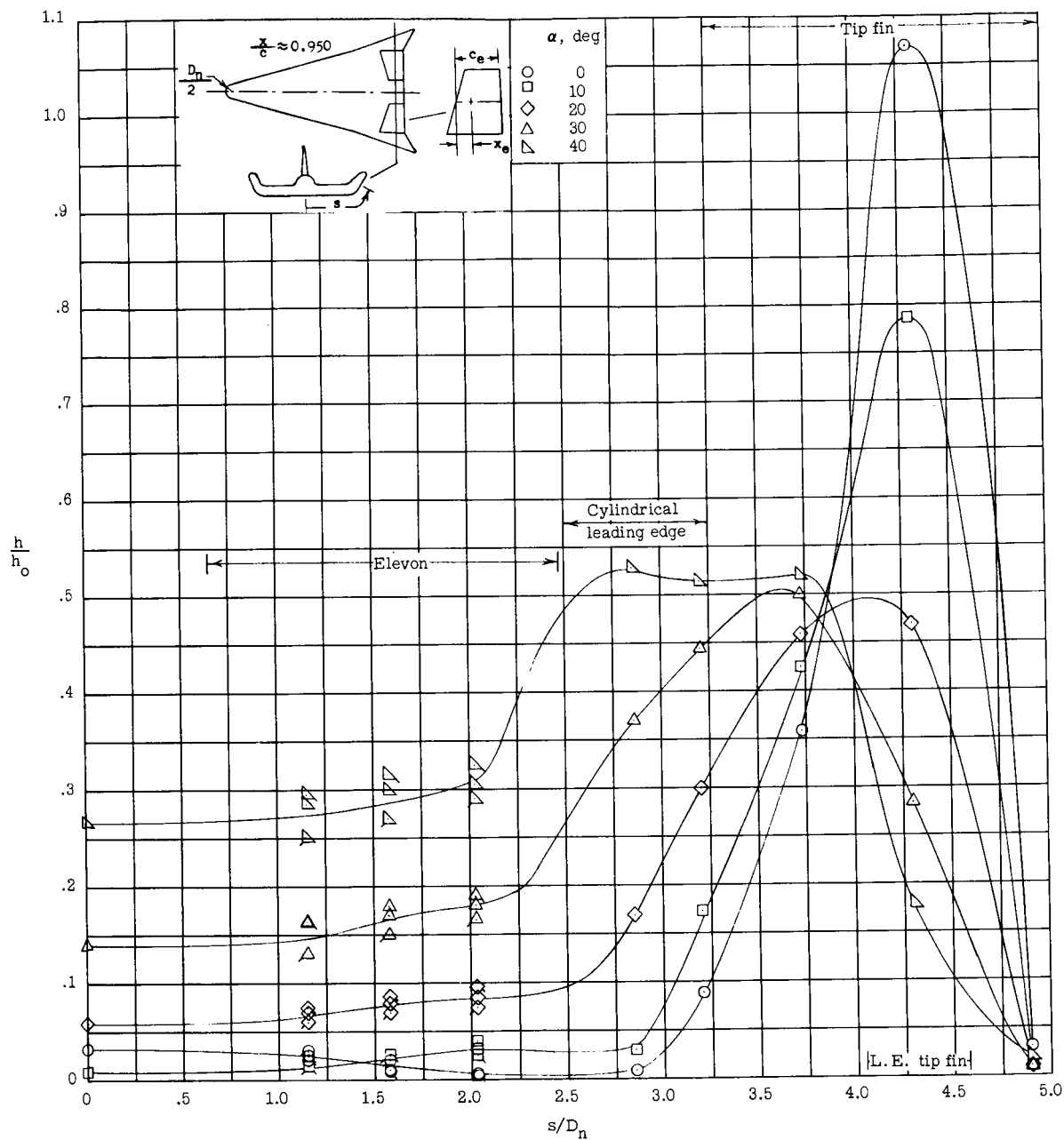
(b) $R_c = 0.77 \times 10^6$.

Figure 11.- Spanwise distributions of heat-transfer ratio on HL-10 with roughness at angle of attack at station $x/c \approx 0.950$. $\delta_e = 0^\circ$.



(c) $R_c = 2.70 \times 10^6$.

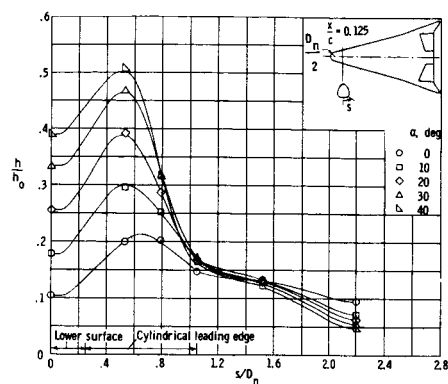
Figure 11.- Continued.



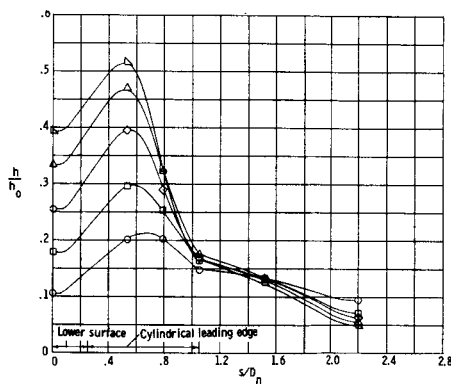
(d) $R_c = 6.58 \times 10^6$.

Figure 11.- Concluded.

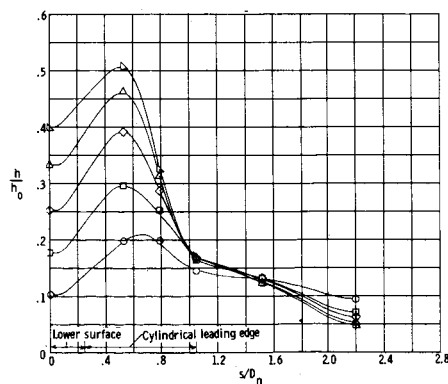
UNCLASSIFIED



(a) $\delta_e = 0^\circ$.



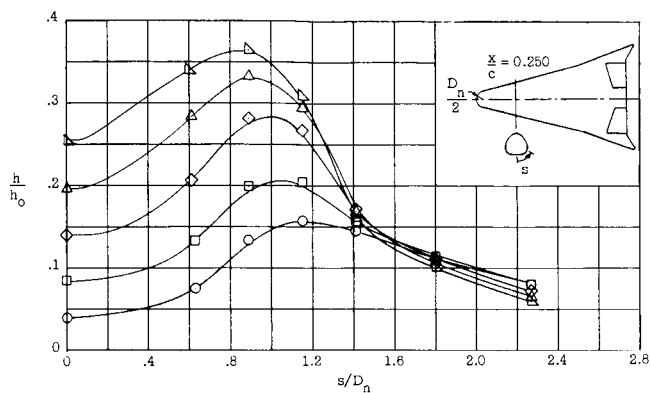
(b) $\delta_e = 15^\circ$.



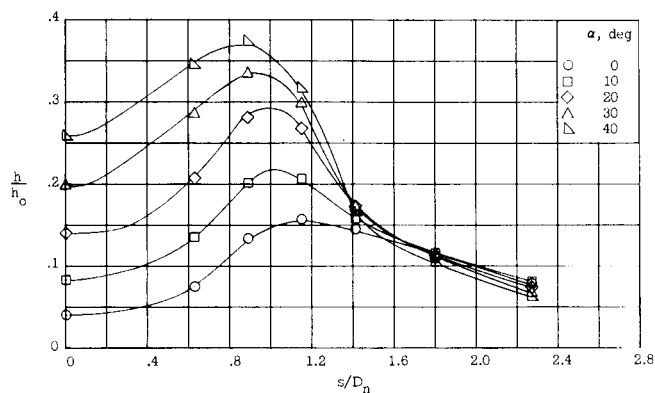
(c) $\delta_e = 30^\circ$.

Figure 12.- Spanwise distribution of heat-transfer ratio on HL-10 without roughness at station $x/c = 0.125$. $R_c = 6.58 \times 10^6$.

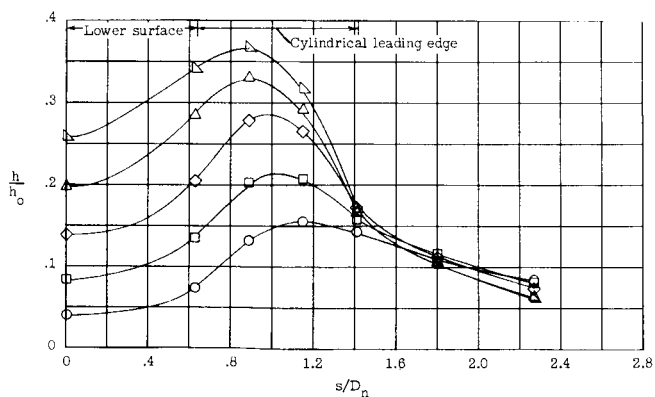
UNCLASSIFIED



(a) $\delta_e = 0^\circ$.



(b) $\delta_e = 15^\circ$.

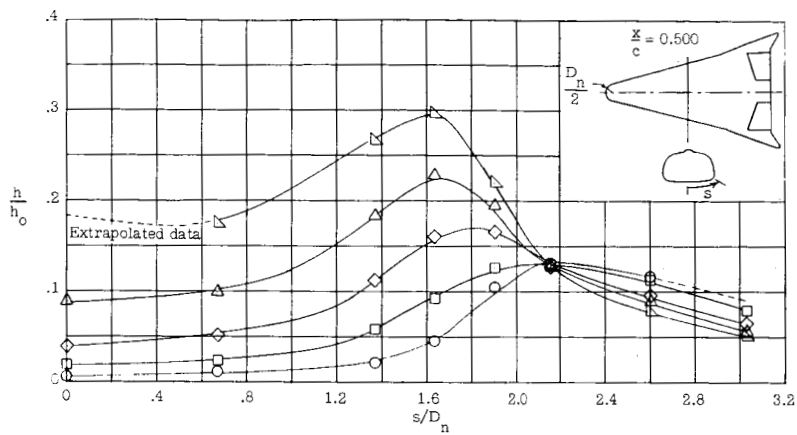


(c) $\delta_e = 30^\circ$.

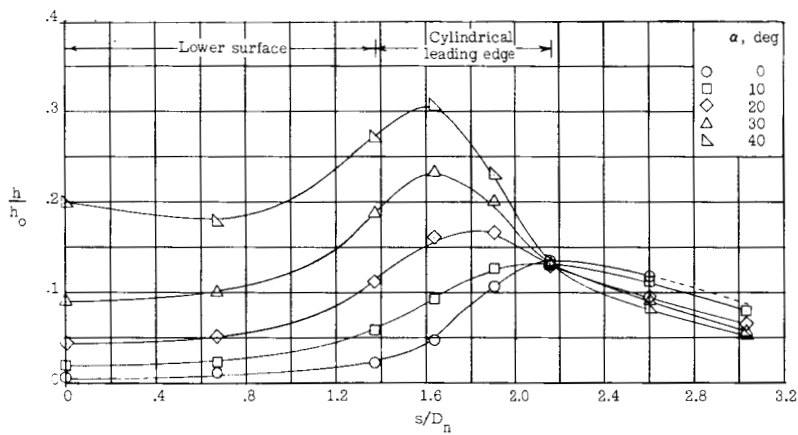
Figure 13.- Spanwise distribution of heat-transfer ratio on HL-10 without roughness at station $x/c = 0.250$. $R_c = 6.58 \times 10^6$.

UNCLASSIFIED

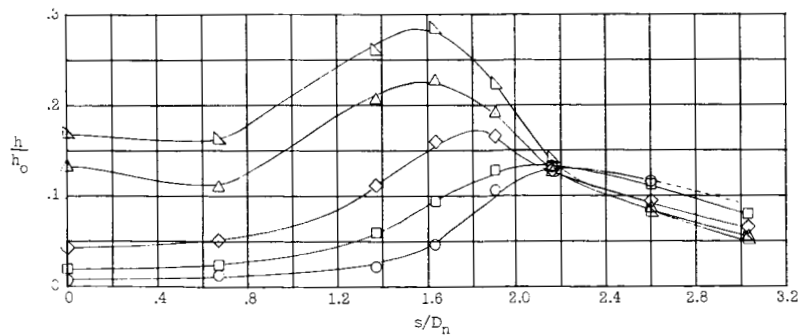
~~CONFIDENTIAL~~



(a) $\delta_e = 0^\circ$.



(b) $\delta_e = 15^\circ$.



(c) $\delta_e = 30^\circ$.

Figure 14.- Spanwise distribution of heat-transfer ratio on HL-10 without roughness at station $x/c = 0.500$. $R_c = 6.58 \times 10^6$.

~~CONFIDENTIAL~~

UNCLASSIFIED

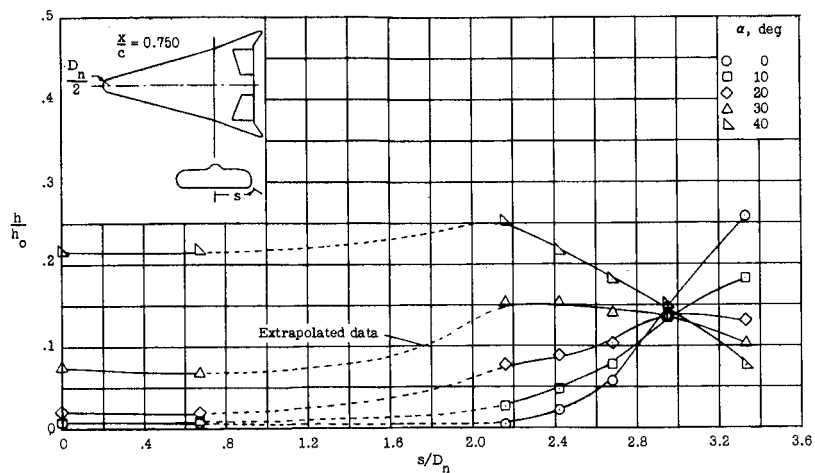
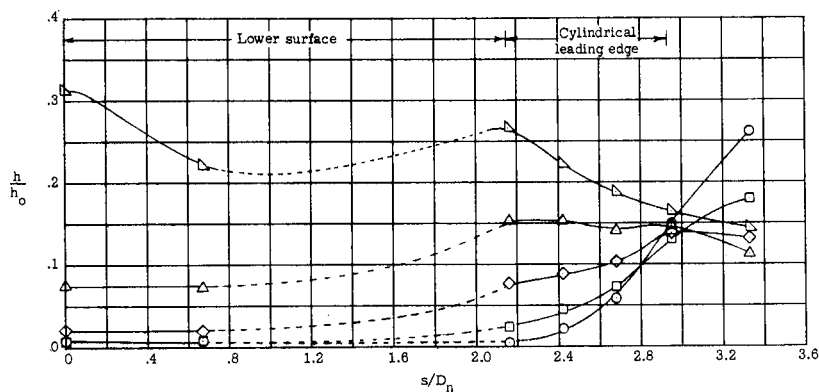
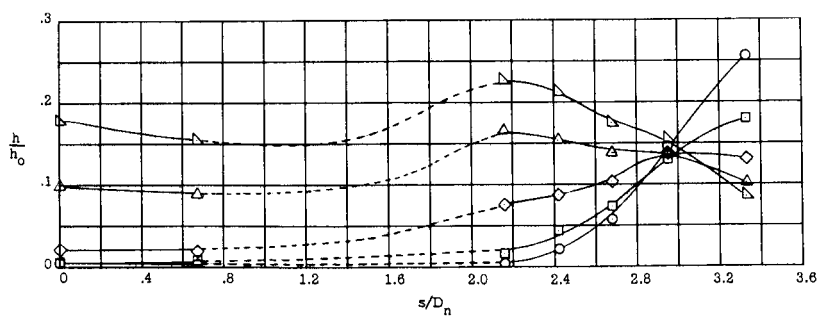
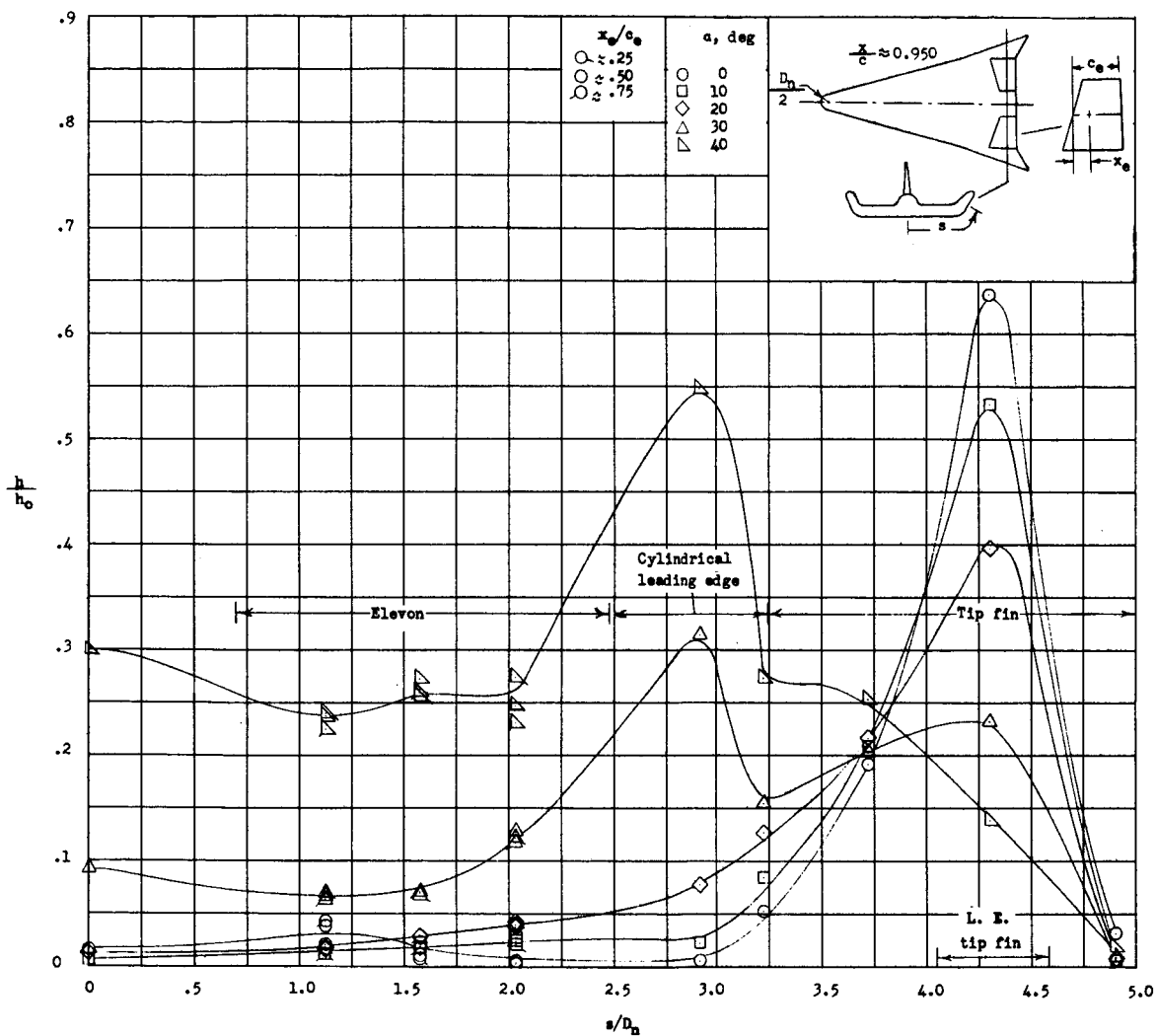
(a) $\delta_e = 0^\circ$.(b) $\delta_e = 15^\circ$.(c) $\delta_e = 30^\circ$.

Figure 15.- Spanwise distribution of heat-transfer ratio on HL-10 without roughness at station $x/c = 0.750$. $R_c = 6.58 \times 10^6$.

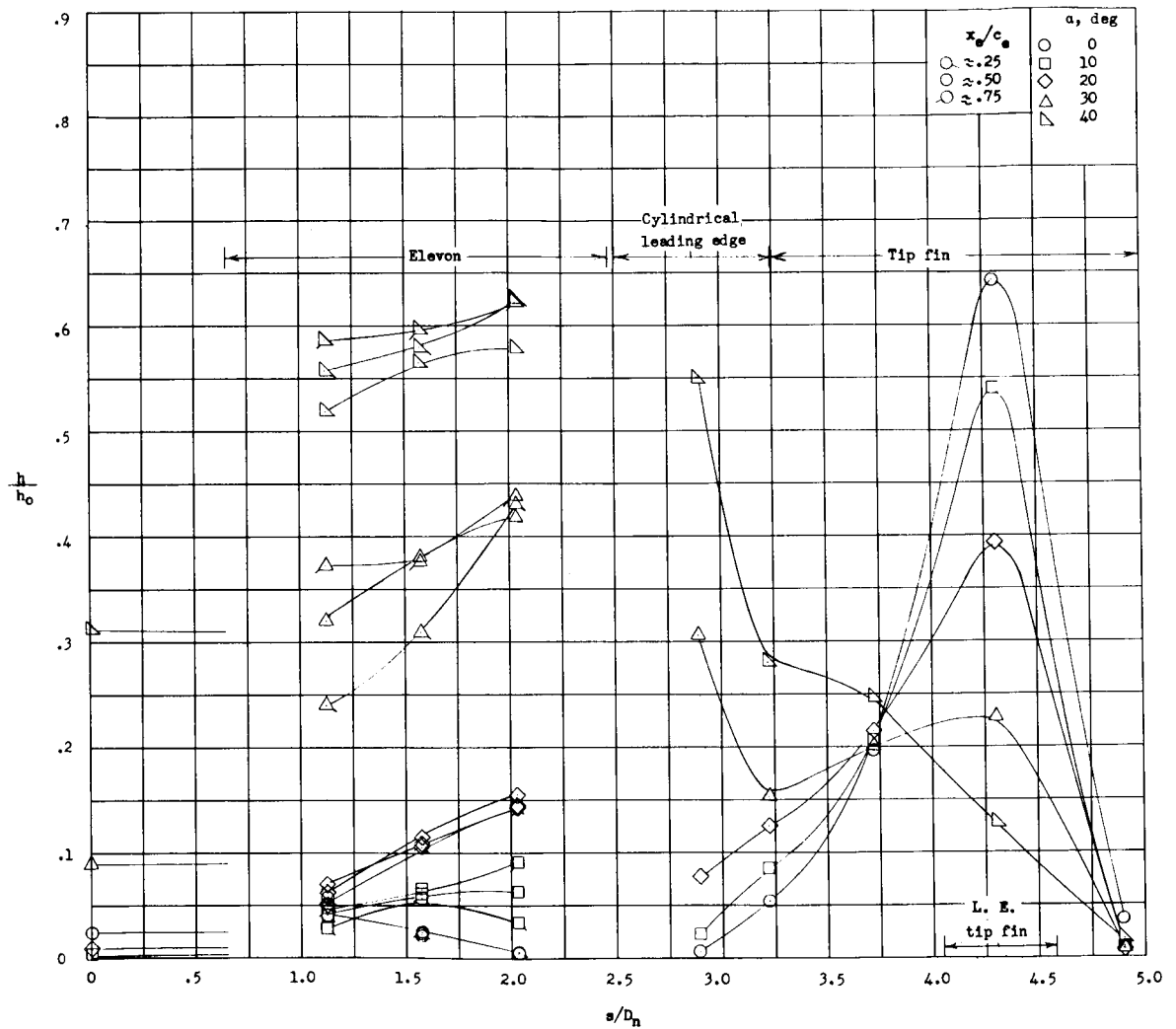
~~CONFIDENTIAL~~
UNCLASSIFIED



(a) $\delta_e = 0^\circ$.

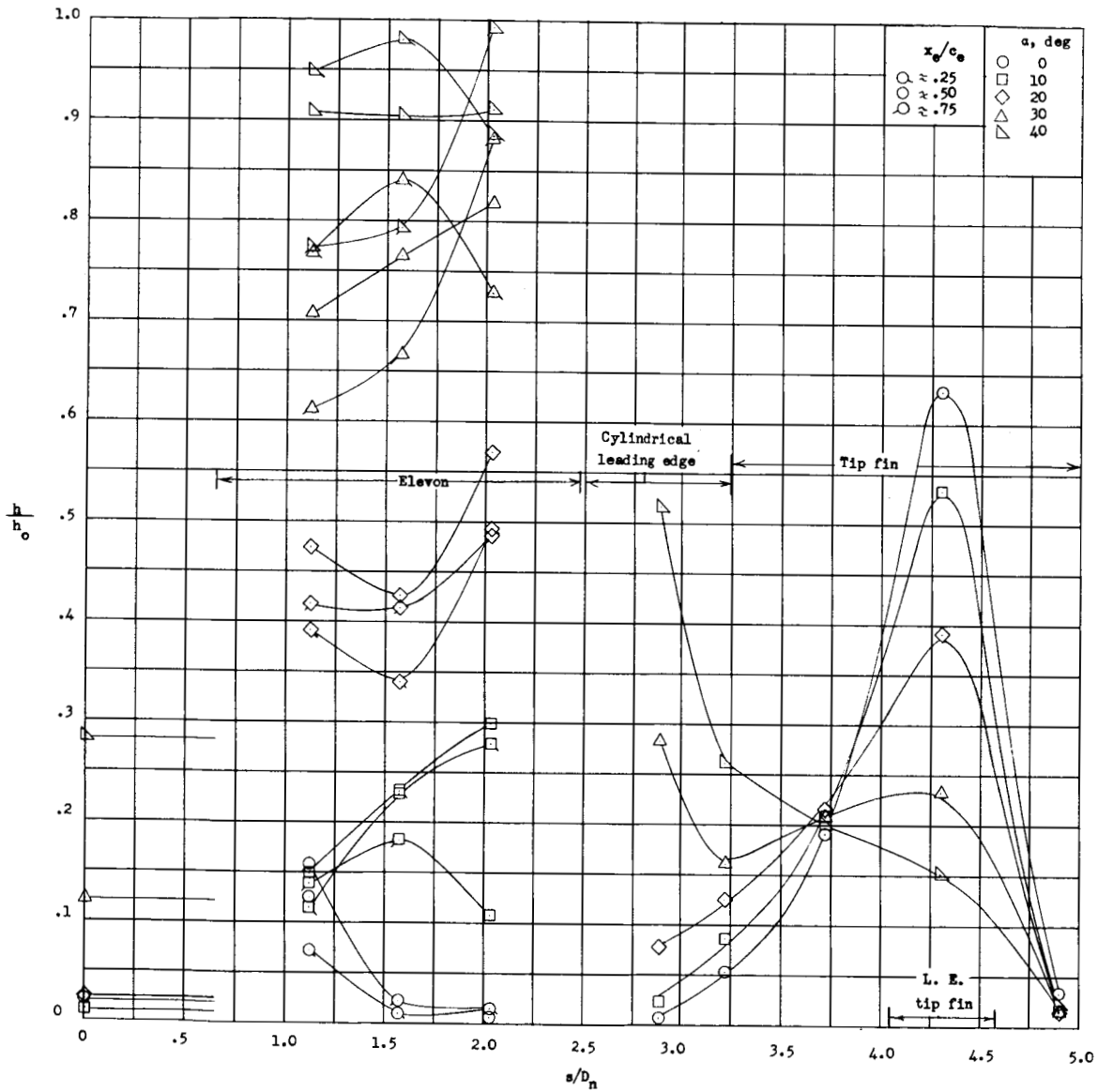
Figure 16.- Spanwise distribution of heat-transfer ratio on HL-10 without roughness at station $x/c \approx 0.950$. $Re = 6.58 \times 10^6$.

~~CONFIDENTIAL~~
UNCLASSIFIED



(b) $\delta_e = 15^\circ$.

Figure 16.- Continued.



(c) $\delta_e = 30^\circ$.

Figure 16.- Concluded.

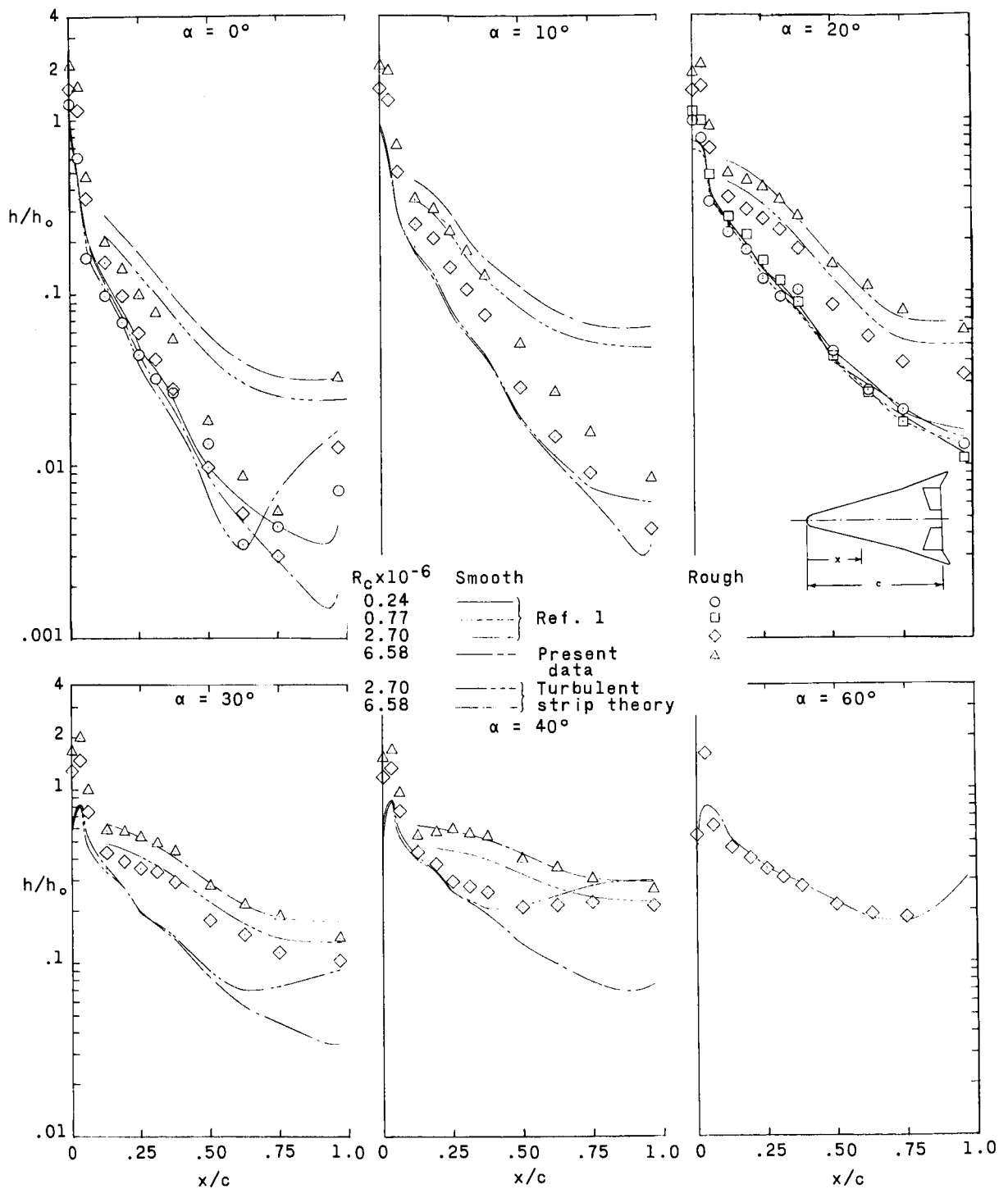
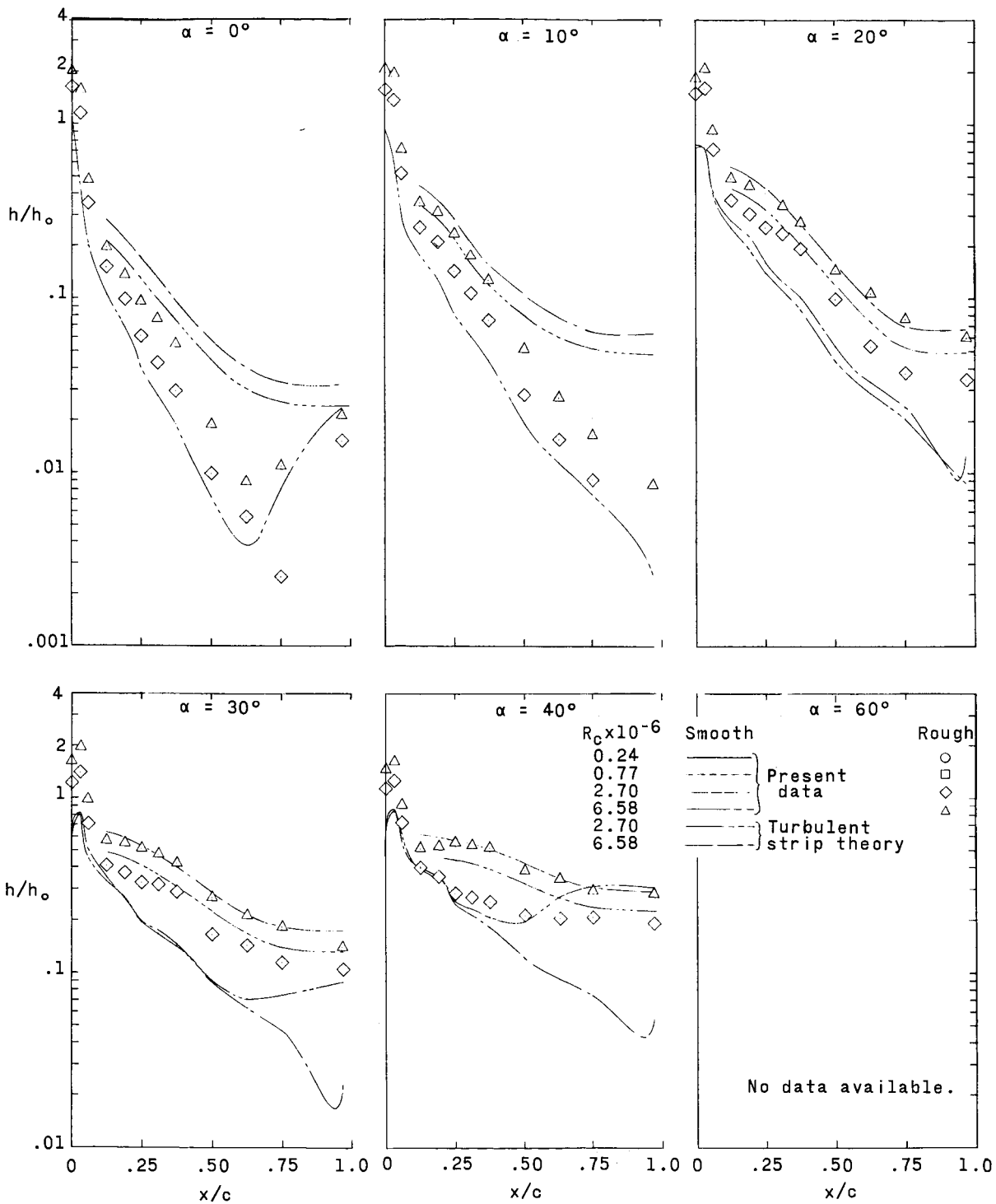
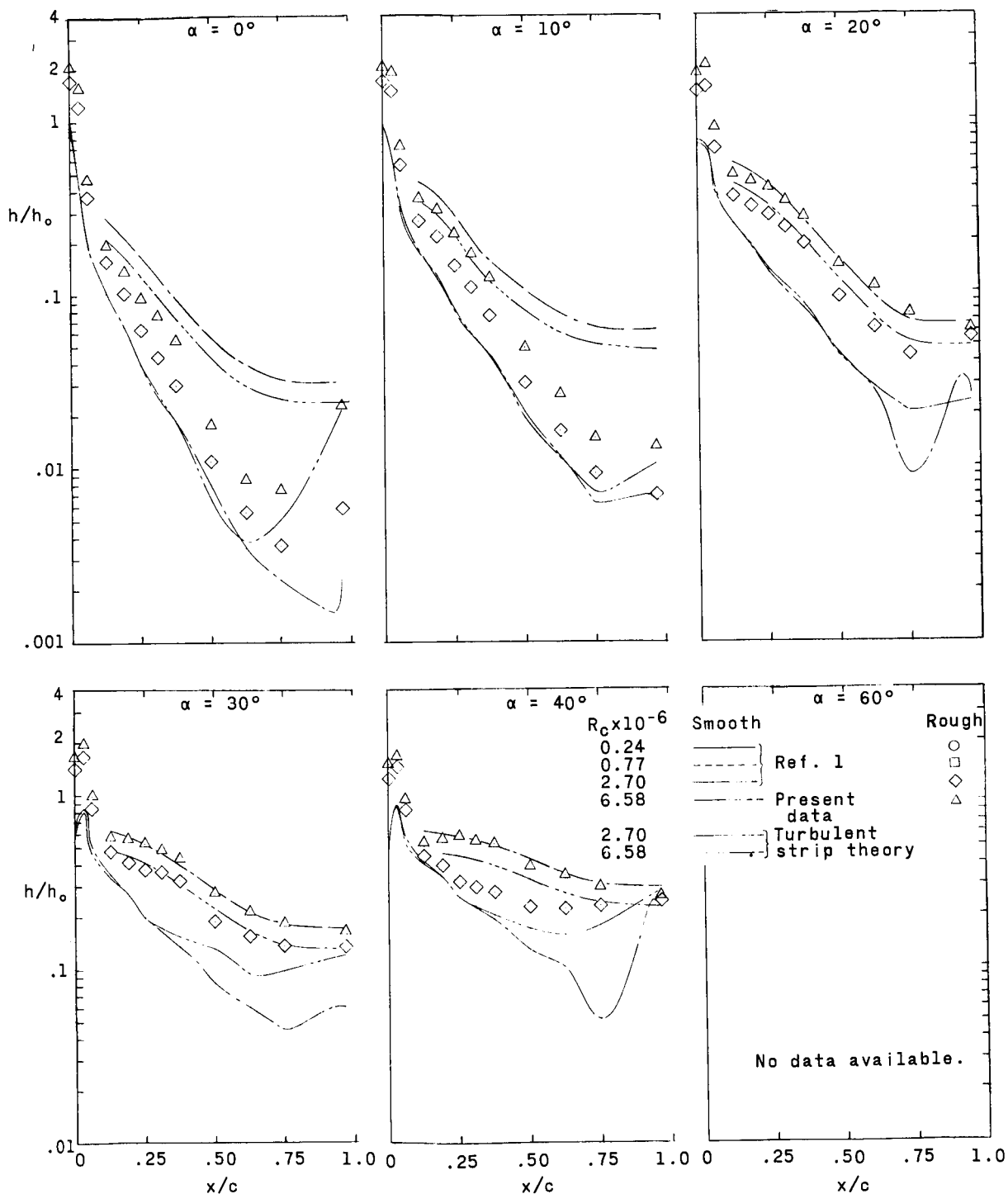
(a) $\delta_e = 0^\circ$.

Figure 17.- Effect of roughness on variation of heat-transfer ratio along model center line.



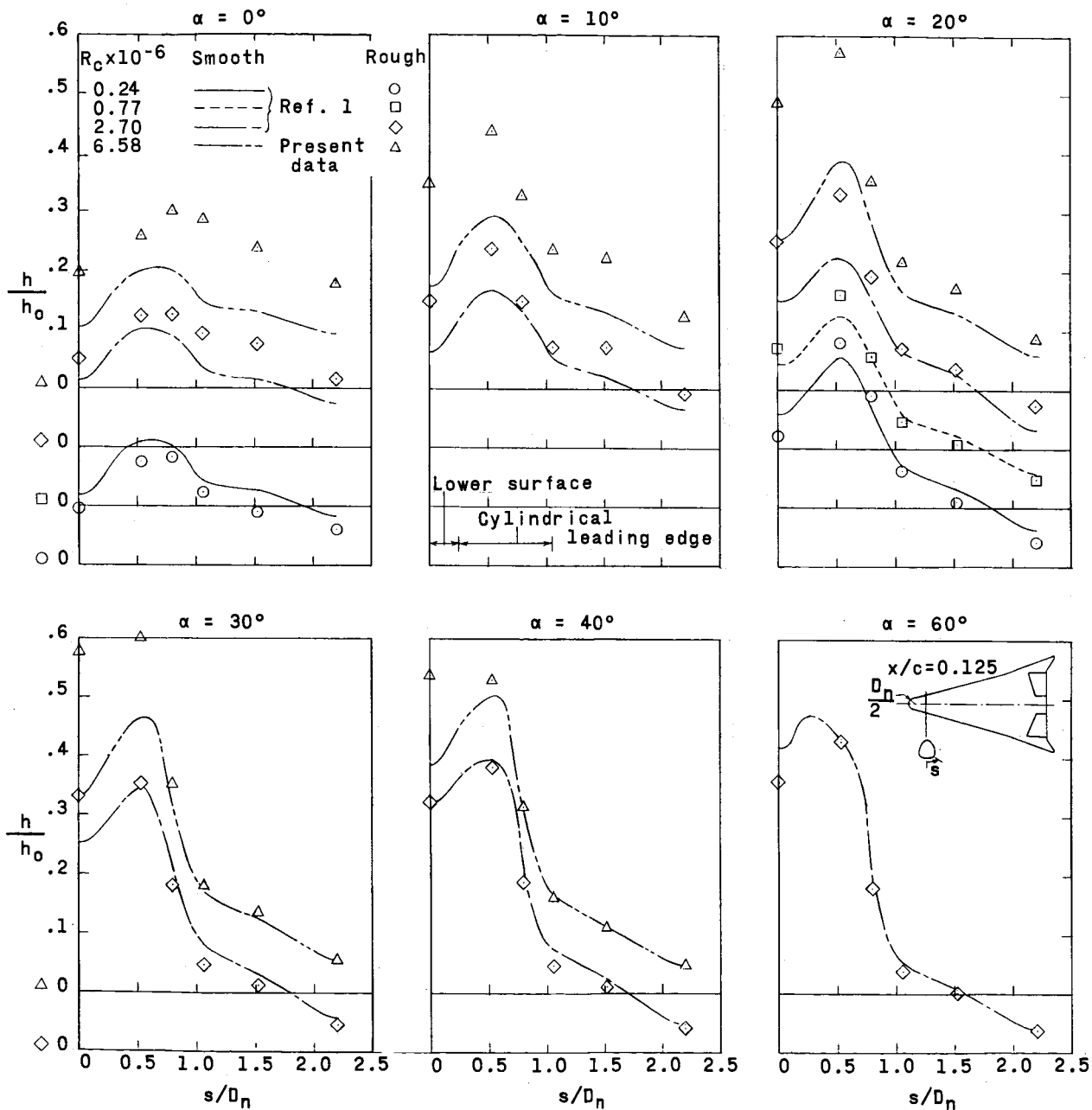
(b) $\delta_e = 15^\circ$.

Figure 17.- Continued.



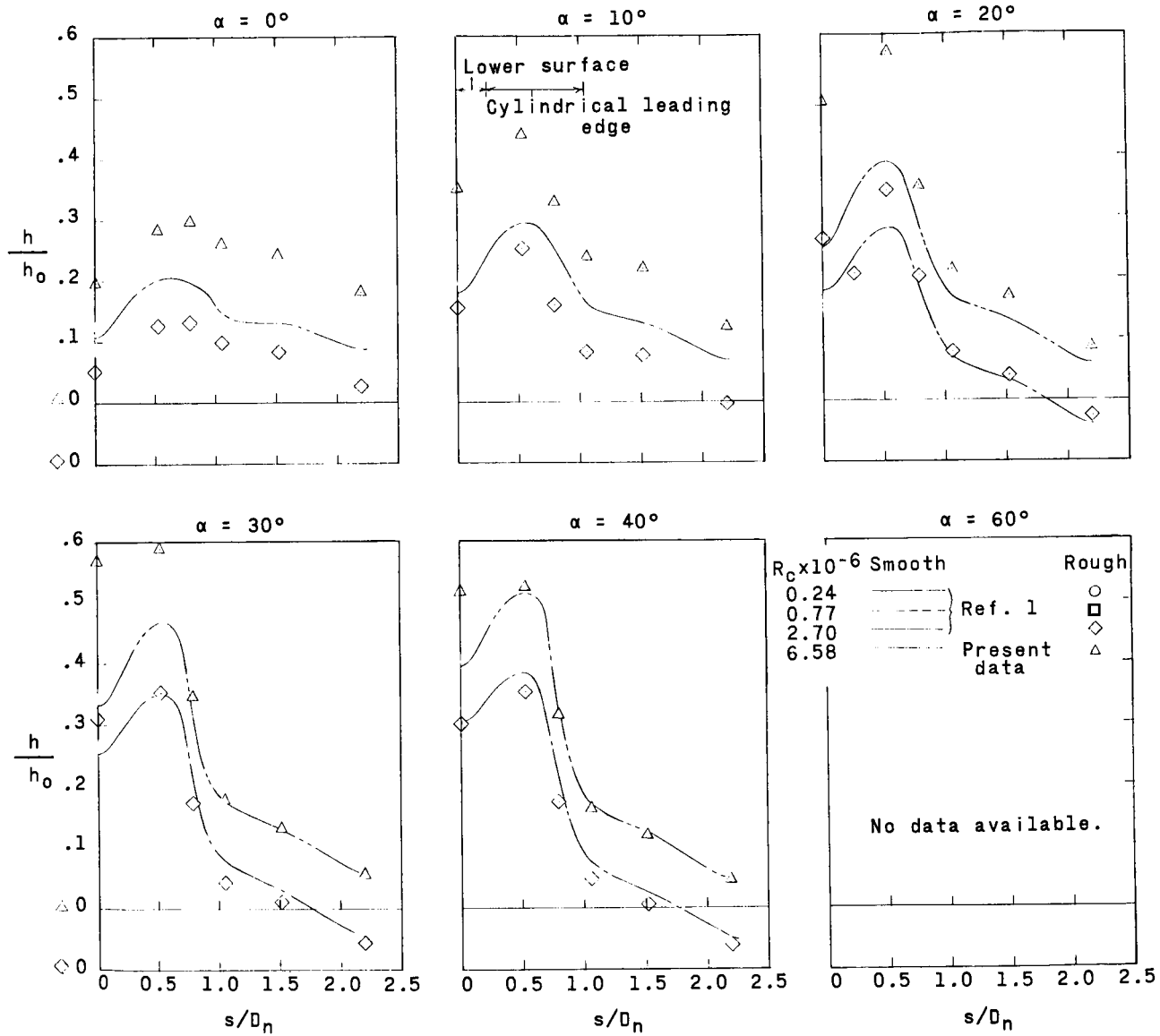
(c) $\delta_e = 30^\circ$.

Figure 17.- Concluded.



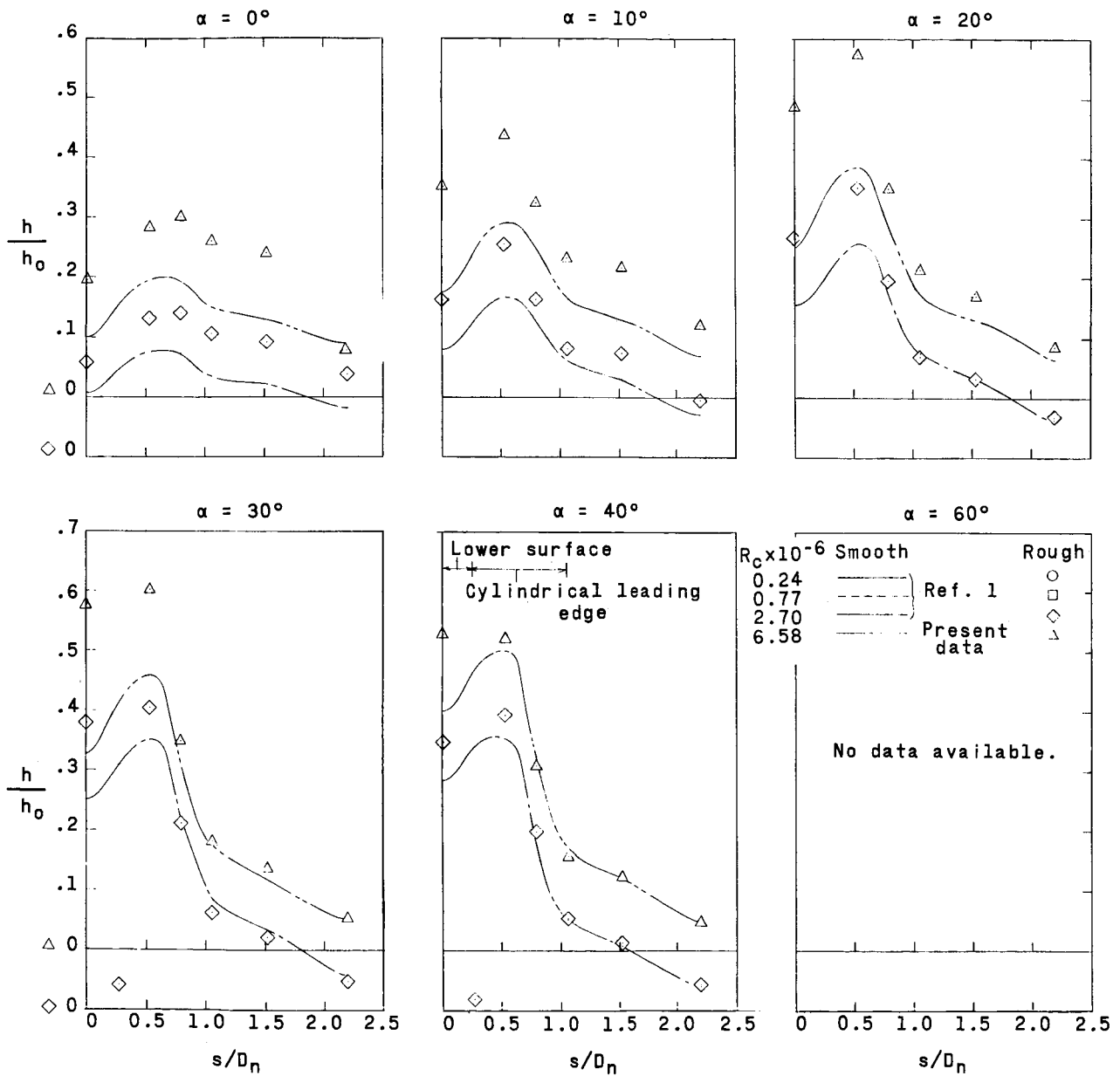
(a) $\delta_e = 0^\circ$.

Figure 18.- Effect of roughness on spanwise variation of heat-transfer ratio
at $x/c = 0.125$.



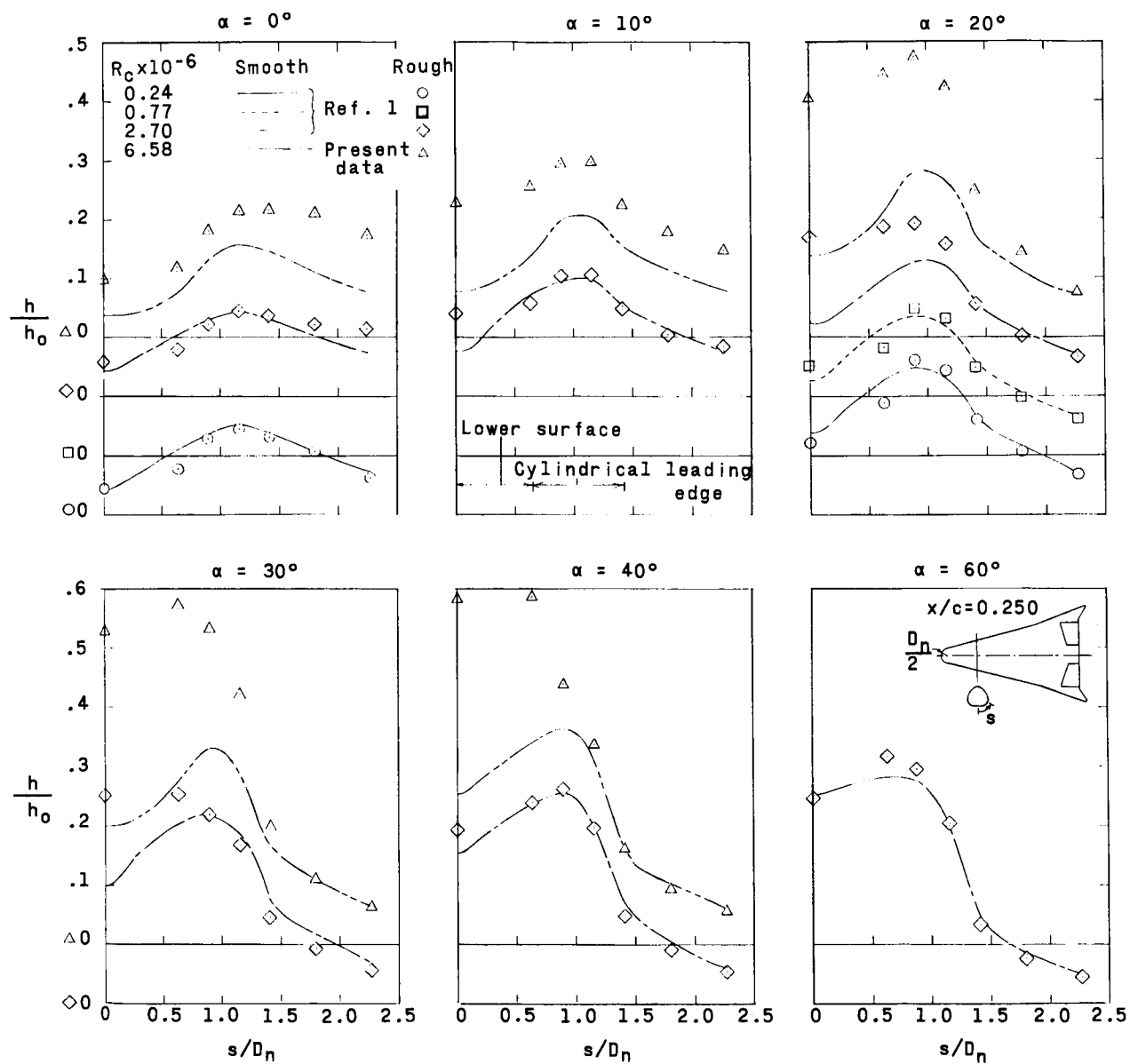
(b) $\delta_e = 15^\circ$.

Figure 18.- Continued.



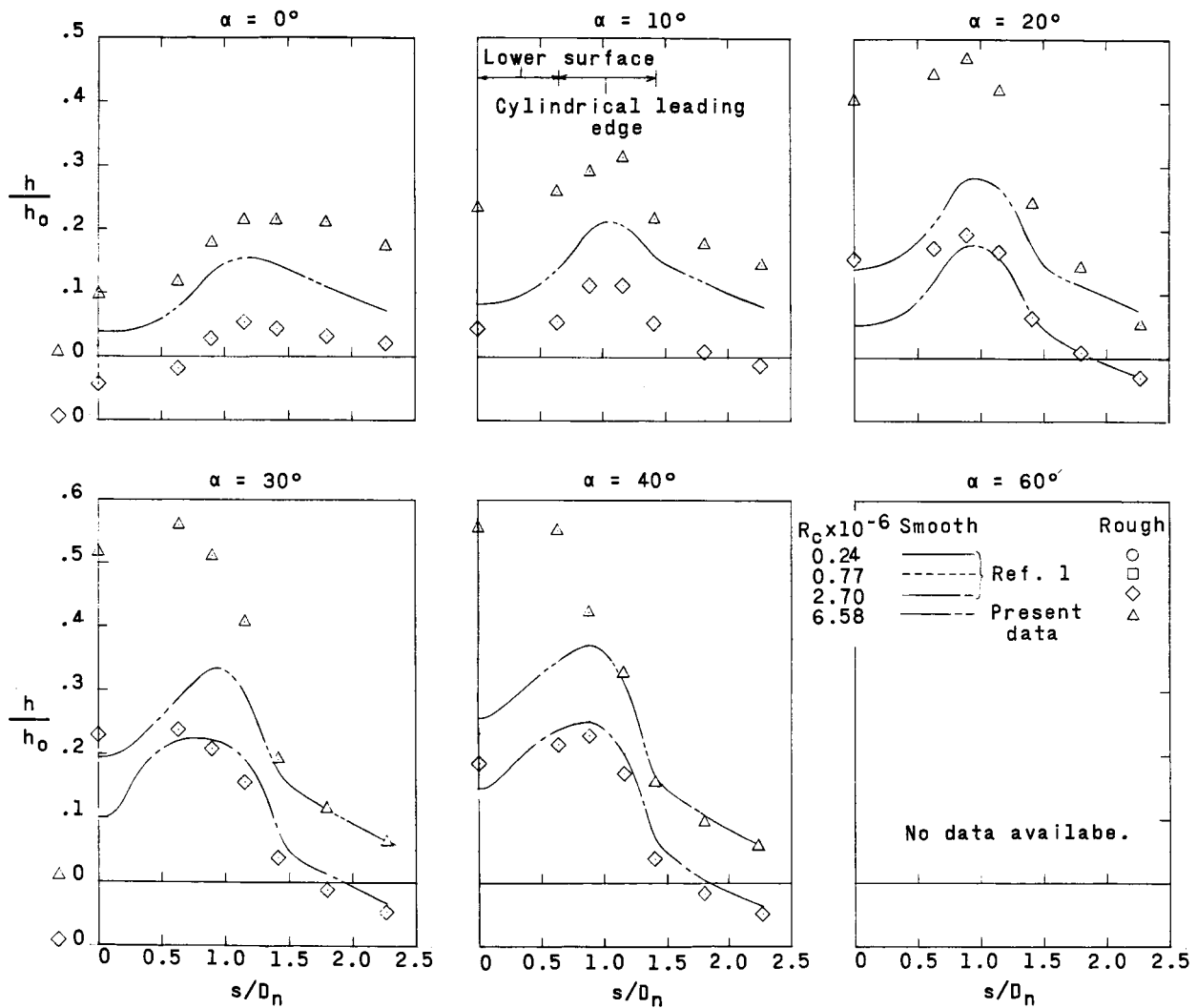
(c) $\delta_e = 30^\circ$.

Figure 18.- Concluded.



(a) $\delta_e = 0^\circ$.

Figure 19.- Effect of roughness on spanwise variation of heat-transfer ratio at $x/c = 0.250$.



(b) $\delta_e = 15^\circ$.

Figure 19.- Continued.

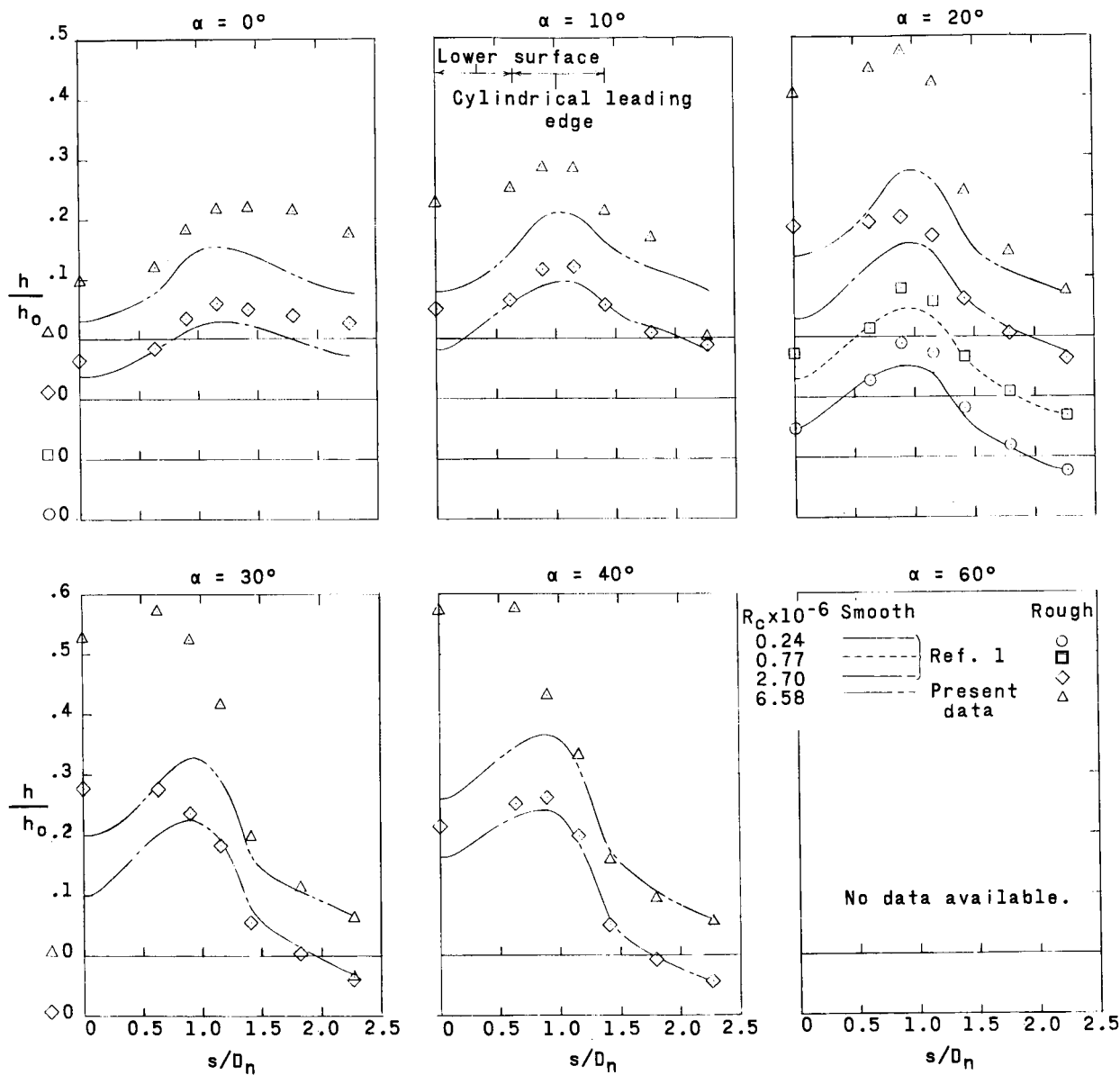
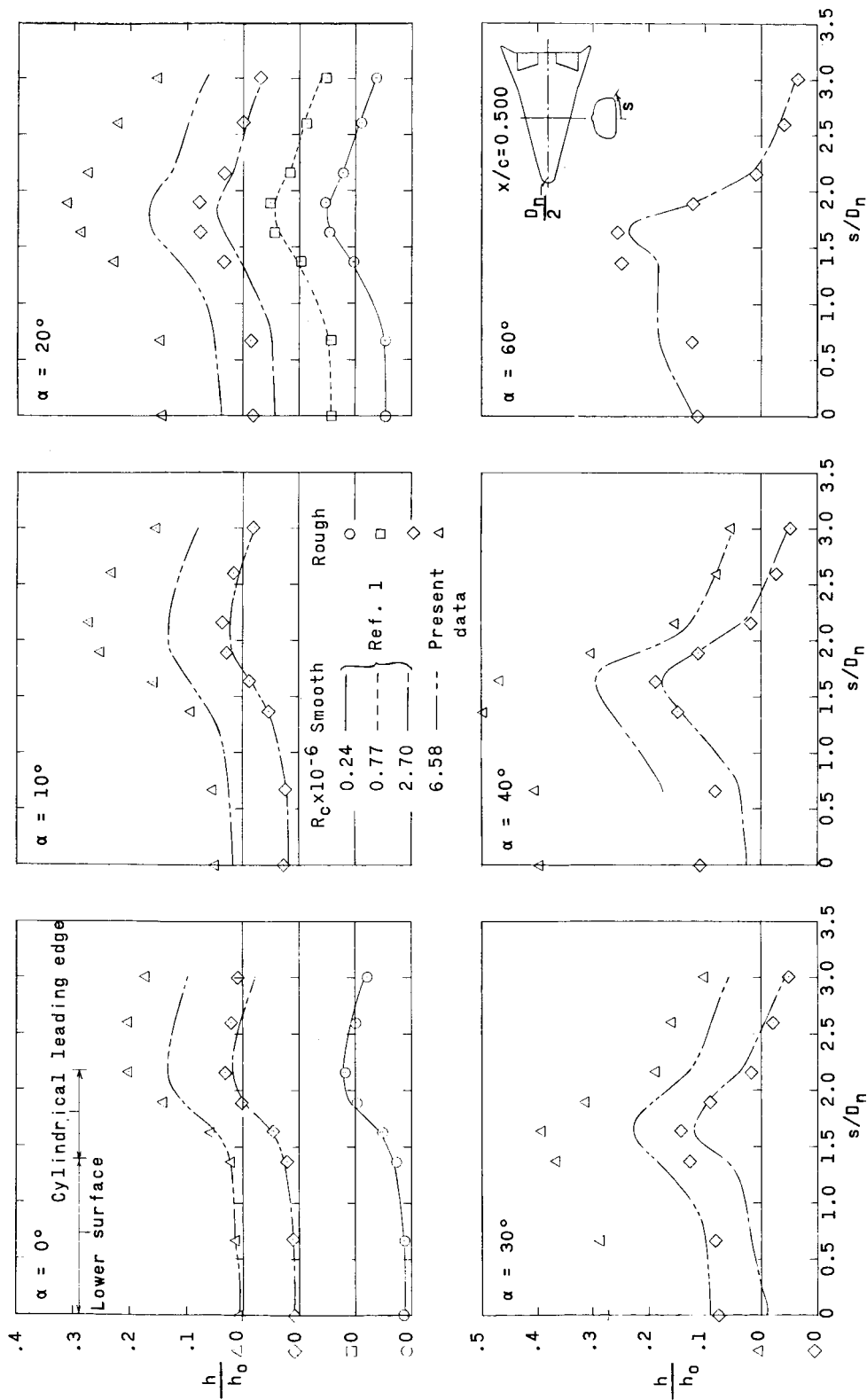
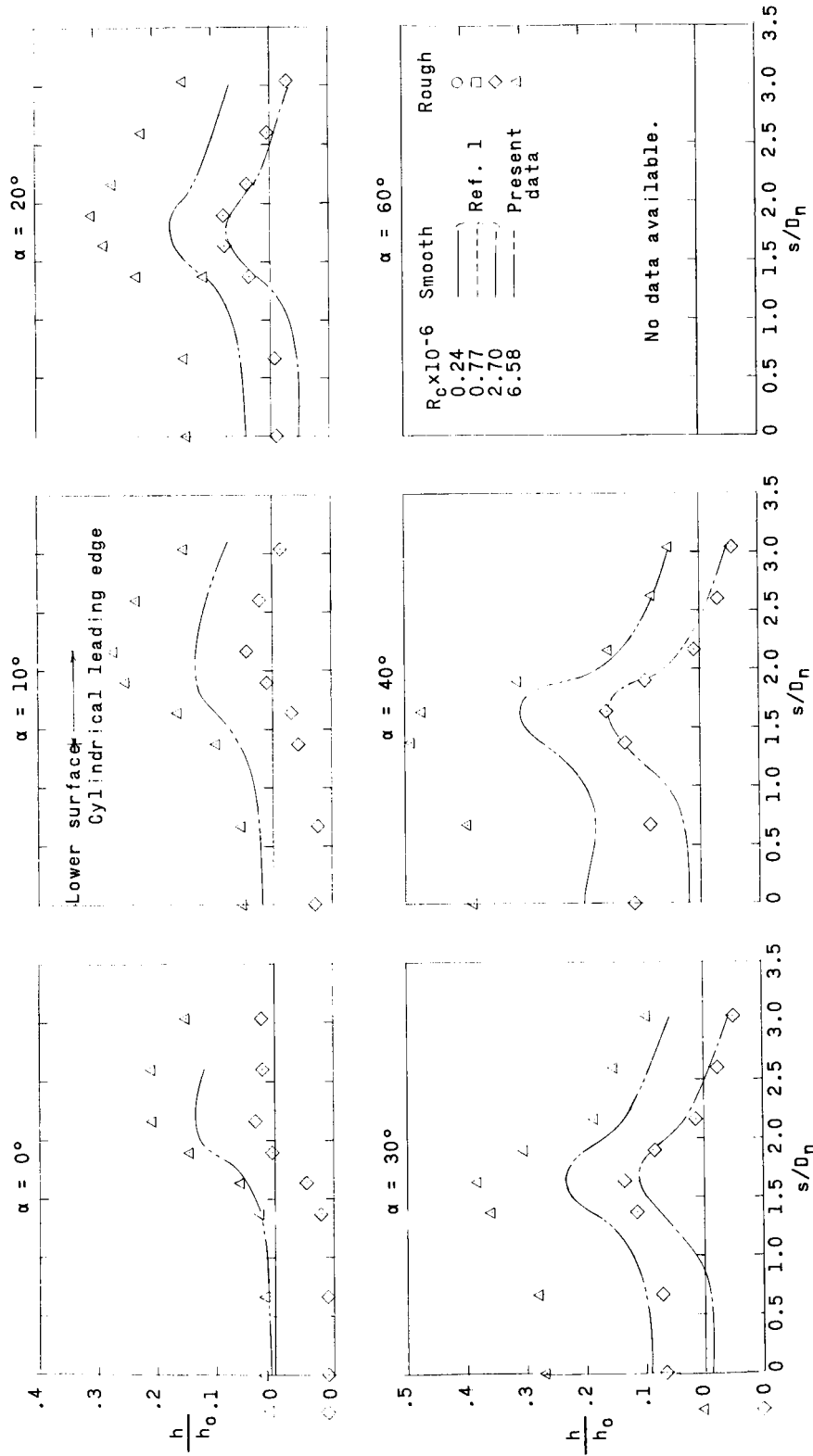
(c) $\delta_e = 30^\circ$.

Figure 19.- Concluded.



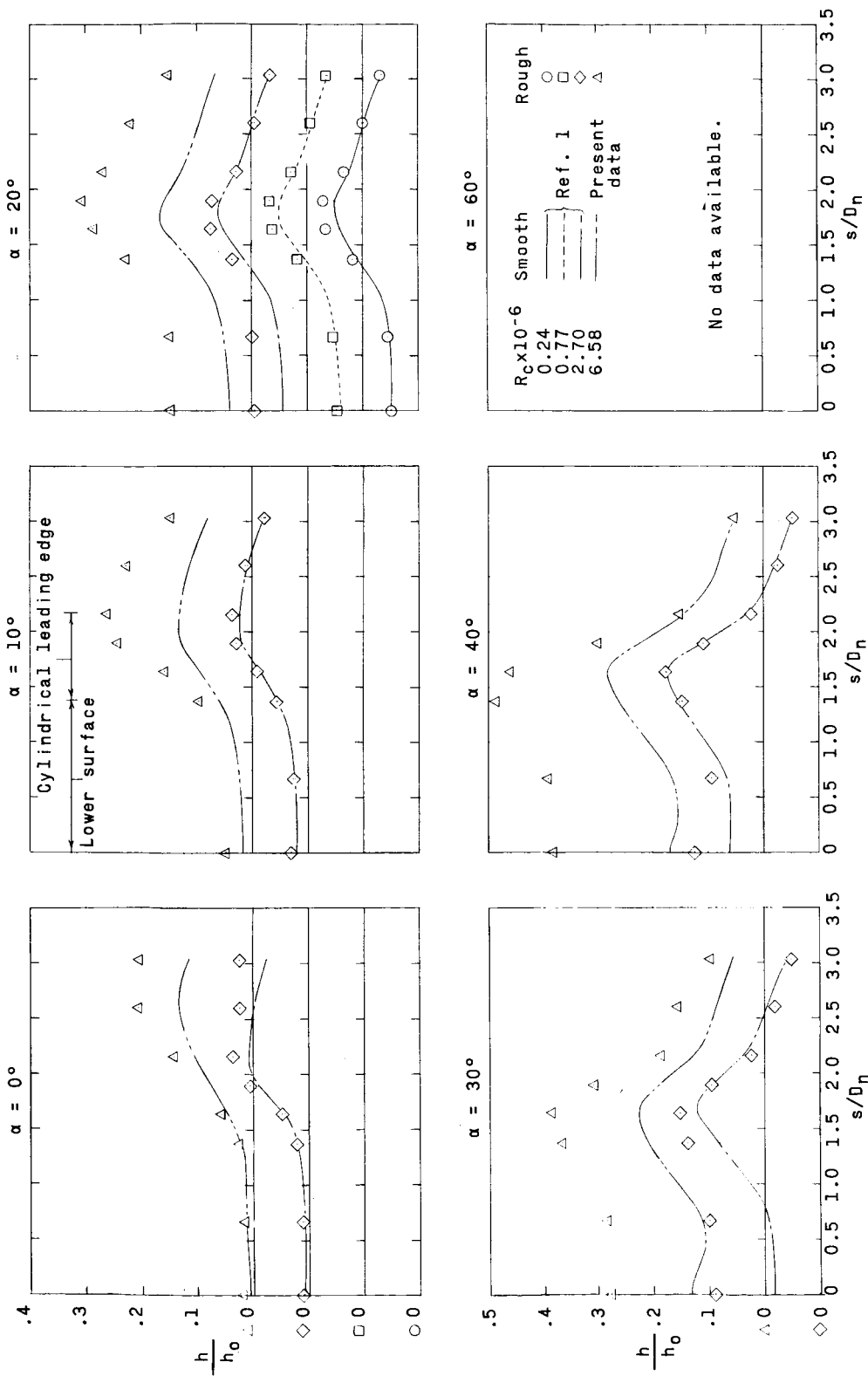
(a) $\delta_e = 0^\circ$.

Figure 20.- Effect of roughness on spanwise variation of heat-transfer ratio at $x/c = 0.500$.



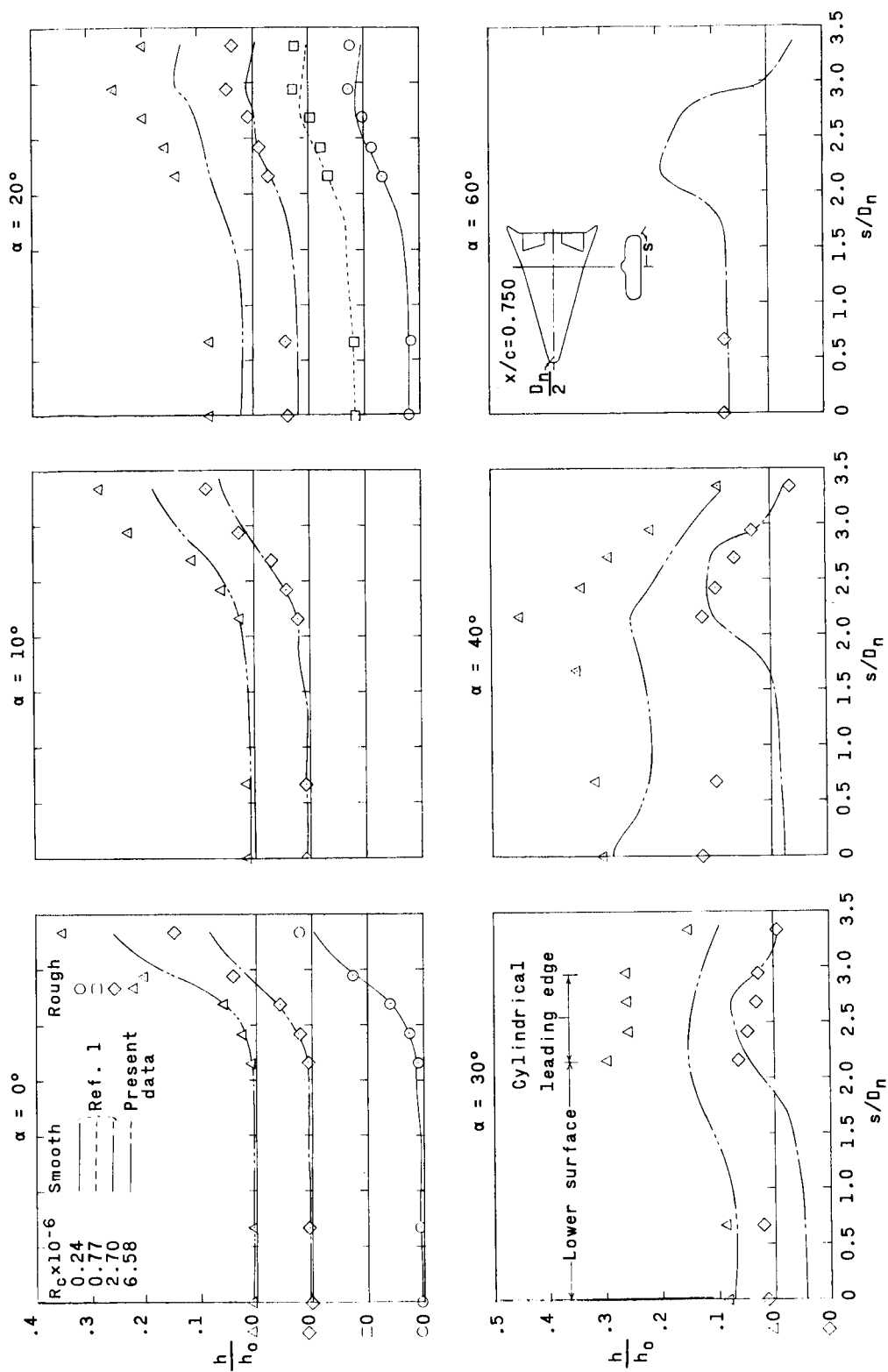
(b) $\delta_e = 15^\circ$.

Figure 20.- Continued.



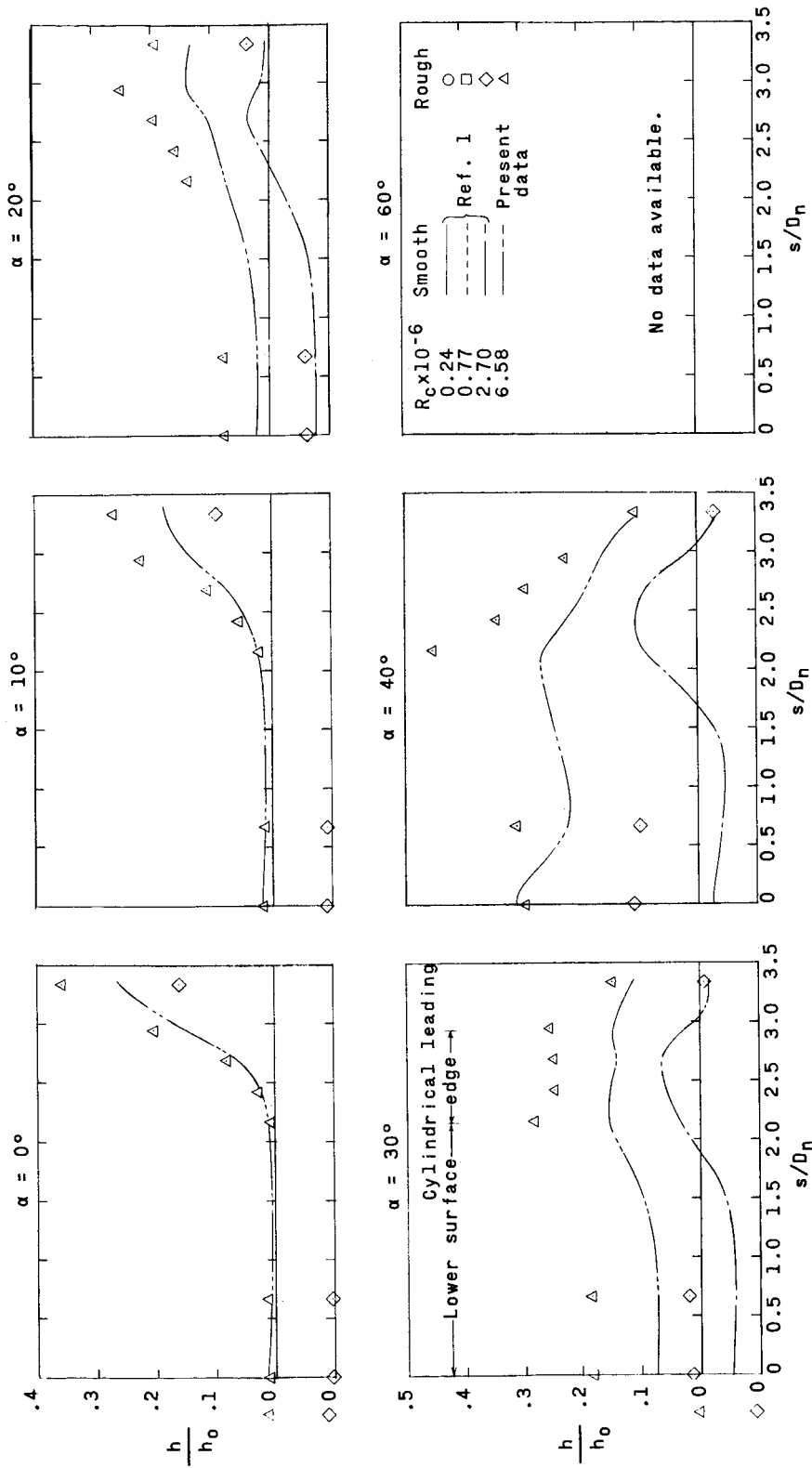
(c) $\delta_e = 30^\circ$.

Figure 20.- Concluded.



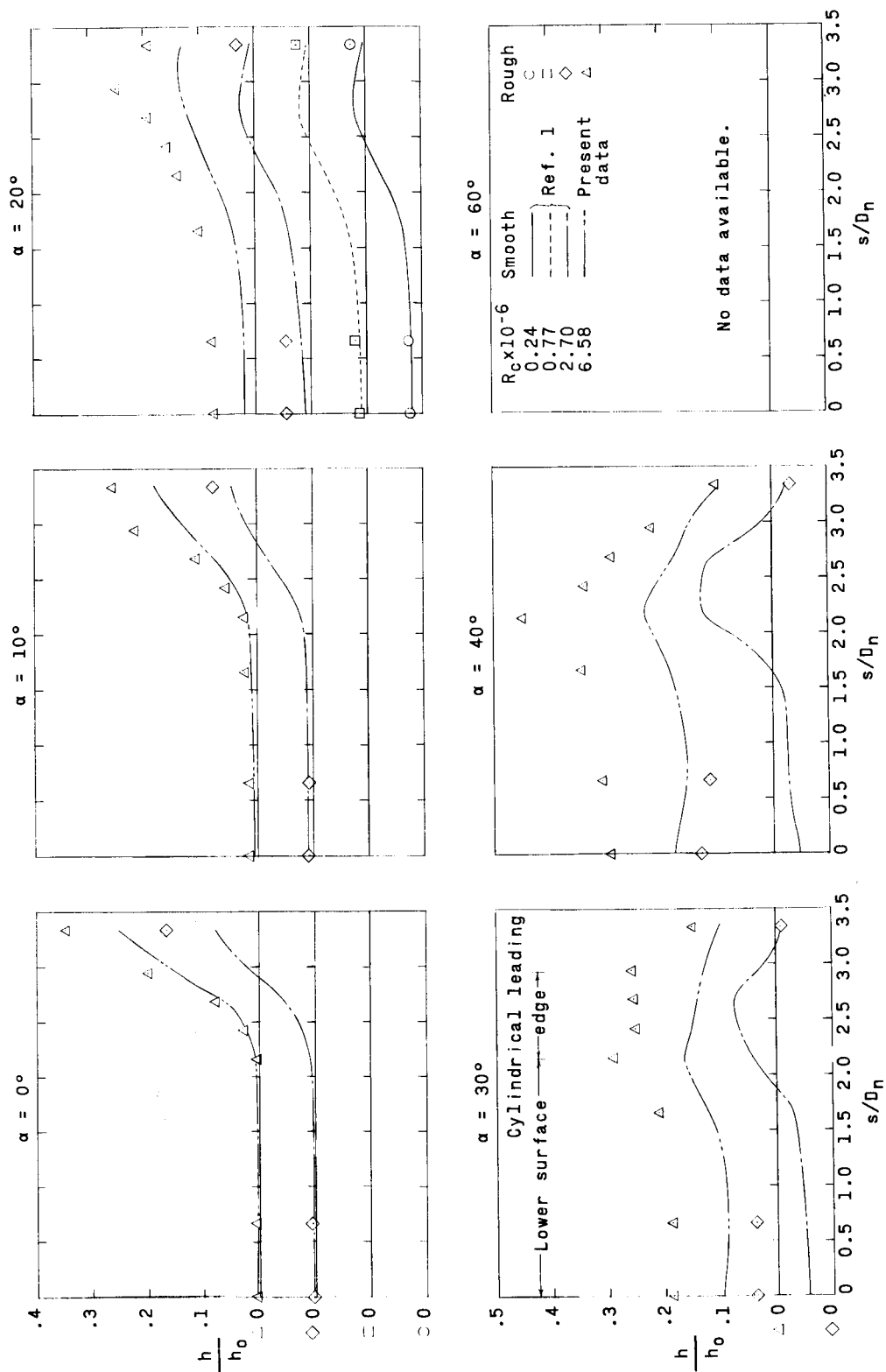
(a) $\delta_e = 0^\circ$.

Figure 21.- Effect of roughness on spanwise variation of heat-transfer ratio at $x/c = 0.750$.



(b) $\delta_e = 150^\circ$.

Figure 21.- Continued.



(c) $\delta_e = 30^\circ$.

Figure 21.- Concluded.

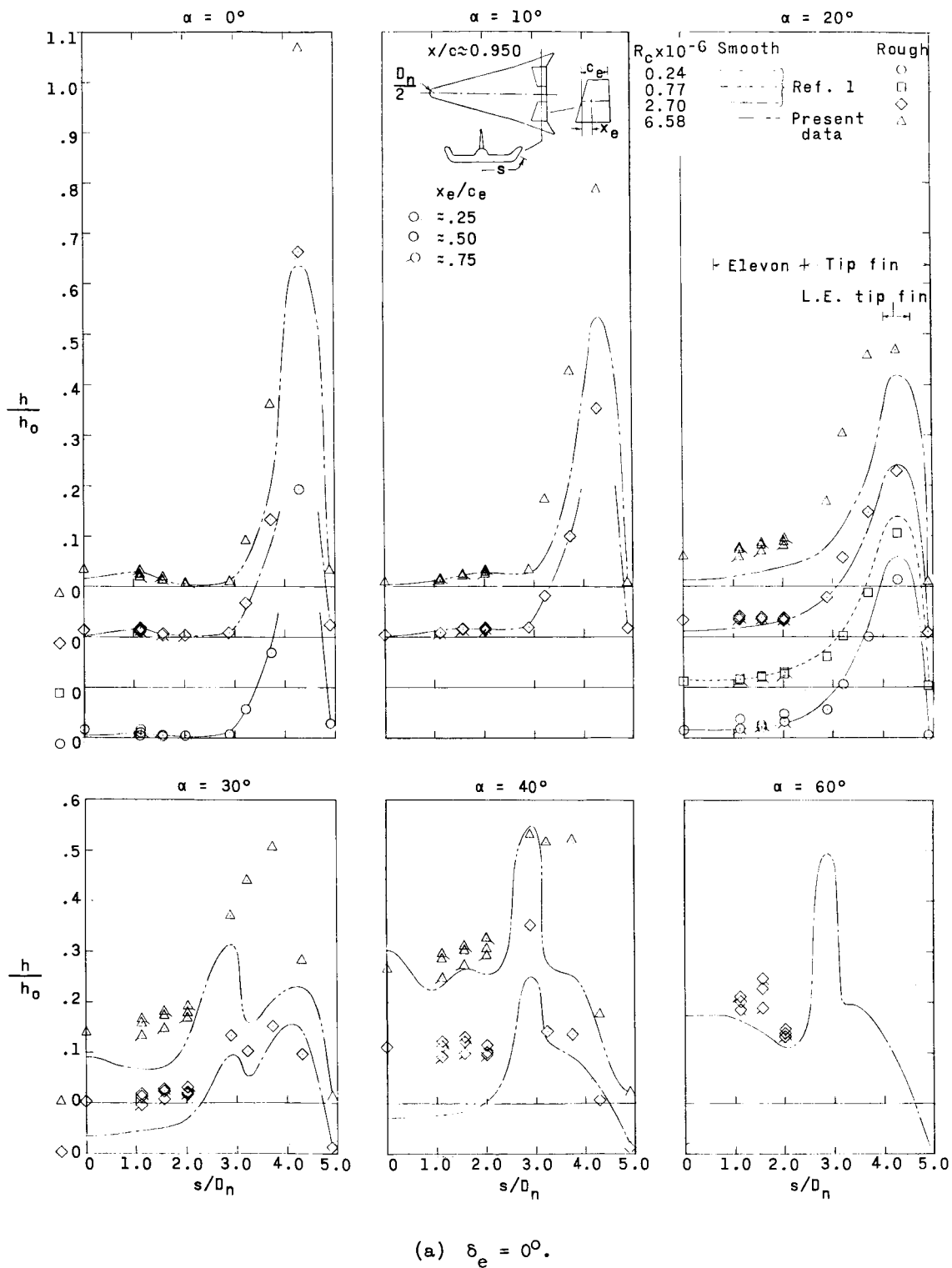
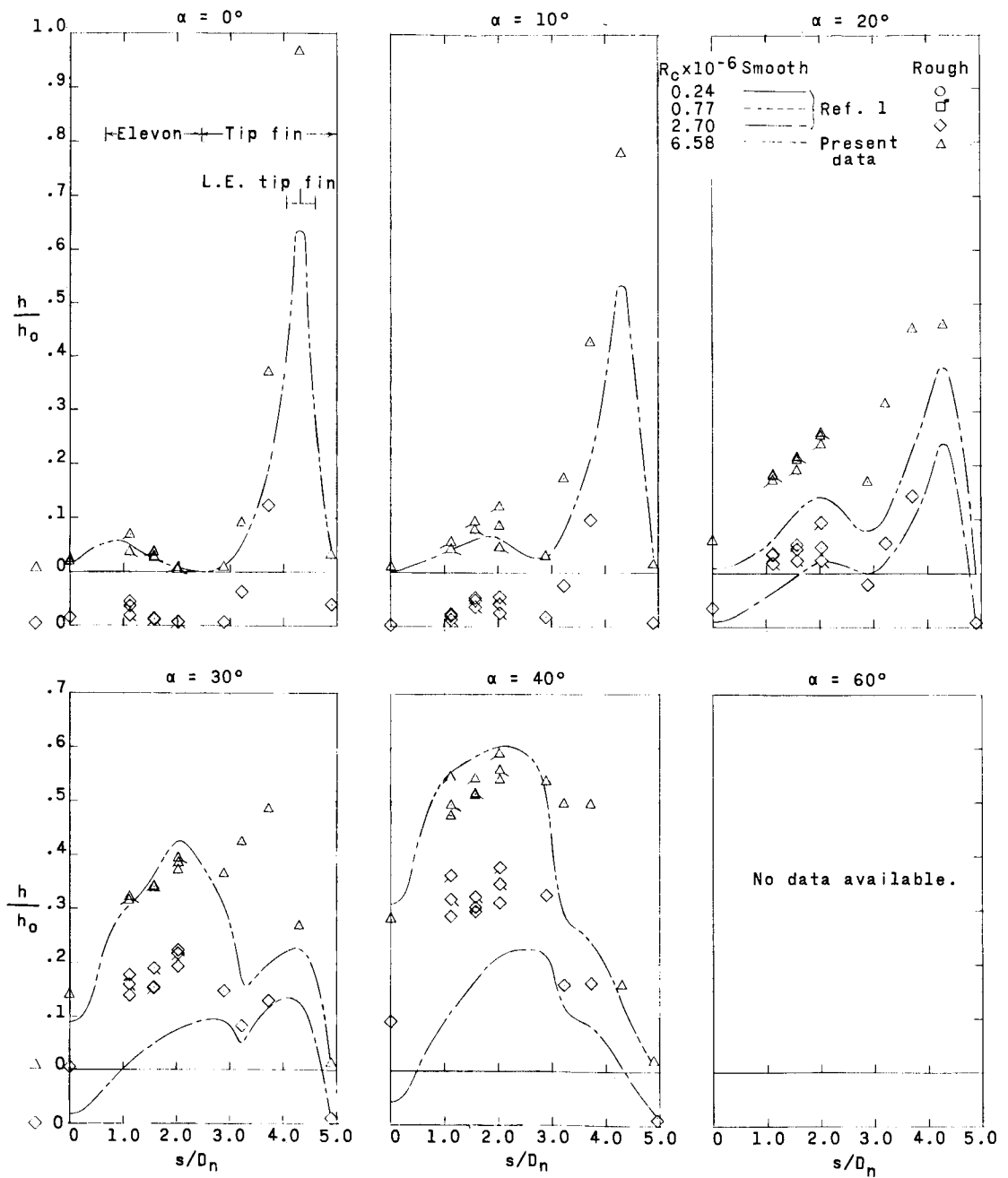
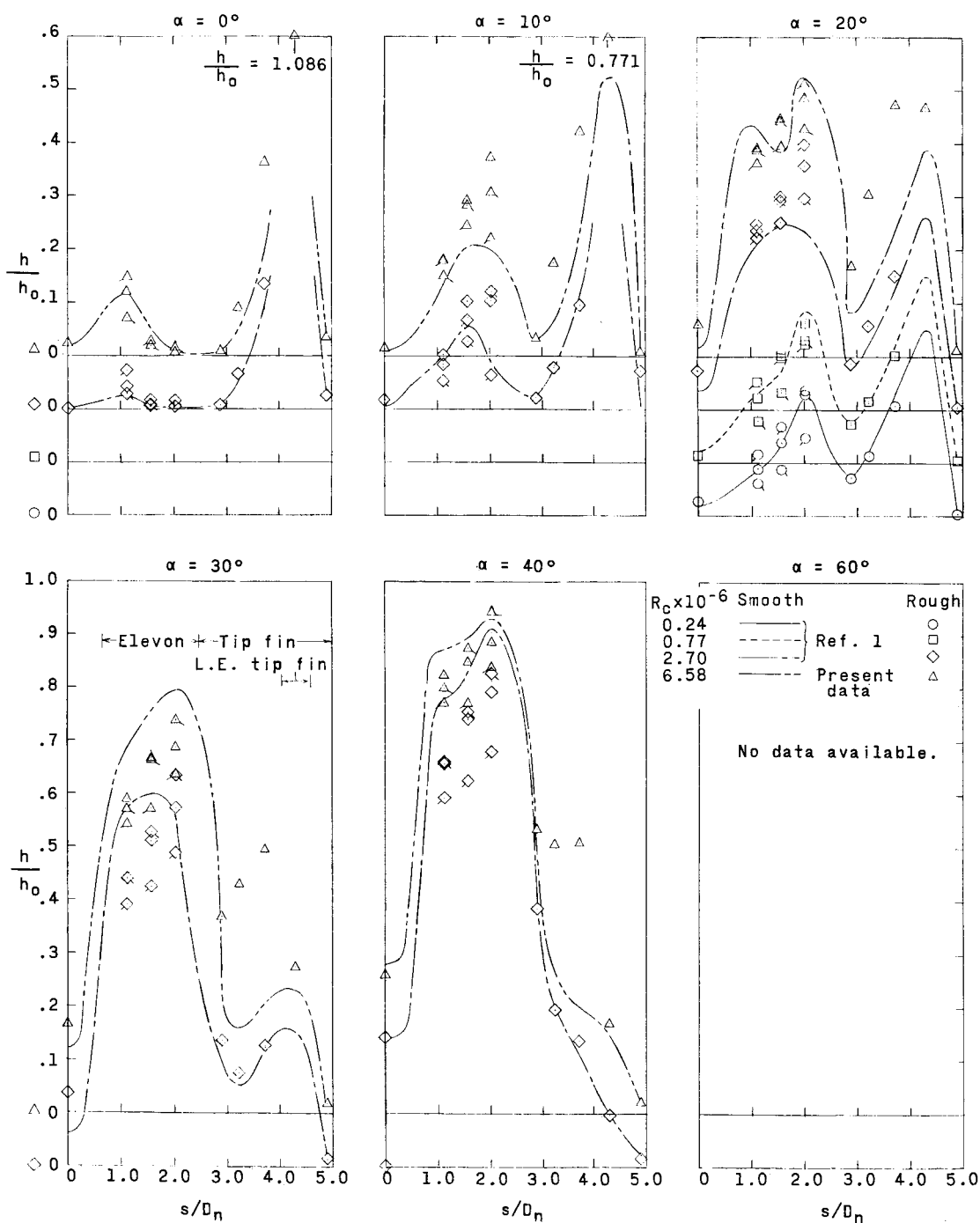


Figure 22.- Effect of roughness on spanwise variation of heat-transfer ratio at $x/c \approx 0.950$.



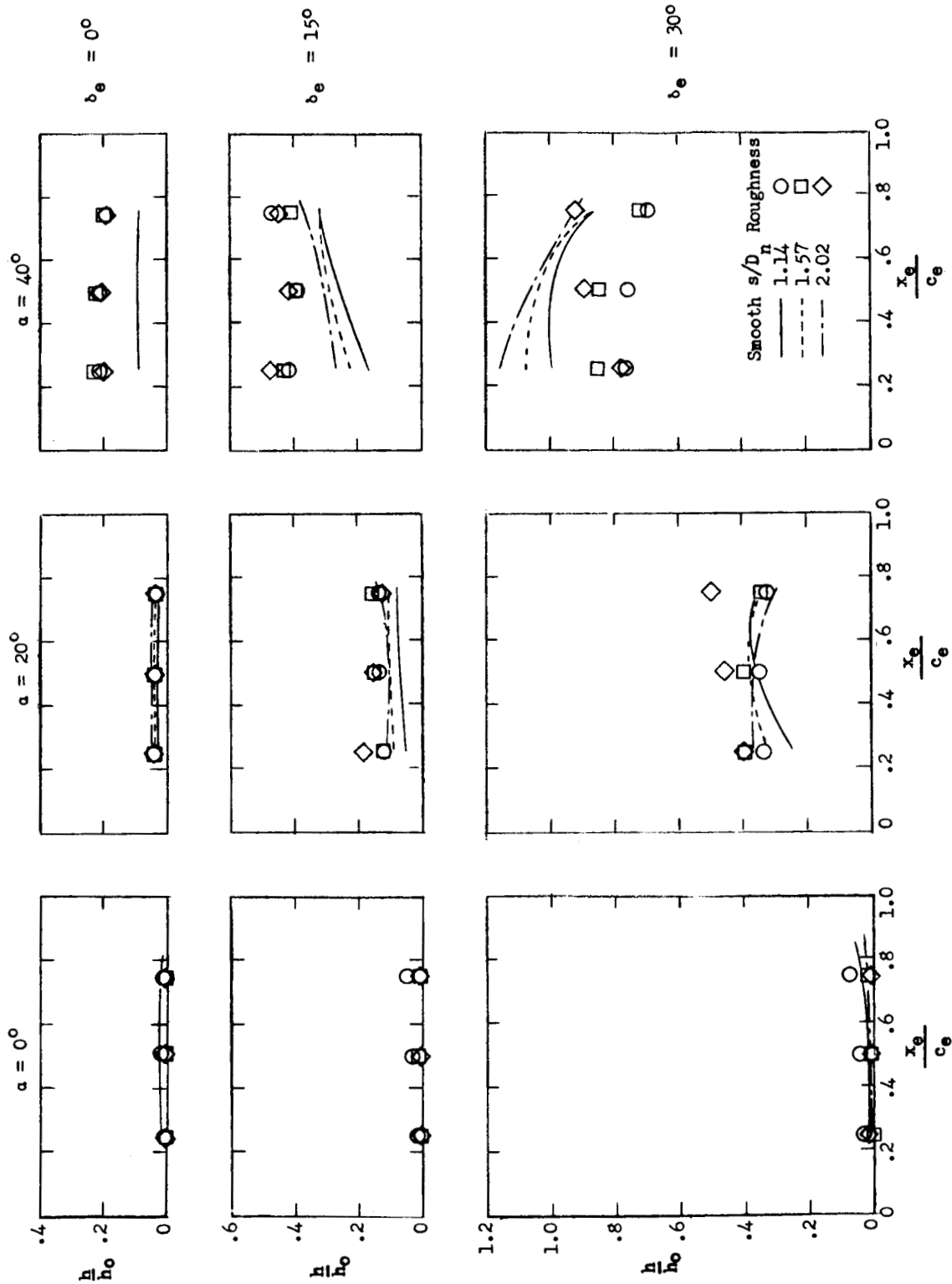
(b) $\delta_e = 15^\circ$.

Figure 22.- Continued.



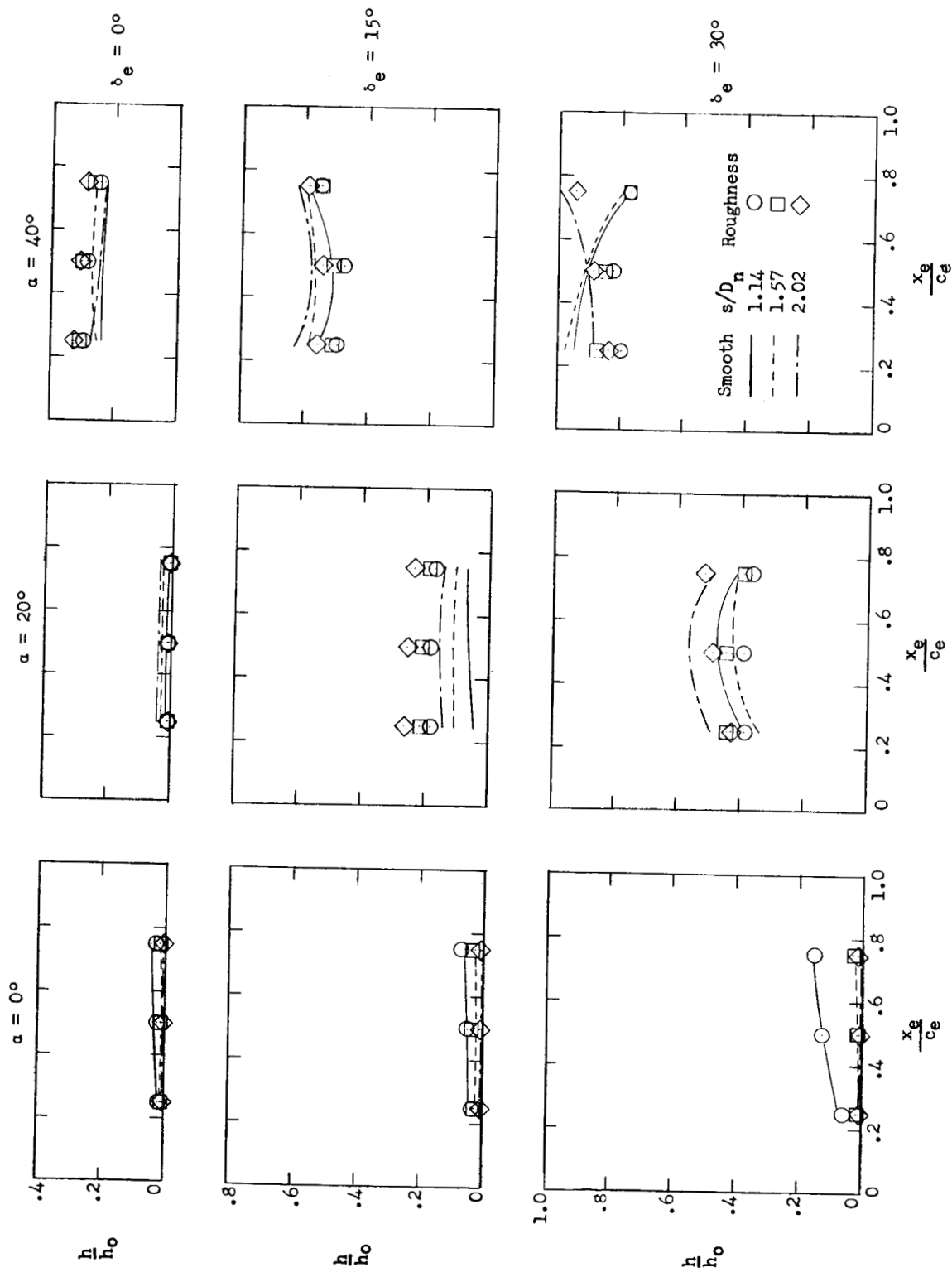
(c) $\delta_e = 30^\circ$.

Figure 22.- Concluded.



(a) $R_c = 2.70 \times 10^6$.

Figure 23.- Chordwise distribution of heat-transfer ratio on elevons.



(b) $R_c = 6.58 \times 10^6$.

Figure 23.- Concluded.

~~CONFIDENTIAL~~
UNCLASSIFIED

"The aeronautical and space activities of the United States shall be conducted so as to contribute . . . to the expansion of human knowledge of phenomena in the atmosphere and space. The Administration shall provide for the widest practicable and appropriate dissemination of information concerning its activities and the results thereof."

—NATIONAL AERONAUTICS AND SPACE ACT OF 1958

NASA SCIENTIFIC AND TECHNICAL PUBLICATIONS

TECHNICAL REPORTS: Scientific and technical information considered important, complete, and a lasting contribution to existing knowledge.

TECHNICAL NOTES: Information less broad in scope but nevertheless of importance as a contribution to existing knowledge.

TECHNICAL MEMORANDUMS: Information receiving limited distribution because of preliminary data, security classification, or other reasons.

CONTRACTOR REPORTS: Technical information generated in connection with a NASA contract or grant and released under NASA auspices.

TECHNICAL TRANSLATIONS: Information published in a foreign language considered to merit NASA distribution in English.

TECHNICAL REPRINTS: Information derived from NASA activities and initially published in the form of journal articles.

SPECIAL PUBLICATIONS: Information derived from or of value to NASA activities but not necessarily reporting the results of individual NASA-programmed scientific efforts. Publications include conference proceedings, monographs, data compilations, handbooks, sourcebooks, and special bibliographies.

Details on the availability of these publications may be obtained from:

SCIENTIFIC AND TECHNICAL INFORMATION DIVISION
NATIONAL AERONAUTICS AND SPACE ADMINISTRATION
Washington, D.C. 20546

UNCLASSIFIED

~~CONFIDENTIAL~~